

DISSERTATION

DEPENDENCE OF THE FORMATION FACTOR ON THE UNSATURATED
HYDRAULIC PROPERTIES OF POROUS MEDIA

Submitted by

Simon A. Lorentz

Department of Chemical and Bioresource Engineering

In partial fulfillment of the requirements
for the degree of Doctor of Philosophy

Colorado State University

Fort Collins, Colorado

Summer 1995

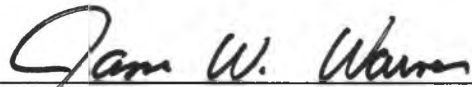
COLORADO STATE UNIVERSITY

May 12, 1995

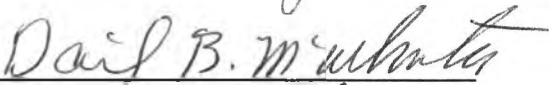
WE HEREBY RECOMMEND THAT THE DISSERTATION PREPARED UNDER OUR SUPERVISION BY SIMON A. LORENTZ ENTITLED DEPENDENCE OF THE FORMATION FACTOR ON THE UNSATURATED HYDRAULIC PROPERTIES OF POROUS MEDIA BE ACCEPTED AS FULFILLING IN PART REQUIREMENTS FOR THE DEGREE OF DOCTOR OF PHILOSOPHY.

Committee on Graduate Work

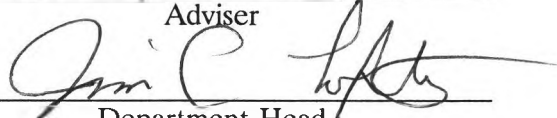








Adviser



Department Head

ABSTRACT OF DISSERTATION

DEPENDENCE OF THE FORMATION FACTOR ON THE UNSATURATED HYDRAULIC PROPERTIES OF POROUS MEDIA

Mathematical models of the hydraulic conductivity are used extensively to predict the movement of liquids in porous media. Included in these models is a description of the physics of flow as well as the nature of the conduits in which the liquids move through the medium. Since these flow channels comprise a complex network of pathways and have significantly varying geometries, the mathematical models developed assume a simplified arrangement and geometry of the flow channels which is termed the formation factor. The simplifications are derived from experimentally determined behavior of the porous media. These simplifications are generalized and used to describe the hydraulic conductivity of all porous media. The pore size distribution information is used to estimate the effective hydraulic radius of the medium. The effects of channel network and geometry are modelled by generalized relationships derived from experimentally determined formation factors or from unsaturated hydraulic conductivity observations. The dependence of the formation factor on the properties of porous media has not been studied.

It is hypothesized that the effects of the channel network and geometry are a function of the pore size distribution or other properties of the porous medium and are thus material specific. It is proposed that a better understanding of the behavior of the hydraulics in porous media can be gained by determining the relationship between the channel geometry and the pore size distribution or other properties.

Therefore, the specific purpose of this study is to:

- Derive a simple mathematical model that describes both the unsaturated hydraulic conductivity as well as the formation factor that represents the channel geometry;
- Determine the pore size distribution and other porous media properties, the formation factors and hydraulic conductivities at various saturations by laboratory experiments on two soils with significantly different pore size distributions;
- Test the model's capability to predict both the formation factor and hydraulic conductivity of the soils so that conclusions can be made about the dependency of the channel geometry or formation factor on the pores size properties of the media; and
- Develop a generalized relationship for the formation factor using porous media properties.

The results of the study indicate that the formation factor increases with increasing pore size distribution index. It also is apparent, however, that the pore formation factor is not uniquely dependant on the pore size distribution index and that the relative size of the pores also may contribute to the dependency of the formation factor on the unsaturated properties of the porous media. In addition, it has been determined that the dynamic flow process is influenced by the formation factor to a greater degree than is the static ion diffusion process.

Simon A. Lorentz
Chemical and Bioresource Engineering Department
Colorado State University
Fort Collins, CO 80523
Summer 1995

ACKNOWLEDGMENTS

The author gratefully acknowledges the support, encouragement, patience, and the sound and stimulating advice of his major professor, Professor David B. McWhorter. His guidance and interest have contributed immeasurably to the success of this author's venture into this daunting topic. The author also thanks the committee members, Professor Deanna Durnford, Professor Robert Ward and Professor Jim Warner, for their advice and patience and for adding value to the study by reviewing the document and offering sound and useful comments.

Sincere thanks are extended to Mrs. Elaine Dean, who provided unfailing encouragement throughout the study and constant support in compiling and printing the document. The author also thanks Mr. John Brookman for the expert construction of laboratory equipment and for his welcomed advice on laboratory procedures. The author is grateful to Professor Deanna Durnford for the many hours spent in discussing the subject material in this study. Other friends, too numerous to mention, have been instrumental in encouraging the author in the completion of this work and their concern is gratefully appreciated.

The author is especially grateful to his wife, Yvonne, and sons, Andrew and Liam, for their ceaseless encouragement and infinite patience during the time spent completing this work. The author gratefully acknowledges their unselfish sacrifice in supporting this effort.

Support for this work also has come from teaching assignments provided by the Department of Chemical and Bioresource Engineering, Colorado State University, from

research projects, and from a bursary provided by the South African Foundation for Research Development.

DEDICATION

A. M. D. G.

TABLE OF CONTENTS

<u>Chapter</u>	<u>Page</u>
1 INTRODUCTION	1
2 LITERATURE REVIEW	4
2.1 Capillary Models	5
2.1.1 Capillary Model Development	5
2.1.2 The Formation Factor in Capillary Models	9
2.2 Statistical Models	19
2.2.1 Statistical Model Development	19
2.2.2 The Formation Factor in Statistical Models	21
2.3 Evaluation of Hydraulic Models	22
2.4 Other Functional Forms of Hydraulic Conductivity	26
3 THEORETICAL DEVELOPMENT	29
3.1 Unsaturated Hydraulic Conductivity	29
3.2 Solute Diffusion	31
4 METHODOLOGY	34
4.1 Materials	34
4.2 Water Retention Tests	36
4.3 Diffusion Half Cell Tests	39
4.4 Unsaturated Hydraulic Conductivity Short Column Tests	41
5. RESULTS AND DATA ANALYSIS	44
5.1 Water Retention Analysis	44
5.2 Diffusion Half Cell Results	46
5.3 Hydraulic Conductivity Results	51
6 ANALYSIS AND DISCUSSION	57
6.1 Diffusion Half-Cell Analysis	57
6.2 Saturated Hydraulic Conductivity Analysis	59
6.3 Unsaturated Hydraulic Conductivity Analysis	67

7	CONCLUSIONS AND RECOMMENDATIONS	75
7.1	Problem Summary	75
7.2	Summary of This Study	76
7.3	Conclusions	78
7.4	Recommendations	79
	REFERENCES	80
	APPENDIX A DIFFUSION HALF-CELL RESULTS	83
	APPENDIX B HYDRAULIC PROPERTIES OF TESTED MATERIALS	108
	APPENDIX C HYDRAULIC PROPERTIES OF MATERIALS EXTRACTED FROM THE LITERATURE	113

LIST OF TABLES

<u>Table</u>	<u>Description</u>	<u>Page</u>
5.1	Results of Brooks-Corey analysis	46
5.2	Results of the diffusion half-cell measurements	49
5.3	Parameter optimization of the water retention (WR) and hydraulic conductivity (HC) characteristics: Ottawa sand	55
5.4	Parameter optimization of the water retention (WR) and hydraulic conductivity (HC) characteristics: Poudre sand mix	56
6.1	Results of the diffusion formation factor, D_e/D_o (or $B\theta^n$) analysis	59
6.2	Saturated hydraulic conductivity analysis	60
6.3	Summary of porous media properties used in the k_oT analysis	62

LIST OF FIGURES

<u>Figure</u>	<u>Description</u>	<u>Page</u>
2.1	Schematic representation of the porous medium	6
2.2	Schematic representation of a uniform capillary model	11
2.3	Schematic representation of a constricted capillary model	16
4.1	Particle size distribution for the Poudre sand mix and the Ottawa sand.	35
4.2	Thin sections through the Poudre sand mix (right) and the Ottawa sand (left): Approximate magnification x60.	36
4.3	Schematic section of the controlled outflow cell.	37
4.4	Schematic section of the diffusion half-cell apparatus.	40
4.5	Schematic section of the short column hydraulic conductivity apparatus.	42
5.1	Water retention analysis by Brooks and Corey model: Ottawa sand.	45
5.2	Water retention analysis by Brooks and Corey model: Poudre sand.	46
5.3a	Half cell diffusion results for Ottawa sand. $S=0.974$	47
5.3b	Half-cell water contents for Ottawa sand. $De/D0=0.99$	47
5.4a	Half cell diffusion results for Poudre sand mix. $De/Do=0.43$	47
5.3b	Half-cell water contents for Poudre sand mix. $S=0.896$	47
5.5a	Diffusion half-cell results: Ottawa sand. $De/Do=0.15$	48
5.5b	Half-cell water content for Ottawa sand. $S=0.084$	48
5.6a	Diffusion half-cell results: Poudre sand mix. $De/Do=0.18$	48
5.6b	Half-cell water content for Poudre sand mix. $S=0.284$	48

<u>Figure</u>	<u>Description</u>	<u>Page</u>
5.7a	Example of the titration result: Poudre sand: Test 1, Cell 6.	49
5.7b	Example of the titration result: Ottawa sand: Test 11, Cell 5.	49
5.8	Hydraulic conductivity analysis: Ottawa sand, Condition 1.	51
5.9	Hydraulic conductivity analysis: Poudre sand mix, Condition 1.	52
5.10	Water retention curves: Ottawa sand, Condition 1.	52
5.11	Water retention curves: Poudre sand mix, Condition 1.	52
5.12	Hydraulic conductivity analysis: Ottawa sand, Condition 3.	53
5.13	Hydraulic conductivity analysis: Poudre sand mix, Condition 3.	54
5.14	Water retention curves: Ottawa sand, Condition 3.	54
5.15	Water retention curves: Poudre sand mix, Condition 3.	54
6.1	Variation of the effective diffusion coefficient/free diffusion coefficient ratio with saturation for Poudre sand mix and Ottawa sand. (Error bars denote 2σ)	58
6.2	k_0T versus pore size distribution index, λ at saturation.	61
6.3	$B\theta$ versus the pore size distribution index, λ at saturation.	64
6.4	Comparison of predicted and measured saturated hydraulic conductivities	66
6.5	Variation of B with S_e , showing the value of B derived from the regression analysis in 6.2 for the Poudre sand mix (solid line) and Ottawa sand (broken line).	67
6.6	Variation of $n+m$ with effective saturation, S_e for the Poudre sand mix and the Ottawa sand.	68
6.7	Unsaturated hydraulic conductivity for the Poudre sand mix (B-C)	69
6.8	Unsaturated hydraulic conductivity for the Ottawa sand (B-C)	70
6.9	Variation of $n+m$ with effective saturation, S_e using the Van Genuchten retention relationships.	71

<u>Figure</u>	<u>Description</u>	<u>Page</u>
6.10	Unsaturated hydraulic conductivity relationships for the Poudre sand mix (V-G).	72
6.11	Unsaturated hydraulic conductivity relationships for the Ottawa sand (V-G).	73

LIST OF SYMBOLS

Variable	Definition	Units
A	Cross sectional area of porous normal to the direction of bulk flow	cm ²
A _p	Total cross sectional area of liquid occupied pore space	cm ²
\bar{a}	Cross sectional area of a constricted single conduit model	cm ²
a	Cross sectional area of single conduit model	cm ²
a _p	Cross sectional area of pore space	cm ²
b	Tortuosity exponent	
B	Formation factor constant	
C	Solute concentration	g/cm ³
C _o	Initial solute concentration	g/cm ³
C _{ext}	Solute concentration of solution extracted from half-cell	g/cm ³
D	Fractal dimension of pore space	
D _o	Diffusion coefficient in liquid	cm ² /s
D _e	Effective diffusion coefficient in porous medium	cm ² /s
EC _b	Electrical conductivity of bulk porous medium	
EC _w	Electrical conductivity of liquid in porous medium	
F	Formation factor	
g	Acceleration due to gravity	cm/s ²
H	Total hydraulic head	cm
h _b	Air entry capillary pressure head	cm

Variable	Definition	Units
h_c	Capillary pressure head	cm
\bar{J}	Solute flux	g/s
$K(\theta)$	Hydraulic conductivity	cm/s
K_s	Saturated hydraulic conductivity	cm/s
$K_r(\theta)$	Relative hydraulic conductivity	
k_o	Shape factor	
l	Straight line length in the direction of bulk flow	cm
l_e	Length parallel to the average pore velocity	cm
l_o	Length measured from the center of the diffusion half-cell	cm
l	Pore tortuosity factor	
m	Pore constriction/tortuosity factor (dynamic)	
M	Van Genuchten retention characteristic parameter	
M_k	Hydraulic conductivity matching factor	
M_d	Mass of dry diffusion half-cell sample	g
M_w	Mass of wet diffusion half-cell sample	g
n	Pore constriction/tortuosity factor (static)	
n_p	Number of pore size classes	
N	Van Genuchten retention characteristic parameter	
N_i	Number of pores with radius less than R_i	
P_b	Air entry capillary pressure	mbar
P_c	Capillary pressure	mbar
Q	Volumetric liquid flow rate	cm ³ /s
q	Darcy flux	cm/s

Variable	Definition	Units
\bar{R}^2	Weighted mean value of the square of the hydraulic radius	cm ²
$\overline{R_e^2}$	Effective weighted mean value of the square of the hydraulic radius	cm ²
R_b	Resistance of bulk soil	ohm/cm
r	Pore radius	cm
r_e	Effective pore radius	cm
R	Pore radius	cm
R^2	Regression coefficient	
s	Pore radius	cm
S_e	Effective liquid saturation	
S	Liquid saturation	
S_r	Residual liquid saturation	
t	Time	
T	Tortuosity	
T_s	Tortuosity at saturation	
\bar{v}_p	Average pore velocity	cm/s
\bar{v}_s	Average pore velocity component parrallel to bulk flow	cm/s
V_p	Volume of liquid in pore space	cm ³
V_s	Volume of solution initially in half-cell cylinder	cm ³
V	Bulk volume of porous medium	cm ³
α	Van Genuchten retention characteristic parameter	cm ⁻¹
α_{ls}	Angle of liquid/solid contact	

Variable	Definition	Units
β	Constriction compensation factor	
λ	Brooks-Corey pore size distribution factor	
μ	Liquid viscosity	g/cm.s
θ	Volumetric liquid content	
θ_e	Volumetric liquid content effective in flow	
θ_r	Residual liquid content not contributing to the flow	
θ_s	Saturated liquid content	
ϕ	Porosity	
ϕ_e	Effective porosity	
ρ	Density of water	g/cm ³
ρ_o	Resistivity of bulk porous medium	ohm
ρ_w	Resistivity of water	ohm
σ_s	Standard deviation of saturation measurements	
σ_θ	Standard deviation of water content measurements	
ϕ	Matric potential	cm

CHAPTER 1

INTRODUCTION

Mathematical models have been used to estimate the conductivity of fluids in unsaturated porous media since the turn of the century. The more commonly used models are invariably based on conduit or channel flow of the fluid within the pore space and typically include two distinguishable aspects. The first is a description of the physics of the fluid flowing in the pore channels, and the second is a description of the distribution of the sizes of these channels. Paramount to the description of the physics of the fluid flow is some definition of the channel geometry that would include the channel size, shape or constrictivity, and tortuosity. The size distribution is generally derived from volume-based pore size distributions inferred from liquid retention measurements. The effects of the constrictivity and tortuosity of the flow paths are represented by the formation factor.

In general, the formation factor is described by a lumped parameter dependant only on the effective saturation. Formation factors in hydraulic conductivity models have been derived either by observations made from electrical conductivity or ion diffusion in porous media that are then transposed to the hydraulic conductivity model, or by comparison of a theoretical model with measured hydraulic conductivity data. Research into the properties of the porous media that affect the formation factor has not been forthcoming. The reasons for this shortcoming include the fact that:

- Experimental observation of the three fundamental characteristics of the porous media have seldom been made on the same material through a complete range of saturations (Mualem and Friedman, 1991). These three

characteristics are: the liquid retention or pore size distribution characteristic, the ion diffusion or electrical conductivity behavior, and the hydraulic conductivity characteristics.

- Formation factors observed from ion diffusion or electrical conductivity experiments where the fluid phase is static have been transposed into hydraulic models that represent a dynamic fluid (Dullien, 1992).
- No specific investigations have been concluded on the dependency of the formation factor on the pore space characteristics of porous media (Wyllie and Spangler, 1952; Lenhard *et al.*, 1991).

It is the hypothesis of this study that the channel geometry comprising the formation factor is material specific and not dependent only on the effective saturation. The purpose of this work is, therefore, as follows:

- To determine the properties of the material that contribute to the channel geometry. In particular, it is the focus of this study to determine the dependence of the channel geometry on the pore size distribution index and other properties defining the pore space.
- To develop a model to predict hydraulic conductivities based on these properties and compare its predictive capabilities using the results of laboratory tests.

In order to achieve these purposes the following tasks have been performed.

The literature describing the historic, common and recent models has been reviewed. These are briefly described with specific reference to the way in which the channel geometry is treated. The literature review includes a description of experimental evidence of the factors affecting the channel geometry. Also included in the literature review is an

assessment of the performance of common models based on the reporting of comparative studies.

A theory has been developed in the light of the approaches suggested in the literature, which includes the effects of material dependent parameters affecting the channel geometry. A series of laboratory tests have been performed to derive the parameters that are included in the model and to serve as a source of data to test the model's performance. Specifically, detailed water retention curves have been measured for two sandy porous media with significantly different pore size distributions. Half-cell diffusion tests have been conducted at a range of water contents, and the unsaturated hydraulic conductivity of these materials has been measured by a short column method.

The results of these tests have been used to derive the model parameters and assess the validity of the assumptions implicit in the model. A generalized formulation of hydraulic conductivity has been derived using the data of 24 different porous media extracted from the literature. A comparative analyses of other common models also has been conducted using the data derived in this study. The study concludes with a summary of the findings resulting from these tasks and presents recommendations for future study based on the results, observations and analyses in this study.

CHAPTER 2

LITERATURE REVIEW

The literature describing the development of mathematical models of unsaturated hydraulic conductivity and the parameters affecting these models is extensive. Consequently, the research reviewed in this study has been limited to those works that are most relevant to the focus of this investigation. Specifically, this review is confined firstly to the more prominent historic research that has led to commonly used methods of describing the unsaturated hydraulic conductivity. Where possible, the methods are grouped to clearly define the different approaches to developing the unsaturated hydraulic conductivity models. Secondly, more recent approaches are summarized where these are applicable to this present study. In addition, the scope of the whole review is restricted to a discussion of how the concepts of tortuosity, constrictivity and geometry of the pore liquid are visualized in the formation factor and subsequently integrated into models of porous media.

These concepts are typically found in research in two different aspects of pore liquid geometry. The first is the development of models to describe the unsaturated hydraulic conductivity of porous materials. The second is the development of models and relationships to describe the formation factor of porous media and their use in describing the electrical conductivity and solute diffusion in unsaturated porous media. Observations made from electrical conductivity and diffusion experimentation are transposed to describe the formation factors in hydraulic conductivity models. In addition to describing the concepts visualized in these different areas of research, this review will show that the physical properties of the porous media have not always been used consistently in developing models of the formation

factors from electrical conductivity and solute diffusion behaviour in the media. Also the review will show that the concepts developed in the research into electrical conductivity and solute diffusion have not been fully integrated into the development of unsaturated hydraulic conductivity models.

Two distinctive methods have been commonly used to describe the unsaturated hydraulic conductivity based on conduit flow. The first type of these methods are referred to as capillary model and the second as statistical models (Dullien 1992). In order to discuss the different approaches of conceptualizing the formation factor of the porous media, it is necessary to develop the general equations used to describe the hydraulic conductivity. The different techniques for representing the formation factor are then highlighted.

2.1 Capillary Models

Capillary models are derived from the Kozeny-Carman theory in which the porous medium consisting of a complex network of channels is considered to be a single conduit of complex shape but of constant average area as shown in Figure 2.1. In the developments that follow it is important to distinguish between the porous medium itself and the single conduit model of the medium.

2.1.1 Capillary Model Development

In the capillary model, the hydraulic radius concept of flow in a channel is assumed to hold, and thus, the average pore velocity, \bar{v}_p can be represented by a Hagen-Poiseuille equation

$$\bar{v}_p = \frac{\rho g}{k_o \mu} \bar{R}^2 \frac{dH}{d\ell_e} \quad 2.1$$

where \bar{R}^2 is a weighted mean value of the square of the hydraulic radius (Corey, 1986) and

is developed further later. $dH/d\ell_e$ is the hydraulic gradient along the average effective flow path represented by the single conduit model as shown in Figure 2.1. The factor k_o accounts for the average effective shape of the conduit. The other terms are defined in the list of symbols. The velocity, \bar{v}_s parallel to the direction of bulk flow is related to \bar{v}_p by

$$\bar{v}_s = \frac{\ell}{\ell_e} \bar{v}_p \quad 2.2$$

where ℓ is measured parallel to the direction of the net bulk flow.

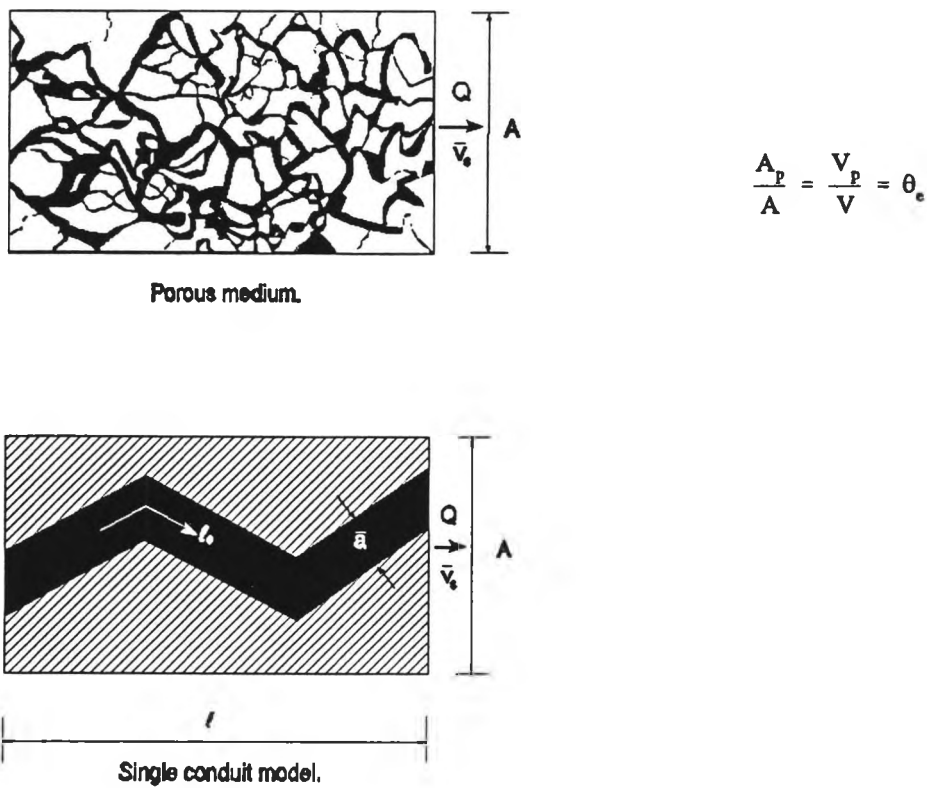


Figure 2.1. Schematic representation of the porous medium.

The velocity, \bar{v}_s can then be written as

$$\bar{v}_s = \frac{\rho g}{k_o \mu} \frac{\ell}{\ell_e} \bar{R}^2 \frac{dH}{d\ell_e} \quad 2.3$$

The pressure gradient can also be expressed as $\frac{\ell}{\ell_e} \frac{dH}{d\ell}$ and so

$$\bar{v}_s = \frac{\rho g}{\mu k_o} \left(\frac{\ell}{\ell_e} \right)^2 R^2 \frac{dH}{d\ell} \quad 2.4$$

The velocity, \bar{v}_s represents the average velocity of the combination of all the pores of the porous medium parallel to the direction of bulk flow. The volumetric flow rate, Q , can then be expressed as

$$Q = \bar{v}_s A_p \quad 2.5$$

where A_p is the combined area of the pores that contribute to the flow in the porous medium. The Darcy flux is the volumetric flow rate per unit area and is expressed as

$$\frac{Q}{A} = q = K \frac{dH}{d\ell} \quad 2.6$$

where A is the cross-sectional area of the bulk porous medium and K is the hydraulic conductivity that is dependent on the water content of the medium.

It is assumed that the amount of water effective in the flow process can be expressed as an area ratio as well as a volume ratio of the porous medium. That is,

$$\theta_e = \frac{A_p}{A} = \frac{V_p}{V} = \theta - \theta_r \quad 2.7$$

where V_p is the volume of liquid contributing to the flow, and V is the bulk volume of the porous medium, θ is the water content, and θ_r is the residual water content considered not to contribute to flow. θ_e is the effective water content in the flow process.

The unsaturated hydraulic conductivity can now be expressed as

$$K(\theta) = \theta_e \frac{\rho g}{\mu k_o} \left(\frac{\ell}{\ell_e} \right)^2 \overline{R^2} \quad 2.8$$

where the inverse of $\left(\frac{\ell}{\ell_e} \right)^2$ is normally referred to as the tortuosity, T , and so Equation 2.8

can be written as

$$K(\theta) = \theta_e \frac{\rho g}{\mu} \frac{1}{k_o T} \overline{R^2} \quad 2.9$$

This is a typical representation of the unsaturated hydraulic conductivity derived from capillary flow concepts and is expressed in different final forms by numerous authors (Carman, 1937; Purcell, 1949; Wyllie and Spangler, 1952; Laliberte *et al.*, 1966; Corey, 1986). The effective hydraulic radius term has been defined by Corey (1986) as the area weighted average of the square of the hydraulic radii of the individual channels making up the single tube conduit. The effective hydraulic radius term can thus be expressed as

$$\overline{R^2} = \frac{\int_0^{S_e} r^2 dS_e}{S_e} \quad 2.10$$

where r is the hydraulic radius of the individual channels. These radii can be determined using the Laplace equation,

$$r = \frac{\sigma \cos(\alpha_{ls})}{P_c} \quad 2.11$$

where σ is surface tension, α_{ls} is the angle of contact between liquid and porous material, and P_c is the capillary pressure. Inserting 2.10 and 2.11 into 2.9 and assuming $\alpha = 0$, yields,

$$K(\theta) = \phi_e \frac{\sigma^2 \rho g}{\mu} \frac{1}{k_o T} \int_0^{S_e} \frac{dS_e}{P_c^2} \quad 2.12$$

where ϕ_e is the effective porosity, $\theta_s - \theta_r$.

This form of the conductivity equation is commonly referred to as the Burdine equation as the form was originally developed by Burdine (1953). Various expressions have been formulated for the relationship between effective saturation and capillary pressure so that the integral in Equation 2.12 can be evaluated. Laliberte *et al.* (1966) used the Brooks-Corey relationship for effective saturation and capillary pressure,

$$S_e = \left(\frac{P_b}{P_c} \right)^\lambda \quad 2.13$$

and were able to simplify the expression for the hydraulic conductivity. The use of different relationships for representing the water retention characteristics in the hydraulic conductivity model is further examined in Chapter 5.

Dullien (1992) develops a relationship similar to Equation 2.9, except that the capillaries are assumed to consist of periodically repeating tube sections of different length and radii. Recognizing that the smallest diameter in the tube section sequence is likely to control the conductivity, the effective diameter of the single conduit model is estimated using an integral of a bivariate pore size distribution function incorporating a certain range of pore sizes close to the controlling throat diameter.

2.1.2 The Formation Factor in Capillary Models

Together with the type of capillary models described above has been the use of formation factors to determine the influence of the geometry of the pore liquid in the complex pore structure. Formation factors, therefore, represent the tortuous nature and the

periodic constrictivity of the flow paths. Relationships describing the variation of formation factor with saturation have either been deduced from $K(\theta)$ measurements or from independent observation of the diffusion of solutes or electrical conductivity in variably saturated porous media. Independent measurements of diffusion or electrical conductivity behavior requires some model of the pore structure so that the observations can be transferred to the hydraulic conductivity model. There are two shortfalls to this approach. First, the models are a 2-D representation of the 3-D pore structure, and in general, consider only the tortuous nature of the flow paths and not the effects of constrictivity. Second, the observations of diffusion or electrical conductivity are made with a static fluid system, whereas the fluid is in motion during measurements of hydraulic conductivity. The implications can be readily appreciated by observing that the diffusion or electrical conductivity processes are dependant on the net sectional area of flow paths, whereas the hydraulic conductivity is dependant on the number of individual flow paths that comprise the net area (Dullien, 1992).

The formation factor, F , has been used to represent the variation of the tortuosity, T , by

$$F = \frac{1}{T}$$

and is generally defined as

$$F = \frac{\text{Electrical conductance of the bulk porous medium}}{\text{Electrical conductance of the liquid}} = \frac{EC_s}{EC_w}$$

where EC_s is the electrical conductivity of the bulk soil with negligible matrix electrical conductivity.

In order to use the formation factor to derive the tortuosity ratio dependence, researchers have resorted to simplified models of the porous medium similar to that used in deriving the hydraulic conductivity equation. Inherent in the derivation of the tortuosity factor, however, is an assumption of the relationship between the net effective length of the

single conduit model of the porous medium and the water content of the medium itself. In the use of these simplified models, two conflicting approaches have been adopted.

The first, adopted by Cornell and Katz (1953); Perkins *et al.* (1956); and Rhoades (1976); among others, is illustrated by referring to Figure 2.2.

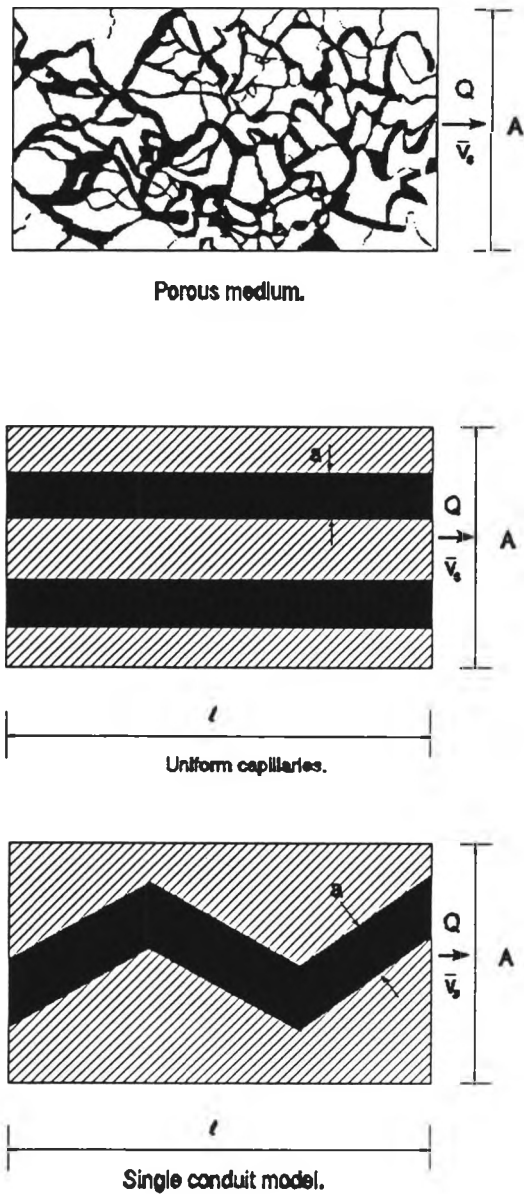


Figure 2.2. Schematic representation of a uniform capillary model.

In this approach, the porous medium is considered as a bundle of uniform capillaries. A single tortuous conduit of the same area, a , as a set number of the straight uniform capillaries is taken to represent the tortuosity of the porous medium. The single conduit is considered to have the same volumetric liquid content as the uniform capillary representation of the porous medium (Dullien, 1992). In the illustration shown, the number of uniform capillaries is two and so the single conduit's effective length, ℓ_e , must be twice the straight line length of the capillaries.

Deriving the tortuosity in terms of the effective diffusion coefficient, an expression for the diffusive flux through the single conduit, \bar{J} , is written as

$$\bar{J} = D_o a \frac{\partial C}{\partial \ell_e} \quad 2.14$$

where D_o is the bulk diffusion coefficient of the diffusing solute, and C is the mass of the solute per unit volume of liquid. Writing the concentration gradient in the direction parallel to the bulk diffusion yields

$$\bar{J} = D_o a \frac{\ell}{\ell_e} \frac{\partial C}{\partial \ell} \quad 2.15$$

The flux, \bar{J} , in these developments is taken to be parallel to the bulk diffusion transport. The area, a , of the conduit is related to the liquid content, θ , by

$$\frac{a \ell_e}{A \ell} = \theta \quad 2.16$$

and so Equation 2.15 can be written as

$$\bar{J} = D_o A \theta \left(\frac{\ell}{\ell_e} \right)^2 \frac{\partial C}{\partial \ell} \quad 2.17$$

Applying this diffusion flux in a mass balance of a transient diffusion experiment yields

$$\theta \frac{\partial C}{\partial t} = D_o \theta \left(\frac{\ell}{\ell_e} \right)^2 \frac{\partial^2 C}{\partial \ell^2} \quad 2.18$$

or

$$\frac{\partial C}{\partial t} = D_o \left(\frac{\ell}{\ell_e} \right)^2 \frac{\partial^2 C}{\partial \ell^2} \quad 2.19$$

If an effective diffusion coefficient, D_e , describes the flux per unit bulk area of porous medium, it can be written as

$$D_e = D_o \left(\frac{\ell}{\ell_e} \right)^2 \quad 2.20$$

then Equation 2.19 can be written as

$$\frac{\partial C}{\partial t} = D_e \frac{\partial^2 C}{\partial \ell^2} \quad 2.21$$

The ratio of these effective diffusion coefficients to the liquid diffusion coefficient has been applied to transient experiments and shown to yield (Porter *et al.*, 1960)

$$\frac{D_e}{D_o} = B\theta \quad 2.22$$

where B is a constant.

The tortuosity term is thus reported to be related to the liquid content by

$$\left(\frac{\ell}{\ell_e} \right)^2 = B\theta \quad 2.23$$

A similar development is presented by researchers using the electrical conductivity (Cornell and Katz, 1953; Rhoades *et al.*, 1976). Here, the resistance of the bulk soil, R_b , is represented by

$$R_b = \rho_b \frac{\ell}{A} \quad 2.24$$

where ρ_b is the resistivity of the porous medium.

Since only the liquid part of the medium is available for current flow and the average length of flow is increased to ℓ_c in the single conduit model, the resistance of the medium is

$$R_b = \rho_w \frac{\ell_c}{a} \quad 2.25$$

where ρ_w is the resistivity of the liquid.

Thus,

$$R_b = \rho_w \left(\frac{\ell_c}{a} \right) = \rho_o \left(\frac{\ell}{A} \right) \quad 2.26$$

and the formation factor, F , defined earlier can be written as

$$\frac{1}{F} = \frac{\rho_o}{\rho_w} = \frac{\ell_c}{a} \frac{A}{\ell} \quad 2.27$$

Since $\frac{a \ell_c}{A \ell}$ is defined as the liquid content, θ , the formation factor can be written

as

$$\frac{1}{F} = \left(\frac{\ell_c}{\ell} \right)^2 \frac{1}{\theta} \quad 2.28$$

which can be written in terms of electrical conductivity as

$$\frac{EC_b}{EC_w} = \left(\frac{\ell}{\ell_c} \right)^2 \theta \quad 2.29$$

where EC_b and EC_w are the electrical conductivity of the bulk soil and of the liquid,

respectively. Observations of $\frac{EC_b}{EC_w}$ yield

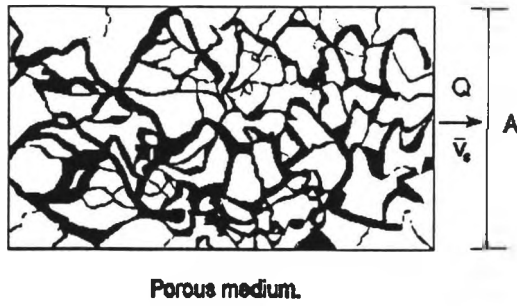
$$\frac{EC_b}{EC_w} = B\theta^2 \quad 2.30$$

and thus the tortuosity defined in this way is again represented by

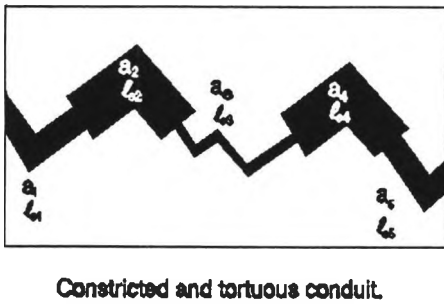
$$\left(\frac{\ell}{\ell_c} \right)^2 = B\theta \quad 2.31$$

Cornell and Katz (1953) have applied this formulation of the tortuosity to the hydraulic conductivity equation. It must be noted, however, that their resulting analyses show a large variation in the shape factor.

A different approach to deriving the tortuosity has been presented by Wyllie and Spangler (1952) and also is used for the diffusion case by Klute and Letey (1958). In this approach, the restriction conduit model with the same volumetric liquid content as the porous medium is not adopted. Since the single conduit model represents the average effective length of the complex conduits of the porous medium, it is not necessary that $\frac{a \ell_c}{A \ell}$ represent



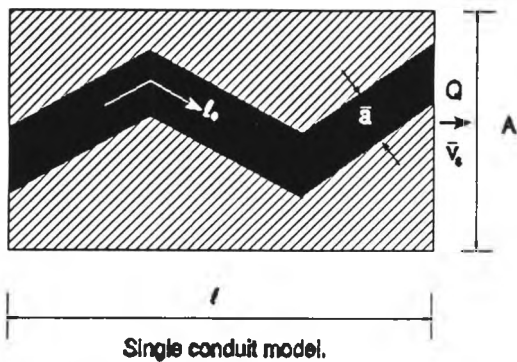
the volumetric water content of the porous medium. In their development Wyllie and Spangler (1952) imply a model such as that represented in Figure 2.3. Proceeding as before with an electrical analogy, the resistance of the bulk soil would be



$$R_b = \rho_o \frac{l}{A} = \rho_w \frac{l_e}{a} \quad 2.32$$

where \bar{a} is now the area of the fictitious single conduit. The formation factor is thus

$$\frac{1}{F} = \frac{\rho_o}{\rho_w} = \left(\frac{l_e}{l} \right) \frac{A}{\bar{a}}$$



Wyllie and Spangler (1952) have defined \bar{a} as

$$\frac{\bar{a}}{A} = \theta \quad 2.33$$

This can be explained by considering the constricted nature of the conduit that models the porous medium as shown in Figure 2.3. In this case, the liquid content would be represented by

Figure 2.3. Schematic representation of a constricted capillary model.

$$\theta = \frac{a_1 l_{e1} + a_2 l_{e2} + a_3 l_{e3} + a_4 l_{e4}}{A l} \quad 2.34$$

The average area, \bar{a} , of the single conduit envisaged would be a weighted average represented by

$$\bar{a} = \frac{\sum_{i=1}^5 a_i \ell_{e_i}}{\ell} \quad . \quad 2.35$$

The formation factor defined is

$$\frac{1}{F} = \frac{\rho_o}{\rho_w} = \left(\frac{\ell_c}{\ell} \right) \frac{1}{\theta} \quad 2.36$$

which is fundamentally different from Equation 2.28. The formation factor can be written in terms of electrical conductivity as

$$\frac{EC_b}{EC_w} = \left(\frac{\ell}{\ell_c} \right) \theta \quad . \quad 2.37$$

Again, experimental observations yield $\frac{EC_b}{EC_w} = B\theta^2$ and so the tortuosity would be

$$\left(\frac{\ell}{\ell_c} \right)^2 = B^2 \theta^2 \quad 2.38$$

which has been adopted by Wyllie and Spangler (1952), Burdine (1953), and Brooks and Corey (1964). It can be seen that this tortuosity term is an order of magnitude of the water content different than that derived in Equation 2.31. It is obvious from the above discussion that the formation factor is dependent on both the tortuous nature of the conduits as well as the constrictivity. It also is evident that adopting a simplified representation of the pore geometry can result in remarkably different representations of the tortuosity and constrictivity.

Indeed, recognizing the difficulty in separating the effects of tortuosity from those of constrictivity, Arah and Ball (1994) have developed a model in which tortuosity is ignored but a functional model is developed in which the pore space is represented as a combination of arterial, marginal and remote channels. The observable results were adequately modelled without a specific representation of tortuosity. Hence, by dividing the pores into different classes, the model was functionally equivalent to the introduction of a tortuosity factor to represent pore convolution.

In analyzing unsaturated relative hydraulic conductivity measurements, Wyllie and Spangler (1953) have reported the exponent of the water content (strictly effective saturation), represented by n in Equation 2.38, to vary from 0.8 to 3.1, which is a significant variation. These authors reflect on the possibility of the pore size distribution affecting this exponent but no specific study has been made in this regard heretofore. The relationship between the exponent and the pore size distribution is, therefore, a primary focus of this present study.

Bear (1972) has expressed the formation factor as a function of tortuosity, T , and porosity, ϕ ,

$$F = C(T)\phi^{-m} \quad 2.39$$

where $C(T)$ is some function of the tortuosity and m is the number of reductions in pore opening sizes or closed-off channels. Bear (1972) reports values of m varying from 1 to 2.

Constrictivity is introduced in the development of the hydraulic conductivity function in statistical models known as "cut and random rejoin" models. The development of this type of model is briefly presented next.

2.2 Statistical Models

Like the capillary models, the statistical models also invoke the Hagen-Poiseuille equation at a single pore scale. The models also characterize the pores by a pore radius, the size distribution which are inferred from the water retention characteristic. The distinguishing feature of statistical models, as grouped in this review, is that the effect of the random variation of pore size on the hydraulic conductivity is modelled using probability theory.

2.2.1 Statistical Model Development

Childs and Collis-George (1950) considered the soil column to be sectioned normal to the direction of flow and the sliced faces to be randomly rejoined. They defined the probability of pores of radius, r , in one face to be connected to pores of radius, ρ , in the other as

$$P(r,\rho) = f(r) f(\rho) dr d\rho \quad . \quad 2.40$$

Assuming that the resistance to flow is dependent only on the smaller of the two interconnected pores and that there is only one connection between the pores, Childs and Collis-George (1950) applied 2.40 to the Hagen-Poiseuille equation to yield,

$$d\bar{q} = M P(r,\rho) \rho^2 \nabla\phi \quad 2.41$$

where ρ is the smaller radius, M is a constant depending on pore geometry and fluid properties and $\nabla\phi$ is the potential gradient. Integrating 2.41 and invoking Darcy's law yields,

$$\begin{aligned}
K(\theta) = & M \int_{\rho=R_{\min}}^{\rho=R(\theta)} \int_{r=\rho}^{r=R(\theta)} \rho^2 f(\rho) f(r) dr d\rho \\
& + M \int_{\rho=R_{\min}}^{\rho=R(\theta)} \int_{r=R_{\min}}^{r=\rho} r^2 f(r) f(\rho) d\rho dr .
\end{aligned} \tag{2.42}$$

Computation of the unsaturated hydraulic conductivity has been found to be considerably improved when the matching factor is derived from a correlation between the measured and estimated hydraulic conductivity. Hence, equations for the unsaturated hydraulic conductivity are expressed as relative to the saturated hydraulic conductivity. Mualem (1986) has presented an analytical solution to Equation 2.42 in terms of the relative hydraulic conductivity as

$$K_r(\theta) = \left[\frac{\int_0^\theta \frac{(\theta - \vartheta) d\vartheta}{\varphi^2}}{\int_0^{\theta_{\text{sat}}} \frac{(\theta_{\text{sat}} - \vartheta) d\vartheta}{\varphi^2}} \right] \tag{2.43}$$

where ϑ is a dummy variable of integration representing the effective water content as a function of φ .

Mualem (1976) conceptualized a model similar to that of Childs and Collis-George, but included a correction factor to account for partial correlation between the two pore radii at either face of a thin slab of porous media. The probability of the pore domain characterized by (r, ρ) is now

$$P(r, \rho) = G(R, r, \rho) f(r) f(\rho) dr d\rho \tag{2.44}$$

where $G(R, r, \rho)$ is a correction factor accounting for the partial correlation of the pores at a given water content, $R(\theta)$. Assuming that there is no bypass between the pores and that the

pore configuration can be replaced by a pair of capillary elements whose lengths are proportional to their radii as

$$\frac{\ell_1}{\ell_2} = \frac{r}{\rho} \quad . \quad 2.45$$

The hydraulic conductivity of the sequel is then found proportional to $r_c^2 = r\rho$. A tortuosity factor, $T(R,r,\rho)$, was also included in the model, and since there is no mechanism to estimate $T(R,r,\rho)$ and $G(R,r,\rho)$ independently, Mualem (1976) assumed both to be a power function of the effective saturation. These assumptions yield

$$K_r(\theta) = S_e^l \left[\frac{\int_0^\theta \frac{d\theta}{\phi}}{\int_0^{\theta_{sat}} \frac{d\theta}{\phi}} \right]^2 \quad . \quad 2.46$$

Although some of the effects of constricted pathways have been included in the formation of the statistical models, it is nevertheless instructive to examine the effective saturation expression that can be considered a part of the formation factor in these models.

2.2.2 The Formation Factor in Statistical Models

Millington and Quirk (1960) have taken account of the effective area for flow by considering the interaction of pores as in the Childs and Collis-George model. However, Millington and Quirk (1960) assume a most probable area of interaction lying between a maximum and minimum pore area, resulting in an expression for the hydraulic conductivity as Equation 2.43 multiplied by a correction factor, S_e^l . The assumptions invoked by these authors result in the exponent, l being $4/3$.

Mualem (1976) compared the expression for unsaturated hydraulic conductivity presented in Equation 2.46 against the measured data of 45 soils and determined an optimum value for the exponent of S_e to be 1/2. This model provided an improved representation of measured values; however, these results and those of other studies indicate that there is no single model that suits every soil (Mualem, 1986). It is worthwhile examining the results of selected studies that comment on the variation of the parameters making up the hydraulic conductivity function, especially those which represent the formation factor. A brief review of these studies is presented in the next section.

2.3 Evaluation of Hydraulic Conductivity Models

A general form of the relative hydraulic conductivity has been developed by Mualem and Dagan (1978) by recognizing that the differences between certain models stem from differences in the conceptualization of the effective pore radius and the effective flow area. The generalized expression can be evaluated making different assumptions about the pore interaction and tortuosity effects to yield three fundamental formulae. These are

$$K_r(\theta) = S_e^l \left[\frac{\int_0^\theta \frac{(\theta - \theta') d\theta'}{\phi^{2+b}}}{\int_0^{\theta_{sat}} \frac{(\theta_{sat} - \theta') d\theta'}{\phi^{2+b}}} \right] \quad 2.47$$

that can be recognized as the generalized Childs and Collis-George model,

$$K_r(\theta) = S_e^l \left[\frac{\int_0^\theta \frac{d\theta'}{\phi^{2+b}}}{\int_0^{\theta_{sat}} \frac{d\theta'}{\phi^{2+b}}} \right] \quad 2.48$$

that is the generalized Burdine model and

$$K_r(\theta) = S_e^l \left[\frac{\int_0^\theta \frac{d\theta}{\phi^{1+b}}}{\int_0^{\theta_{sat}} \frac{d\theta}{\phi^{1+b}}} \right]^2 \quad 2.49$$

that is the generalized Mualem model. Based on the development of the statistical models, the parameter b is often referred to as the tortuosity factor, and l is referred to as the pore interaction parameter although many studies refer to l as the tortuosity factor. Various forms of these expressions have been studied by different authors and have often been derived from first principles with significantly different assumptions concerning the formation factor.

Alexander and Skaggs (1986) have assumed the tortuosity term is related to both the size of pore conducting liquid at the prevalent water content as well as to the saturation as

$$T = C \left(\frac{r}{S} \right)^{\frac{1}{2}} \quad 2.50$$

where C is a constant. Applying this model of the formation factor to the Burdine model as expressed in Equation 2.12 results in the expression Equation 2.48 in which $b = -1$ and $l = 1$. This model was compared to the measured data of 23 soils and found to perform well for sandy and clayey soils. Mishra and Parker, assumed a tortuosity factor $T = 2.5$ and developed the Mualem equation to obtain an expression for the saturated hydraulic conductivity. Applying the Van Genuchten retention function to the hydraulic conductivity model yields

$$K_s = C(\theta_s - \theta_r)^{5/2} \alpha^2 \quad 2.51$$

where C is a constant. The measured saturated hydraulic conductivities of 48 soils were predicted within an order of magnitude that indicates the strong influence of the effective porosity in the hydraulic conductivity.

The interdependence of the parameters in the models also is evident from evaluation with measured data. Stephens and Rehfeldt (1985) examine the sensitivity of the standard Burdine model ($b = 0$ and $l = 2$ in Equation 2.48) to the estimated residual water content, θ_r , while holding the b and l parameters at the standard values and optimizing the Van Genuchten retention characteristic parameters. Predicted hydraulic conductivities were found to vary by an order of magnitude from those measured, depending on the choice of θ_r . A similar observation was made by Lenhard *et al.* (1991) in studying two-phase flow. These authors report that simulations of the hydraulic conductivity were substantially affected by assuming θ_r of the wetting phase to be zero, but that the effects could be counteracted by invoking a tortuosity factor that diminishes more severely with decreasing water saturation. The model they adopt is equivalent to Equation 2.49 with $b=0$ but with $l = 2$ instead of 0.5 as predicted by Mualem. The authors also speculate on the factor, l , being a function of the pore size distribution index, confirming Wyllie and Spangler's (1952) suspicions.

The study of the dependence of the factor, l , on other more easily observable soil characteristics has been attempted by Schuh and Cline (1990) and by Vereecken (1995). The factor, l , is compared with the particle size fractions, bulk density, organic carbon, Van Genuchten retention characteristic parameters and the total energy of drainage by Schuh and Cline (1990) using 69 data sets. These authors find no trend in l with any of the parameters tested but observe a change in the variability of l for soils with geometric mean particle diameter (G_d) greater than 0.08 mm. For the silty and sandy soils with G_d greater than 0.08 mm, the values of l were significantly less variable than those for clayey soils with G_d less than 0.08 mm. The values of l that were optimized to the data using the Mualem model were

found to vary between a minimum of -8.73 to a maximum of 14.8, but the l parameter data exhibited a geometric mean of 0.63, close to the value of 0.5 predicted by Mualem. Vereecken (1995) permitted optimization of both l and b in evaluating the three models represented in Equations 2.47 to 2.49 against 44 measured hydraulic conductivity data. The Van Genuchten relation was used to describe the measured retention data and simultaneous optimization of retention and hydraulic conductivity data was performed. The optimized l and b values were correlated against textural properties, organic carbon, bulk density and saturated hydraulic conductivity. No acceptable description of the measured data could be obtained from these correlations. However, the parameter l appeared to be more closely associated with textural classes of the soil, while the parameter b was preferably correlated to bulk density and saturated hydraulic conductivity, and thus more related to the structural state of the soil.

The Burdine and Mualem models have been studied by selective optimization of the parameters using large data sets (Van Genuchten and Nielsen, 1985; Yates *et al.*, 1992). The hydraulic conductivity and retention data of 36 measurements on 23 soils were examined by Yates *et al.* (1992). These authors conclude that using parameters optimized on the retention data alone to predict hydraulic conductivity data yields inaccurate comparisons, even when the parameter, l , is permitted to be optimized when predicting the hydraulic conductivity data. Simultaneous optimization of parameters using both retention and conductivity data yields reliable predictions. The parameter, l , however, was found to vary between -5 and 371. The authors offer no explanation for this large variation.

It is clear, therefore, that an examination of the factors affecting the tortuosity and pore interaction in fluid flow would be of value. A simple functional form for the hydraulic conductivity and diffusion in a porous medium that would permit such an examination are developed in Chapter 3. It is expedient, however, to list some additional functional forms for

modelling hydraulic conductivity before the theoretical analysis is attempted. These may give an indication of the parameters affecting the formation factor.

2.4 Other Functional Forms of Hydraulic Conductivity

Fractal analyses have been used to model porous media and develop hydraulic conductivity functions. Rawls *et al.* (1993) model the saturated hydraulic conductivity of a soil with macropore structure as

$$K_s = 4.41 \times 10^{-7} \left(\frac{\phi_m^l}{n_p^2} \right) R_1^2 \quad 2.52$$

where R_1 is the largest pore equivalent for the Sierpinski carpet and is given as

$$R_1 = \frac{0.148}{h_b} \quad 2.53$$

where h_b is the geometric mean bubbling pressure head. The total number of pore size classes, n_p , is given by

$$n_p = -5.7 + 77.0R_1 \quad 2.54$$

and the macropore areal porosity, ϕ_m , is given by

$$\phi_m = \left(\frac{\pi}{1.08 \times 10^4} \right) \left(\frac{D}{2 - D} \right) N_i R_i^2 \quad 2.55$$

where D is the fractal dimension of porosity and N_i is the number of pores with radius less than R_i .

Wong *et al.* (1984) model the electrical conductivity of a saturated porous medium by a random resistance network in which the porosity is varied by a random bond-shrinkage mechanism. They develop the expression for Archie's law as

$$\frac{EC_b}{EC_w} = B\phi^n \quad 2.56$$

and find by analytical development, that the exponent, n , is related to pore size distribution of the medium. Applying the same model to fluid hydraulic conductivity yields

$$K \propto \phi^{n'} \quad 2.57$$

where n' is shown to be greater than n . This indicates that the hydraulic conductivity is more strongly dependent on the tube size fluctuations than the electrical conductivity. It is speculated, therefore, that the formation factors observed from static electrical conductivity or diffusion measurements may not be appropriate for unaltered inclusion in dynamic hydraulic conductivity models.

Models developed using percolation and effective medium theory reveal a strong dependence of the saturated hydraulic conductivity on a characteristic pore size and effective porosity (Katz and Thompson, 1987; Doyen, 1988). The saturated hydraulic conductivity and formation factor are represented, respectively, by Katz and Thompson (1987) as

$$K_s = D r_h^2 \frac{EC}{EC_w} \quad 2.58$$

and

$$\frac{EC_b}{EC_w} = E \phi \frac{r_c}{r_h} S(r_{max}) \quad 2.59$$

where r_h , r_e and r_{max} are determined from the pore size distribution and D and E are constants. Swansen (1981) also presents an analysis using a pressure and porosity ratio to determine saturated hydraulic conductivities.

CHAPTER 3

THEORETICAL DEVELOPMENT

The theoretical development presented here models the unsaturated hydraulic conductivity as well as the solute diffusion process using the same general assumptions of pore topology for the hydraulic flow as well as for the solute flux. The parameters influencing these processes will be evaluated using the diffusion data and then used to formulate a formation factor for the hydraulic conductivity. It is hypothesized that the parameters influencing the solute diffusion process can be used to successfully determine the hydraulic conductivity and that these parameters are related to the pore size distribution.

3.1 Unsaturated Hydraulic Conductivity

The development of the unsaturated hydraulic conductivity proceeds assuming a single conduit channel represents the porous medium (as in Figure 2.3). Accounting for the tortuous nature of the flow as in Equations 2.1 to 2.4, the fluid velocity parallel to the bulk direction of the flow is

$$\bar{v}_s = \frac{\rho g}{\mu k_o} \left(\frac{\ell}{\ell_e} \right)^2 \bar{R}_e^2 \frac{dH}{d\ell} \quad 3.1$$

where \bar{R}_e^2 is the effective square of the hydraulic radius.

It is assumed that the tortuosity ratio is dependant on the water content as

$$\left(\frac{\ell}{\ell_c}\right)^2 = B \theta_c^n \quad 3.2$$

where B and n are parameters dependent on the pore size distribution and properties of the porous media to be examined in Chapter 5.

It is also assumed that the constricted nature of the flow reduces the effective square of the hydraulic radius so that

$$\overline{R_c^2} = \theta_c^m \overline{R^2} \quad 3.3$$

where $1 \leq m \leq 2$ determines the way the pore is constricted and divided into adjoining pores.

The velocity in the pore channel can now be expressed as

$$\overline{v_s} = \frac{\rho g}{k_o \mu} B \theta_c^{n+m} \overline{R^2} \frac{dH}{d\ell} \quad 3.4$$

and with the ratio of the area of flow to the bulk area equal to the water content of the porous medium, the flux can be written as

$$q = \frac{\rho g}{k_o \mu} B \theta_c^{n+m+1} \overline{R^2} \frac{dH}{d\ell} \quad 3.5$$

The unsaturated hydraulic conductivity can now be expressed as

$$K(\theta) = \frac{\rho g}{k_o \mu} B \theta_c^{n+m+1} \overline{R^2} \quad 3.6$$

The hydraulic radius term is expressed as the area weighted average of the square of the hydraulic radii making up the channel or

$$\overline{R^2} = \frac{\sigma^2 \cos^2 \alpha}{S_e} \int_0^{s_e} \frac{dS_e}{P_c^2(\theta)} \quad 3.7$$

The angle of contact, α is taken to be 0 so that the unsaturated hydraulic conductivity is

$$K(\theta) = \phi_e \frac{\rho g \sigma^2}{k_o \mu} B \theta_e^{n+m} \int_0^{s_e} \frac{dS_e}{P_c^2(\theta)} \quad 3.8$$

The special case of $m=n=1$ yields the Burdine equation.

3.2 Solute Diffusion

The flux of solute is dependent on the tortuous nature of the porous medium as is the hydraulic velocity. Without making assumptions about the relation between the effective length ratio of the single tube model and the volume of the liquid in the porous medium, the solute flux in the direction of the bulk transport is expressed similarly to the hydraulic velocity by accounting for the gradient of the concentration and for the component of the flux in the direction of the bulk transport. The flux can thus be written as

$$\overline{J} = a_p \left(\frac{\ell}{\ell_e} \right)^2 D_o \frac{\partial C}{\partial \ell} \quad 3.9$$

The same dependency of the tortuosity is used as in the hydraulic case and it is assumed that the area of solute transport is identical to that of the hydraulic flow. The flux per unit bulk area of the porous medium can now be written as

$$\frac{\overline{J}}{A} = \theta^{n+1} D_o \frac{\partial C}{\partial \ell} \quad 3.10$$

Writing an expression for the mass balance of the solute transport yields

$$\frac{\partial C}{\partial t} = B \theta^n D_o \frac{\partial^2 C}{\partial \ell^2} \quad 3.11$$

and defining an effective diffusion coefficient as

$$D_e = B \theta^n D_o \quad 3.12$$

the mass balance can be written as

$$\frac{\partial C}{\partial t} = D_e \frac{\partial^2 C}{\partial \ell^2} \quad 3.13$$

Solving the mass balance for the concentration along a column comprising two halves that have been joined at time, $t = 0$, where the one half is initially at a solute concentration $C=C_o$ and the other half at $C=0$, yields

$$\frac{C}{C_o} = \frac{1}{2} \operatorname{erfc} \left(\frac{\ell}{2\sqrt{D_e t}} \right) \quad 3.14$$

for a semi-infinite column, and

$$\frac{C}{C_o} = \frac{\ell_o}{L} + \frac{2}{\pi} \sum_{n=1}^{\infty} \frac{1}{n} \exp \left(-\frac{n^2 \pi^2 D_e t}{L^2} \right) \cos \left(\frac{n \pi \ell_o}{L} \right) \sin \left(\frac{n \pi \ell}{L} \right) \quad 3.15$$

for a finite column where ℓ is measured from the end of the column and ℓ_o from the center. The semi-infinite solution is used if the solute has not reached the end of the column and the finite solution if it has. Fitting the solutions to the data from the half cell tests yield the ratio

$$\frac{D_e}{D_o} = B \theta^n \quad . \quad 3.16$$

It can be seen that the exponent describing the formation factor of the diffusion model is different from that describing the hydraulic conductivity formation factor. The water retention characteristics, the diffusion profiles and the unsaturated hydraulic conductivity measurements will be used in Chapter 6 to determine the factors affecting the parameters B, n and m in Equations 3.8 and 3.16. The porous media and the testing procedures are described next.

CHAPTER 4

METHODOLOGY

Three sets of laboratory experiments were conducted to yield data that could be used to determine the pore size distribution, formation factor and unsaturated hydraulic conductivities. These were comprised of a set of detailed water retention measurements, a set of half-cell diffusion tests at various water contents and a set of short column unsaturated hydraulic conductivity measurements. These tests were performed for two different porous media that exhibited a distinctive difference in pore size distribution.

4.1 Materials

Two porous media were chosen that have significantly different pore size distributions. The first medium was made up of a predetermined mix of different size fractions of Poudre sand. The sand medium was prepared by first separating the size fractions of the Poudre sand by wet sieving. Then a predetermined mass of each fraction was mixed together to yield the sand medium that was named Poudre sand mix. No clay fraction was included in the mix. The sand mix was used in this study because it proved to yield a wide pore size distribution as well as conveniently high permeability. The implications of this will be seen in the analysis in Chapter 6.

The second porous medium was a silica sand with a very narrow particle size distribution. This material is known as Ottawa sand, Flintshot 1.8, and was used without

modification. The particle size distribution curves are shown for the two materials in Figure 4.1.

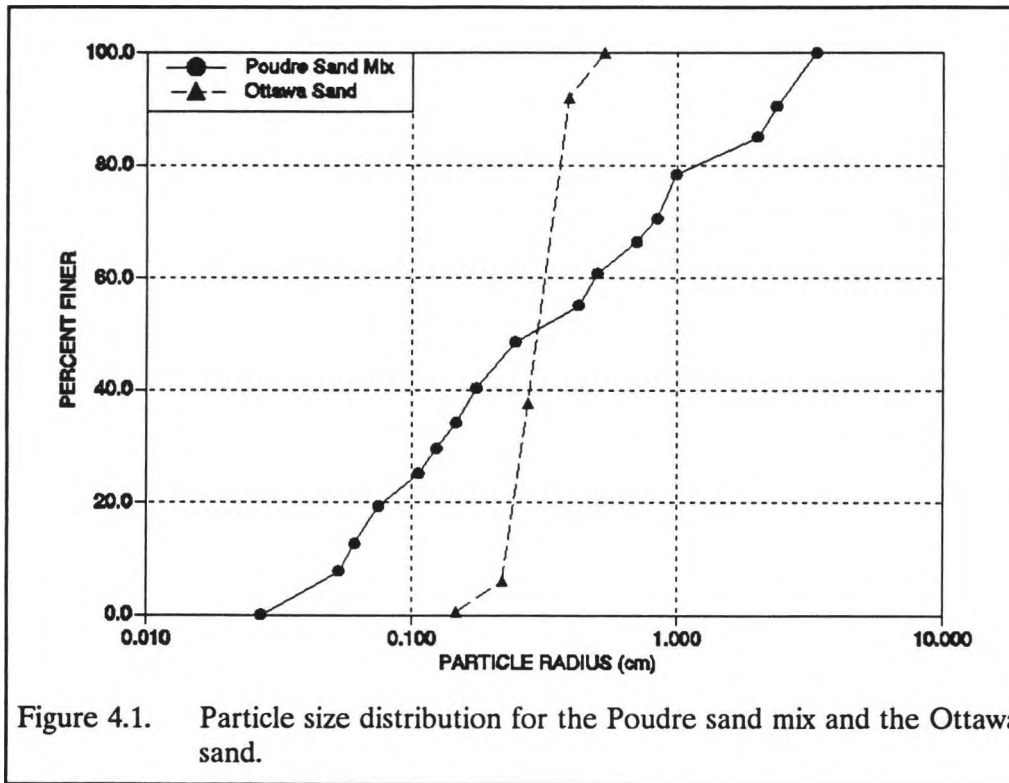
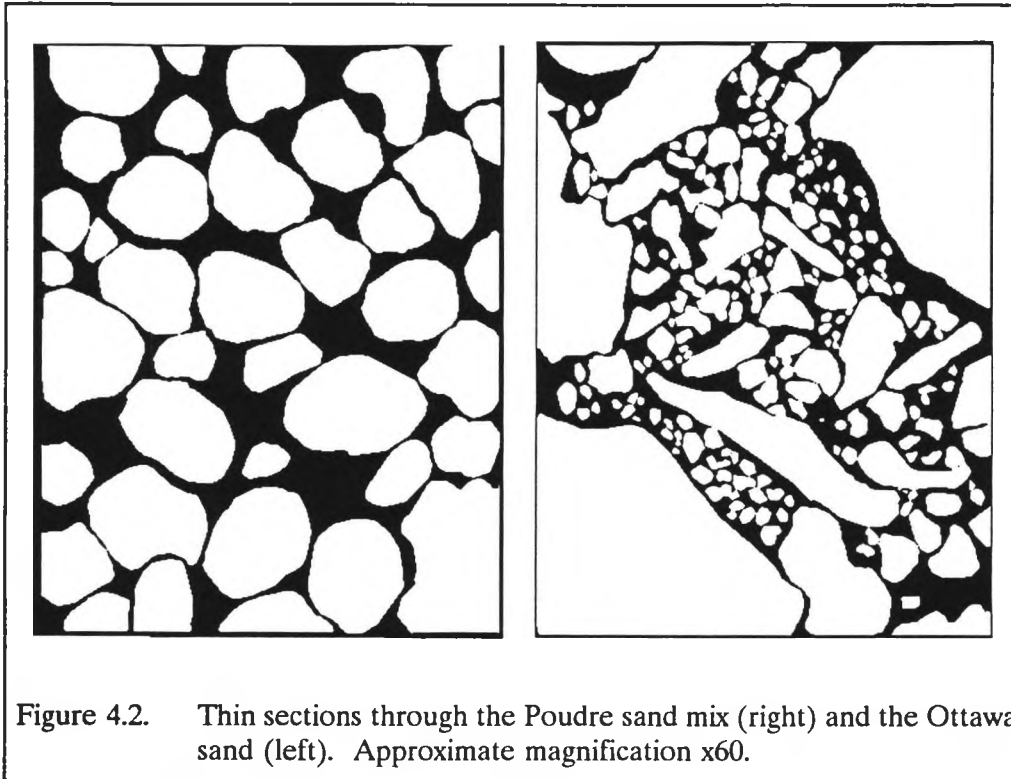


Figure 4.1. Particle size distribution for the Poudre sand mix and the Ottawa sand.

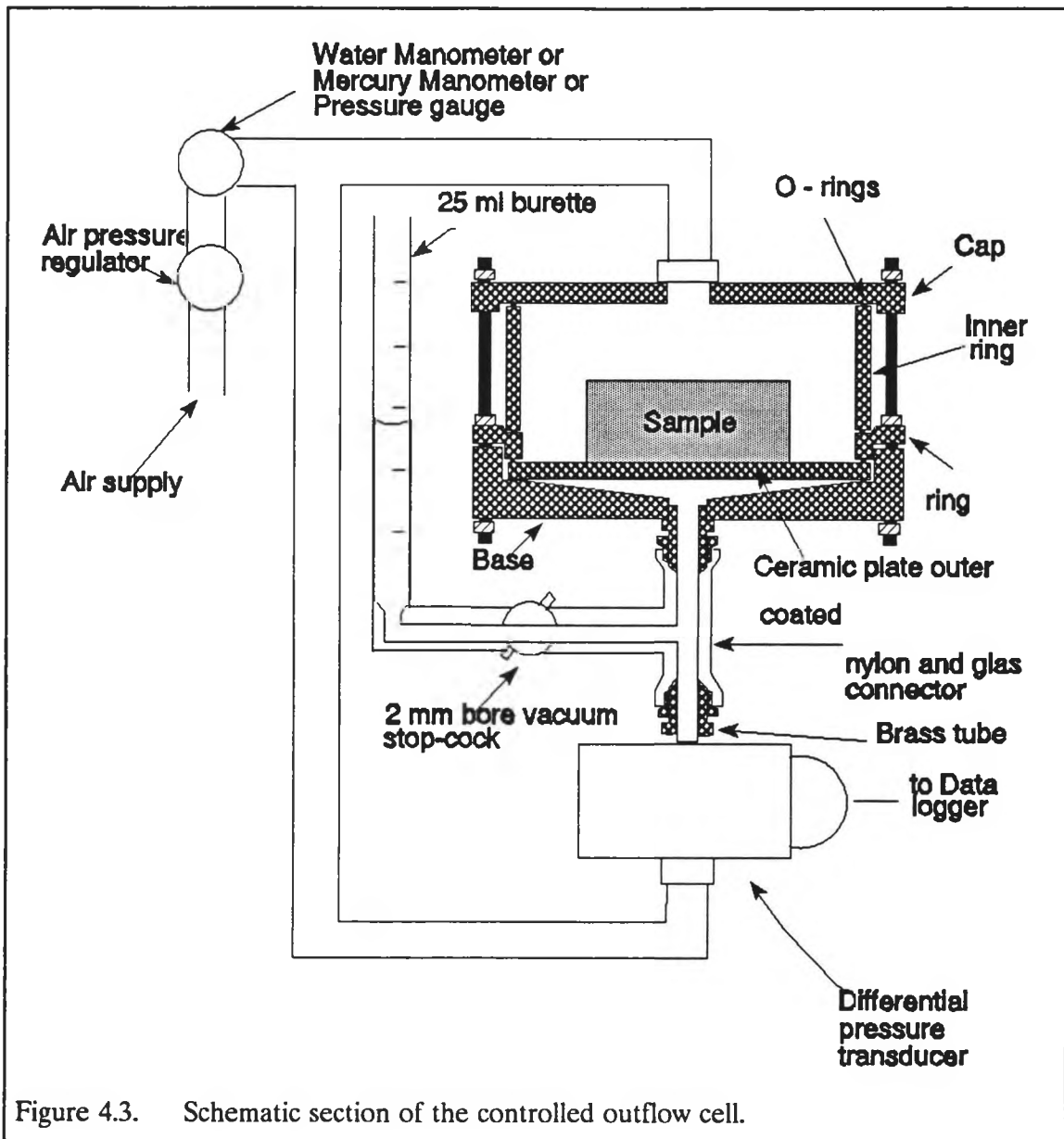
The porous media were prepared in the laboratory by packing the sands in the air-dry state to yield homogeneous packing and similar bulk densities for all the porous media samples for each of the three sets of measurement. The sands were first thoroughly mixed in a container and then poured through a 50 cm long packing tube via a funnel with a 7 mm diameter outflow restriction. Two wire mesh screens at the base of the packing tube serve to further disperse the falling sand particles. Cross sections of the packing geometry of the grains and the particle shapes are shown in Figure 4.2. The sections were prepared by drawing a dyed epoxy into a prepared sample, allowing the epoxy to set, and cutting a thin section of the sample. The section was then polished and photographed using a microscope.



4.2 Water Retention Characteristic

In order to clearly define the pore size distribution, an accurate and detailed water retention curve was measured for each material. The method used to measure these curves was the controlled outflow method and the apparatus was named the controlled outflow cell.

The controlled outflow cell is shown schematically in Figure 4.3. The main components are the base, a retaining ring, an inner ring that houses the sample, the cap and the outflow burette, and T-piece. The materials used in constructing the components are aluminum, brass and glass with rubber O-rings to seal mating surfaces. These materials were chosen to minimize the diffusion of water vapor out of the cell.



The retaining ring clamps a porous stainless steel plate between O-rings in the base and in the retaining ring. The porous plate is machined on its outside edges and sides to form an impervious surface to seal against the O-rings. A reservoir of water is maintained below the porous plate in the base. The water is continuous from the porous plate into the burette and "wet port" of the transducer.

The cap clamps the inner ring to the retaining ring and seals the compartment where the sample rests on the porous plate. The outflow assembly and T-piece are made up of a 25 ml burette, a vacuum stopcock, glass capillary tubing, two Number 7 Ace Glass connectors, and two machined brass fittings. The vertical glass piece allows measurement of the pore water pressure through the connection from the cell to the transducer. On the horizontal leg of the T-piece, the glass stopcock and volumetric burette allow accurate measurement of incremental outflow volumes.

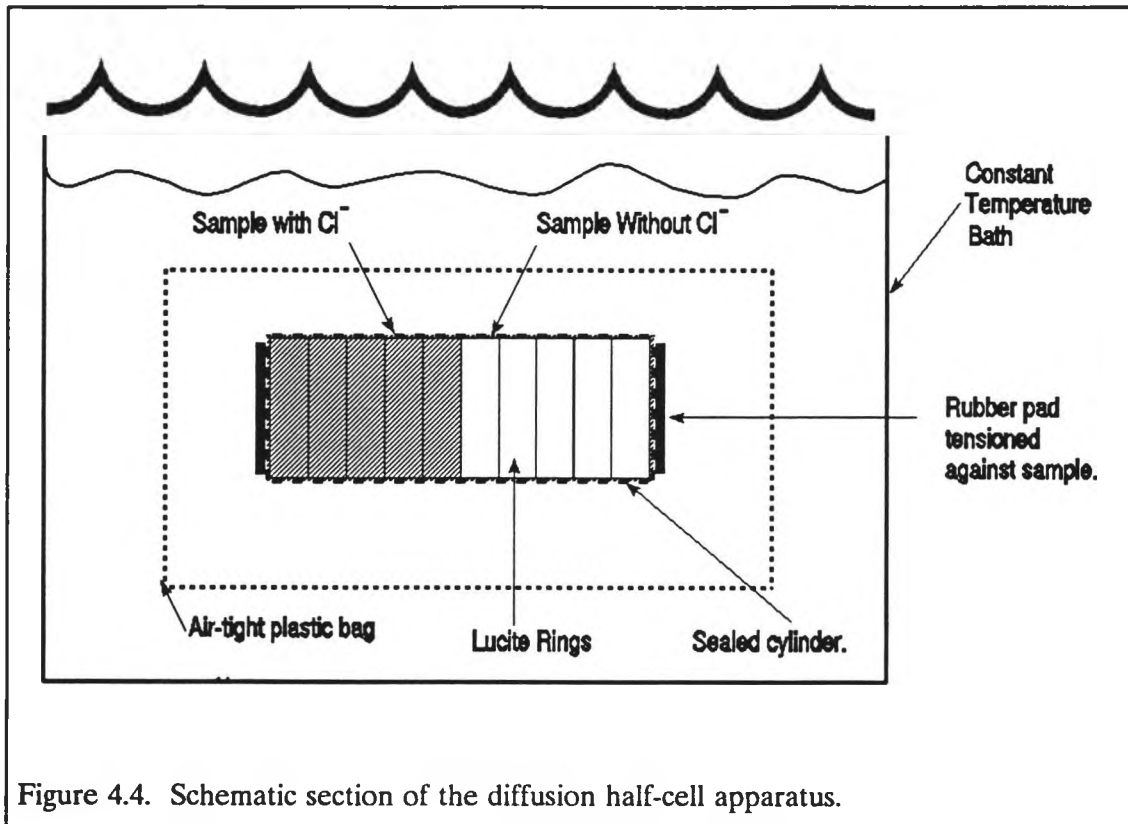
Additional items required for the system are a differential null transducer to measure the difference in pressures of air and water, Poly-flo tubing and connections to provide air pressure to the cell and "dry port" of the transducer, suitable air pressure regulators to provide an accurate, steady air pressure over the range required, an air supply, pressure gauges, and mercury or water manometers to monitor the air pressure.

The general procedure to develop the desaturation curve requires that the glass tubing and transducer "wet port" are first filled with de-aired water. Thereafter the glass T-piece is connected to the cell base and water is allowed to flow into the base. After the sample and porous plate are vacuum saturated, they are placed carefully on the base O-rings without trapping any air bubbles. The plate is then clamped down with the retaining ring. Finally, the cap is secured, and the air hoses are attached to the cap and "dry port" of the transducer as shown in Figure 4.3. To begin the retention curve measurement, air pressure is slowly applied to the cell, with the outflow stopcock in the open position. The pressure at which drainage begins is recorded. Thereafter a predetermined volume of water is allowed to drain from the sample into the burette. The air pressure during this stage is set high enough to allow relatively rapid drainage of the required volume of water but not high enough to induce a large water pressure gradient in the sample. When the predetermined volume of water has drained, the stopcock is closed and the capillary pressure is monitored over time by recording

the pressure difference between the air and pore water as measured by the differential transducer. The pore water pressure slowly equilibrates and the transducer reading stabilizes. Additional points on the drying retention curve are obtained by applying successive increments of pressure, draining incremental volumes of water and establishing equilibrium in the manner described above. The final water content was determined gravimetrically at the end of the test and the intermediate water contents determined from the volume of water extracted at each step.

4.3 Diffusion Half-Cell Tests

The diffusion half-cells were prepared in pairs by packing the sands into cells made up of five lucite cylinders, each 1.15 cm high and 5.03 cm in diameter. The packing procedure was identical to that used in packing the retention characteristic samples. The cylinders were securely taped together with waterproof tape. The configuration of the cells is shown in Figure 4.4. For the duration of the packing process of the sands, an additional cylinder was attached to the top of the cell, and two additional cylinders were attached to the bottom. After the packing was completed, the additional cylinders were carefully removed, and the sand levelled flush with the ends of the cell. This was done to obtain a homogeneous packing throughout the length of the cell. The packing was repeated if the bulk density was not within 10 percent of the required mean for all the tests. A plastic end plate was placed at each end of the cell and held down by rubber bands. This retained the porous medium during the saturation process. The half-cells were then placed on the porous steel plates used in the controlled outflow cell and put into one of two vacuum chambers and a vacuum of 24" of mercury was drawn on each cell and on a solution of either NaCl or NaNO₃ for at least



three hours. The solutions were then allowed to flow into the separate vacuum chambers housing the half-cells and saturate the porous media for 24 hours. After this period the vacuum was released and the samples were left to soak in the solutions for an additional 3 hours. For the diffusion tests at water contents below saturation, the sample and plate was setup in the controlled outflow cell.

Sufficient solution was then drained from each sample until the required matric pressure had been established. The half-cell that was initially saturated with the chloride solution was equipped with a flat rubber gasket at one end. This remained in place throughout the packing, saturation and desaturation processes. After removing the samples from the cells, the rubber gasket was removed from the Cl^- spiked half-cell so that the face of the material was exposed. The faces of each of the half-cells were checked to ensure that they were level and competent for joining together. The two half cells were pressed together

and taped in place. The time of joining was recorded. The open ends of the joined cells were then sealed with wax paper and tape and a tension was applied to hold the cells together using a rubber band. The assembly was then placed in a sealed plastic bag and immersed in a constant temperature bath at $25^{\circ}\text{C} \pm 0.1^{\circ}\text{C}$.

The wetter samples were left to diffuse for 3 to 4 days and the drier samples from 4 to 6 days. After this period, the time was recorded, and the samples were removed and sliced into the 10 individual cylinders. These samples were weighed immediately, dried for 24 hours and weighed dry. Fifty milliliters of deionized water was then added to each sample. The samples and cylinders were thoroughly mixed in this water to dissolve the salt. The water was then extracted and passed through a $0.45\mu\text{m}$ filter. The concentration of the extract, C_{ext} , was then accurately determined by potentiometric titration with AgNO_3 . The concentration of the chloride ion, C , in each sample was determined by

$$C = \frac{C_{\text{ext}} \cdot 50}{V_s}$$

where V_s is the initial volume of water in the sample determined as

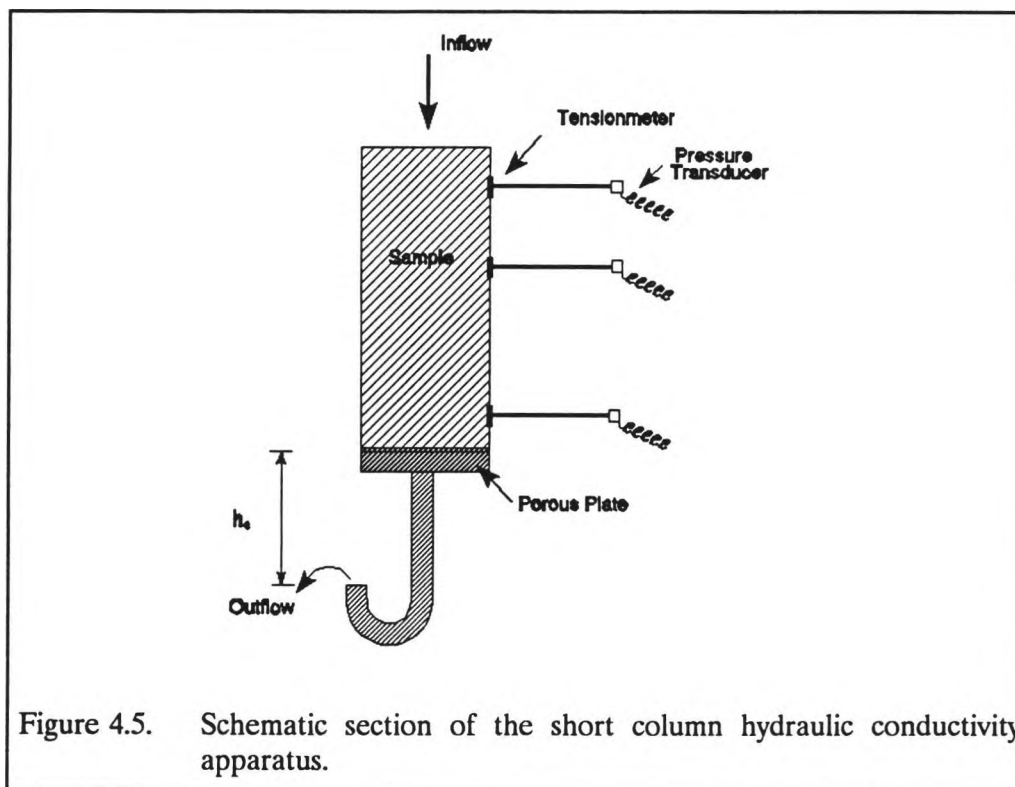
$$V_s = \frac{M_w - M_d}{\rho_w}$$

where M_w is the wet mass of the sample (g), M_d is the dry mass of the sample (g) and ρ_w is the density of water (1 g/cm^3). The concentrations of each segment of the half-cells were plotted with distance along the cell to yield the diffusion curves.

4.4 Unsaturated Hydraulic Conductivity Short Column Tests

The short columns, shown in Figure 4.5, for the unsaturated hydraulic conductivity measurements were constructed out of 3.79 cm diameter lucite tubing. The base was fitted

with a porous steel plate and windows for the tensiometers were machined from the side of the tube. The tensiometers comprised of a rectangular porous plastic pad sealed into a section of lucite cylinder that could fit into the windows of the tube. The cap of the column served to retain the sample, and a filter paper was placed between the sample and cap. The inflow tube was placed into an opening in the cap. The samples were packed into the short columns in the same way as the water retention samples and the diffusion half-cells.



After packing the sample into the column, it was saturated with deionized water in a vacuum chamber. The tensiometers were also vacuum saturated and then set in place in the windows of the column. Pressure transducers accurate to 0.5 cm, were attached to each of the tensiometers and connected to a data logger.

Inflow of deionized water was regulated into the top of the column by two different methods. For the Poudre sand mix sample, a length of small diameter plastic tubing was calibrated for its outflow response to an applied head of water. The column test was then run with a falling head on the length of tubing so that the flux varied continuously, starting at a rate corresponding to the saturated conductivity. The inflow to the Ottawa sand column was regulated with a peristaltic pump. During measurement or equalization phases, the inflow rate was kept constant beginning with a rate that was equal to the saturated hydraulic conductivity. The inflow rate was then slowly reduced to the next lower inflow rate that was again held constant for sufficient time for a stable reading to be made from the tensiometers. During the measurement phases and flow reduction phases of the Ottawa sand and continuously during the test on the Poudre sand mix, a negative pressure was adjusted at the base of the column so that a unit gradient of hydraulic head was induced and maintained in the material between the two upper tensiometers. This was achieved by regulating a negative air pressure in a glass vessel where the outflow tube from the column was sealed.

The hydraulic conductivity was reported as the flux at which unit gradient was established and the tension was reported when the tensiometers indicated a unit hydraulic gradient. Water contents were inferred from the tension measurements using the water retention data.

CHAPTER 5

RESULTS AND DATA ANALYSIS

The results of the laboratory tests on the Ottawa sand and Poudre sand mix materials are presented in this chapter. The pore size distribution parameters are determined for the two sands from the water retention data using the Brooks-Corey model. The diffusion data is presented together with an analysis of the variability of the half-cell water content as well as an analysis of the effective diffusion coefficients. The results of the hydraulic conductivity data are presented with the predicted curves derived from the Burdine model using the Brooks and Corey retention parameters. Finally, an analysis of the water retention and hydraulic conductivity data is performed using parameter optimization to study the parameter combinations for different retention characteristic and hydraulic conductivity models.

5.1 Water Retention Analysis

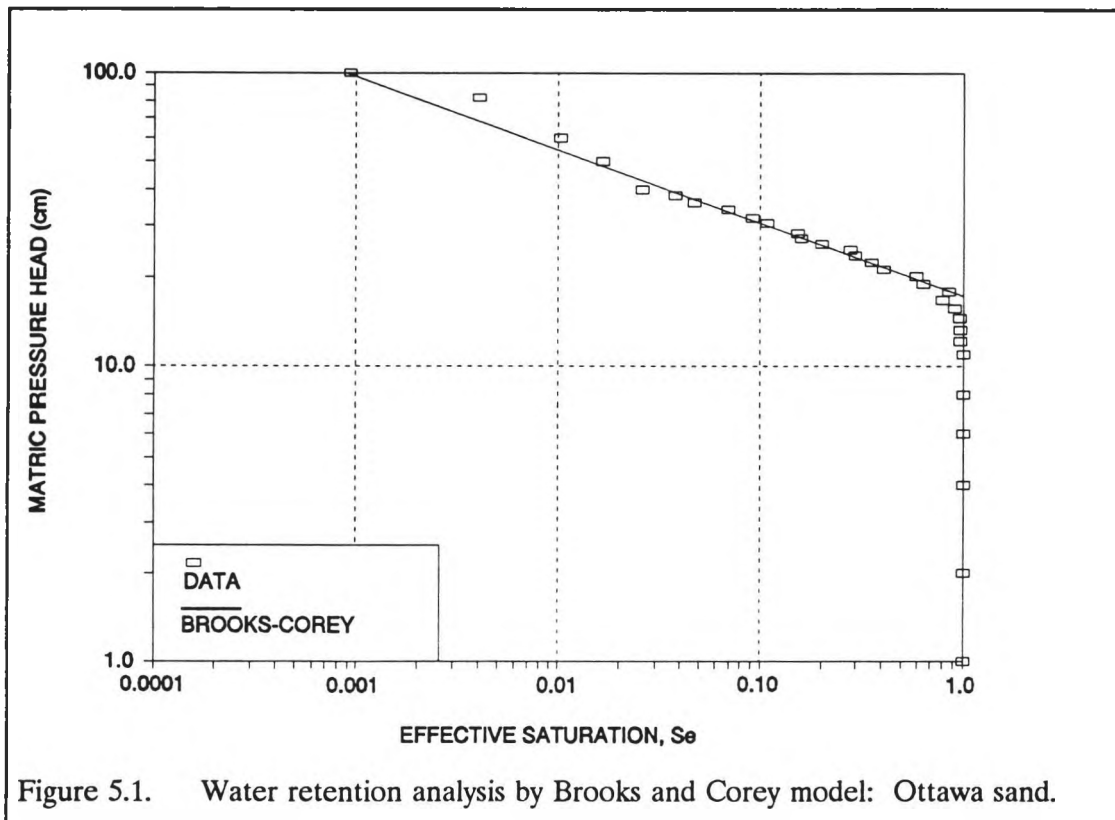
The matric pressure head and the associated water content are calculated from the results of the controlled outflow cell tests. The results are shown in Appendix A and Figures 5.1 and 5.2. The Brooks-Corey parameters are estimated using a logarithmic plot of the matric pressure head, h_c , and effective saturation, S_e , that are related in the Brooks-Corey model as

$$S_e = \left(\frac{h_b}{h_c} \right)^\lambda \quad h_c > h_b \quad 5.1$$

where

$$S_e = \frac{\theta - \theta_r}{\theta_s - \theta_r} \quad 5.2$$

The value of residual water content, θ_r , is chosen such that the h_c - S_e data lie in a straight line on the logarithmic plot as shown in Figures 5.1 and 5.2 for the Ottawa sand and the Poudre sand mix, respectively. The pore size distribution index, λ , and the air entry pressure head, h_b , are then optimized to represent the data. These results are presented in Table 5.1. The optimum R^2 resulting from the parameter adjustment was greater for the Poudre sand mix, 0.9995, than for the Ottawa sand, 0.9897, however, both of these values indicate a satisfactory fit to the data.



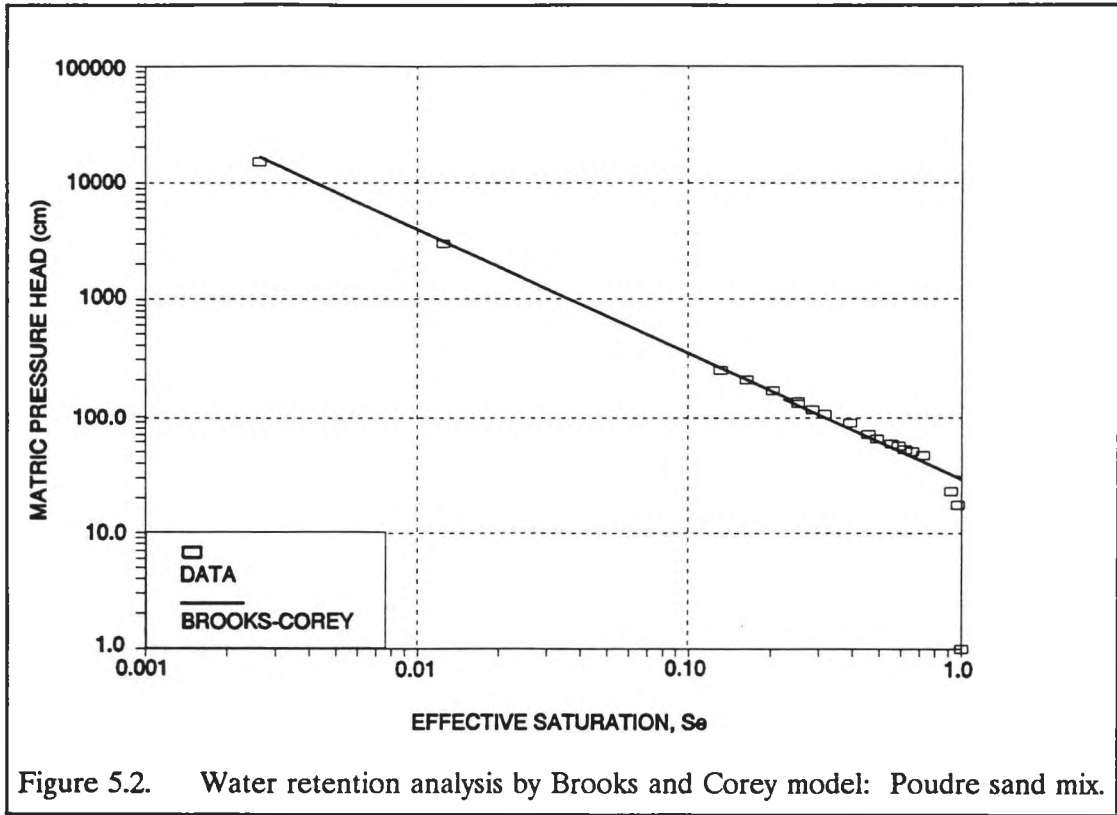


Table 5.1. Results of the Brooks-Corey parameter analysis.

Material	Pore size distribution index	Residual water content	Air entry pressure head (cm)	R ² of log-log regression
Ottawa sand	4.0	0.0187	17.2	0.9897
Poudre sand	0.94	0.0182	30.0	0.9995

5.2 Diffusion Half-Cell Results

The diffusion half-cell data comprise chloride concentration and water content profiles along the length of the cell. These results are presented in Figures A-1 to A-18 in Appendix A together with the tabulated data. Typical diffusion curves for the half-cell tests are shown in Figures 5.3 to 5.6. The figures show the variation of the concentration of the chloride along the length of the column as well as the gravimetric water content in each of the Lucite cylinders.

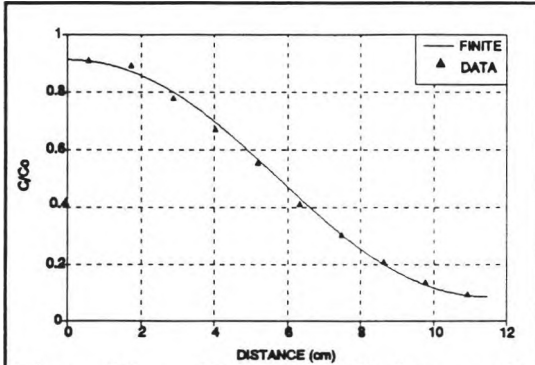


Figure 5.3a. Half-cell diffusion results for Ottawa sand. $S=0.974$.

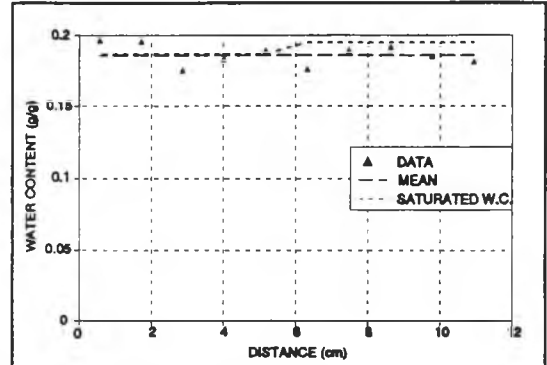


Figure 5.3b. Half-cell water contents for Ottawa sand. $De/Do=0.99$.

At high saturation, the diffusion data are smooth and the effective diffusion coefficient can easily be estimated by fitting the appropriate solution to the data as is shown in Figure 5.3 for the Ottawa sand and in Figure 5.4 for the Poudre sand mix.

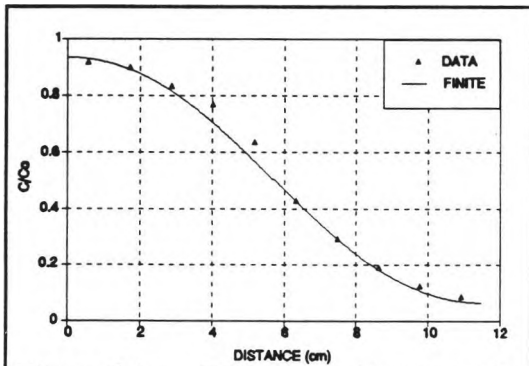


Figure 5.4a. Diffusion half-cell results: Poudre sand. $De/Do=0.43$.

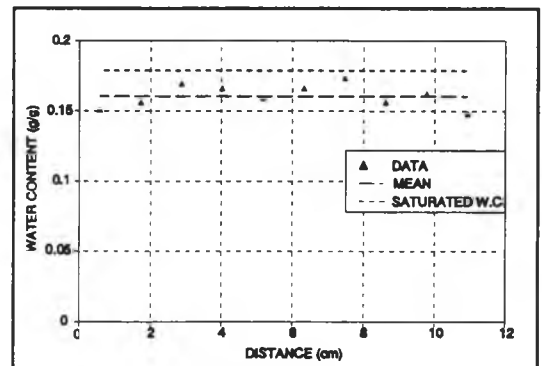
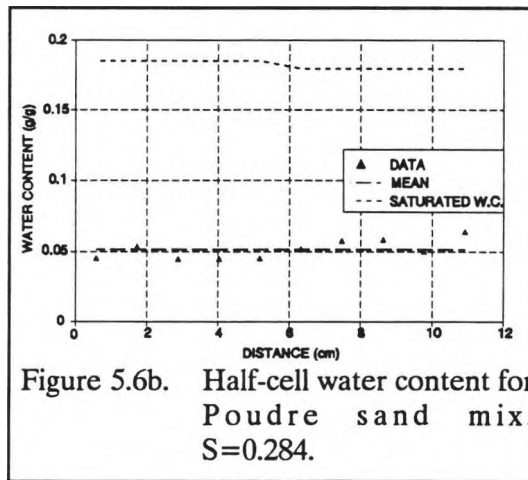
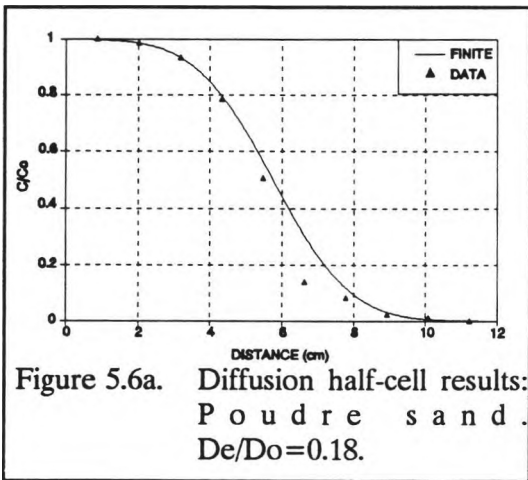
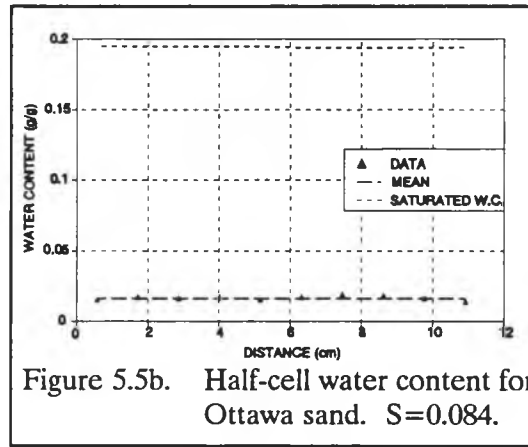
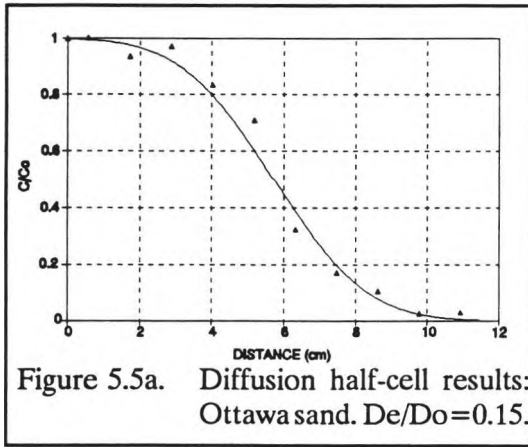


Figure 5.4b. Half-cell water content for Poudre sand mix. $S=0.896$.

At lower saturations in the Ottawa sand, the hydraulic continuity between the two half cells was more difficult to attain than at higher saturations. This can be seen in the step in the concentration at the midpoint of the column as shown in Figure 5.5a. This is not as evident in the Poudre sand results as is shown in Figure 5.6a where reasonably smooth data is obtained at a low saturation of $S = 0.284$. The accuracy of the concentration data diminishes

with decreasing water content. This can be seen in the scatter of the data in Figures 5.5a and 5.6a.



The results of all the diffusion half-cell measurements and the variation of the water contents in the profiles are summarized in Table 5.2. The accuracy of the fitted effective diffusion is examined by first assessing the accuracy of the chloride concentrations. These are affected by the accuracy of the titration and by the dilution ratio that is determined as the volume of water added to the dried cell sample to the volume of water initially in the cell during the diffusion process. The titration accuracy was 0.2 ml of titrant for the moist samples and 0.05 ml for the drier samples and the lower concentrations. Typical titration curves are shown in Figures 5.7a and 5.7b, from which it can be seen that an accuracy of 0.2 ml is conservative,

Table 5.2 Results of the diffusion half-cell measurements.

Half-Cell #	Average bulk density ρ_b (g/cm ³)	Average porosity ϕ	Average water content θ (cm ³ /cm ³)	Standard deviation of θ σ_θ (cm ³ /cm ³)	Average saturation S	Standard deviation of S σ_s	Duration of test (hrs)	D_v/D_o	R ²
Poudre Sand									
Mix	1.782	0.323	0.327	0.013	1.000	0.038	120.0	0.50	0.9949
PS1	1.798	0.316	0.289	0.014	0.896	0.045	168.0	0.43	0.9936
PS2	1.776	0.324	0.242	0.021	0.730	0.064	120.0	0.30	0.9968
PS3	1.774	0.325	0.092	0.013	0.284	0.038	120.0	0.18	0.9863
PS4	1.764	0.329	0.069	0.008	0.205	0.024	180.0	0.14	0.9865
PS5	1.787	0.320	0.131	0.036	0.400	0.112	144.0	0.20	0.9899
PS6	1.784	0.321	0.073	0.007	0.223	0.020	122.0	0.10	0.9957
Ottawa sand									
OS1	1.753	0.339	0.319	0.009	0.943	0.028	101.0	0.97	0.9852
OS2	1.749	0.340	0.029	0.003	0.084	0.008	169.5	0.15	0.9888
OS3	1.760	0.336	0.030	0.003	0.089	0.008	169.5	0.08	0.9972
OS4	1.769	0.335	0.327	0.014	0.974	0.041	84.0	0.99	0.9976
OS5	1.770	0.332	0.326	0.011	0.951	0.032	96.0	0.82	0.9977
OS6	1.765	0.334	0.235	0.045	0.706	0.134	131.0	0.68	0.9995
OS7	1.749	0.340	0.119	0.037	0.348	0.108	129.5	0.40	0.9483
OS8	1.780	0.328	0.114	0.029	0.488	0.089	120.3	0.55	0.9885
OS9	1.740	0.343	0.236	0.030	0.718	0.090	96.3	0.68	0.9965
OS10	1.746	0.341	0.135	0.021	0.392	0.061	121.3	0.46	0.9976
OS11	1.769	0.333	0.084	0.014	0.241	0.056	145.0	0.31	0.9990

since the peak is extremely sharp at the equilibration point. These titration accuracies, together with dilution ratios which vary between 6.2 and 28.2, result in an error in the concentration reported being 3 percent.

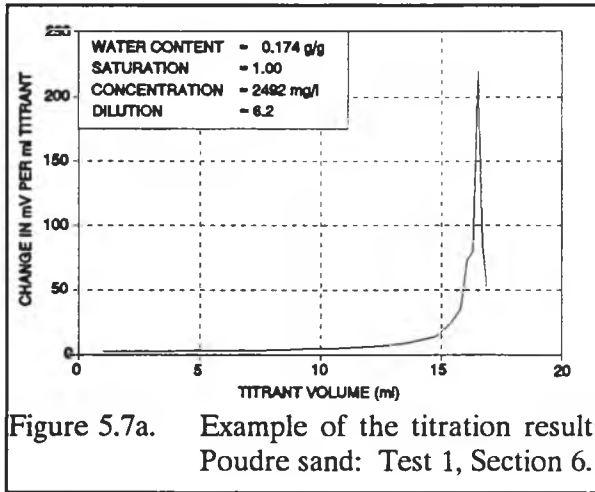


Figure 5.7a. Example of the titration result: Poudre sand: Test 1, Section 6.

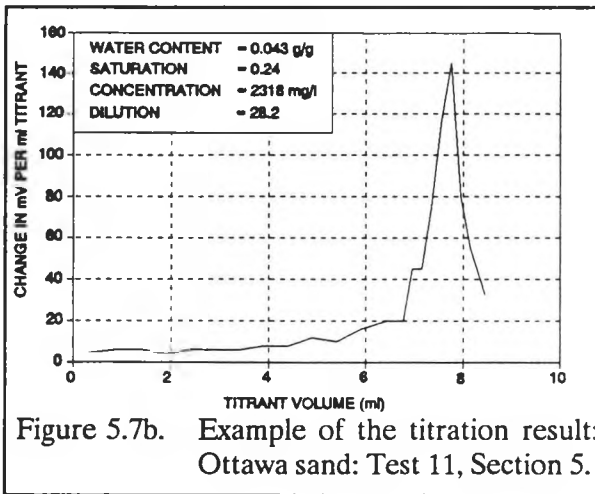


Figure 5.7b. Example of the titration result: Ottawa sand: Test 11, Section 5.

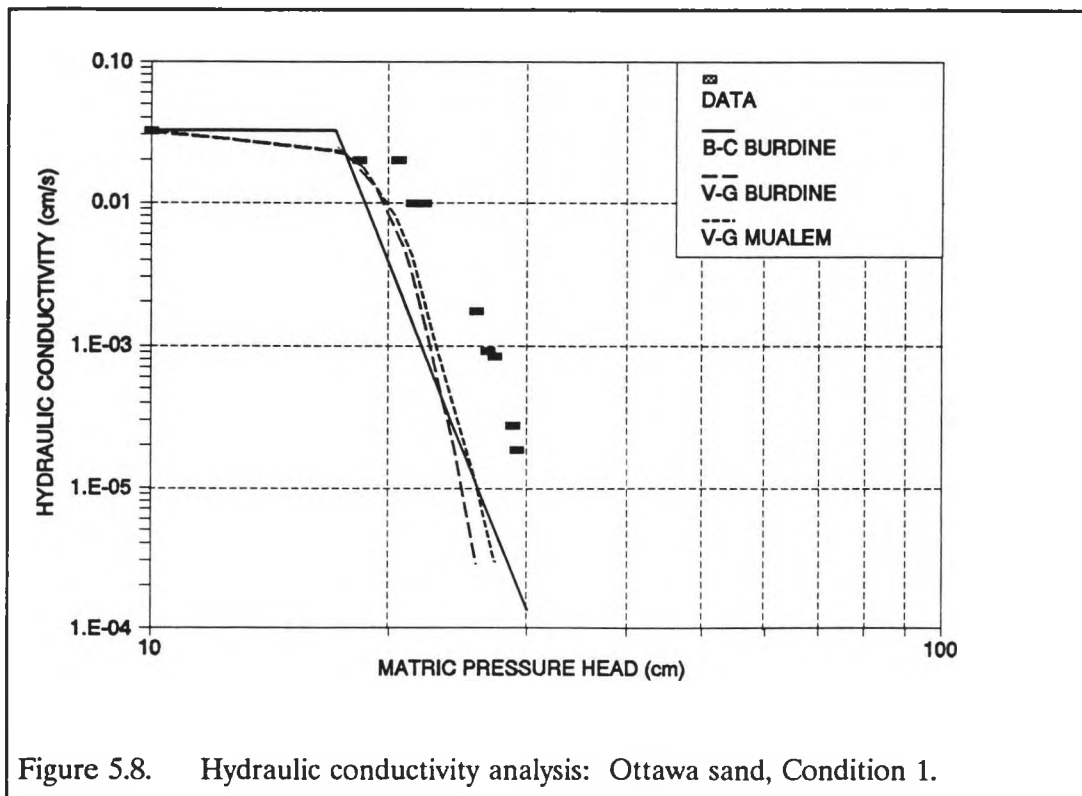
The exercise of fitting the diffusion equation solution to the data as demonstrated in Figures 5.3 to 5.6, was repeated two more times with the concentrations adjusted up and down by 3 percent. The value of the effective diffusion coefficient for each of these exercises was recorded when the

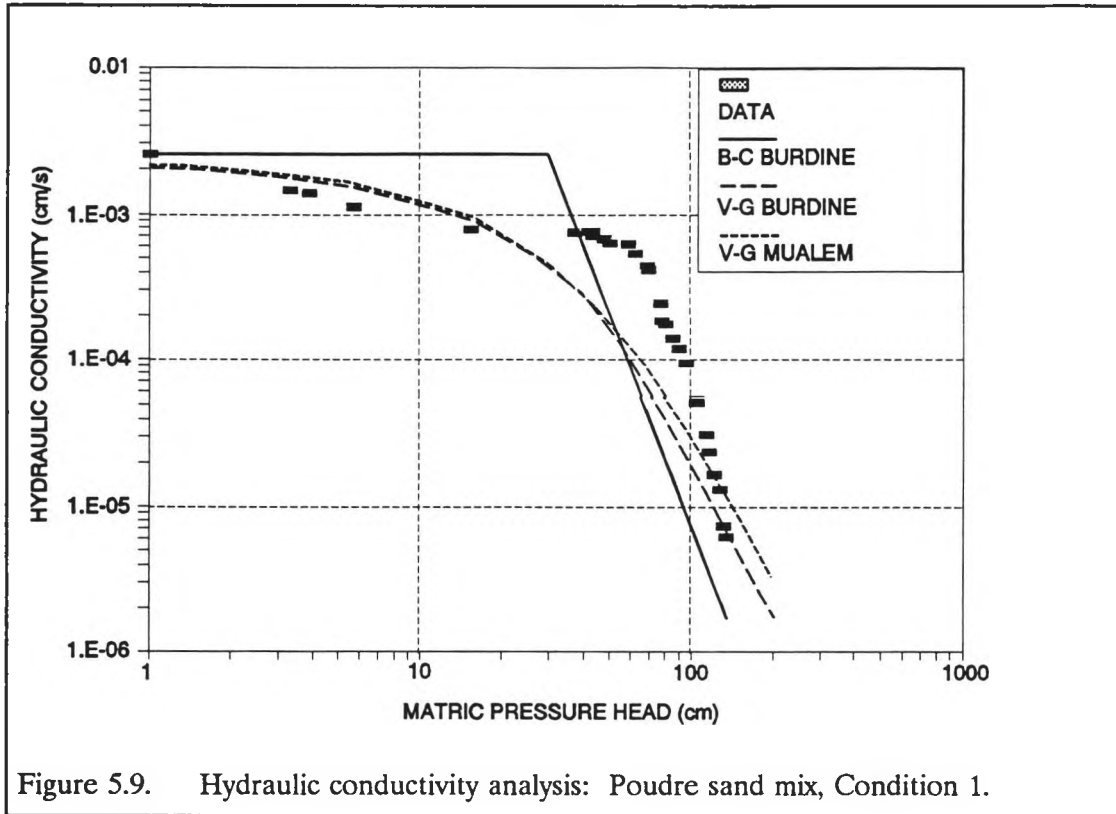
regression of the data with the theoretical solution resulted in the same regression coefficient, (Table 2), that was achieved while fitting the curves to the data without adjustment. The variation of the effective diffusion coefficient determined in this way yielded an accuracy of the ratio, D_e/D_o of 0.02. This accuracy is

presented as error bars in the diffusion half-cell analysis, Figure 6.1, presented in Chapter 6. Confidence in the accuracy of the D_e/D_o ratio is verified further by examining the range of the duration of the half-cell test. The durations vary from 96 to 170 hours, yet the D_e/D_o ratios do not follow a trend with the duration of the tests. Indeed, in the Poudre sand mix, tests that have a similar duration, 120 hours, have resulting D_e/D_o ratios ranging from 0.1 to 0.5.

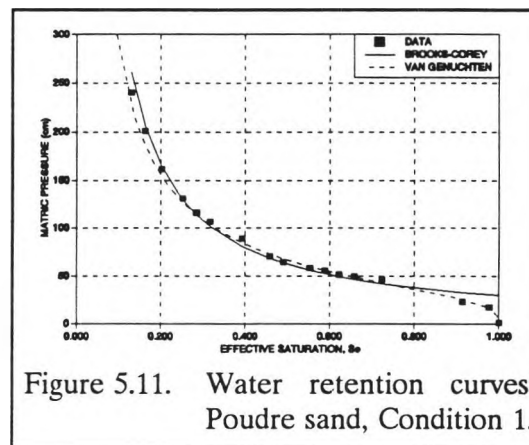
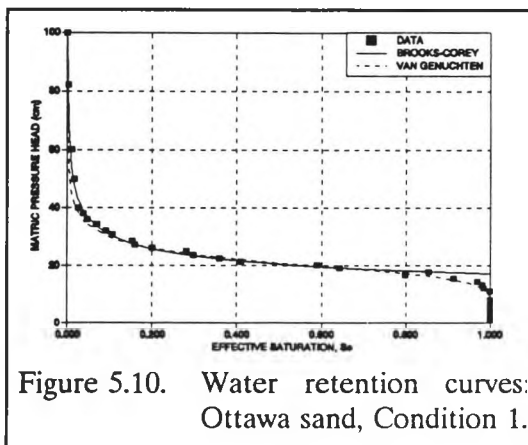
5.3 Hydraulic Conductivity Results

The hydraulic conductivity results are plotted against the matric pressure head on a logarithmic scale as shown in Figures 5.8 and 5.9 for the Ottawa sand and Poudre sand mix, respectively. Theoretical curves defined by the Burdine model using Brooks and Corey retention relationships are plotted with the data in these figures. The parameters used in the hydraulic conductivity curves are those of the Brooks and Corey relationship, derived in 5.1 and the saturated hydraulic conductivities determined in the short column tests. The Brooks-Corey-Burdine relationship, displayed as the straight line in Figures 5.8 and 5.9 does not represent the data adequately, being as much as an order of magnitude in error. Nevertheless, for the sake of completeness, analysis of the water retention and hydraulic conductivity data is continued using additional relationships and parameter sets as indicated by Conditions 1 to 4 in Tables 5.3 and 5.4.





The parameter optimization model, RETC, (Van Genuchten *et al.*, 1991) was used to derive parameters for various conditions. The first condition analyzed allows for optimization of the α (or h_b) and the N (or λ) parameters of the Van Genuchten or Brooks and Corey models in the Burdine or Mualem conductivity models. The results are shown in Figures 5.8 and 5.9,



while the corresponding water retention characteristics are shown in Figures 5.10 and 5.11. The use of the Van Genuchten characteristics in either the Burdine or Mualem model in the concurrent fitting of these theoretical relationships to the retention and hydraulic conductivity data does not result in an improved regression coefficient when compared with the use of the Burdine model with the Brooks and Corey parameters derived in 5.1. In fact, using the Van Genuchten model in the Poudre sand mix analysis results in a considerable decrease in the regression coefficient, from an R^2 of 0.923 using Burdine with Brooks and Corey to an R^2 of 0.9505 using Burdine with the Van Genuchten characteristic, and 0.921 using Mualem with the Van Genuchten characteristic. A less strict optimization rule was used in Condition 3 of Tables 5.3 and 5.4. Here five parameters are freed for optimization. The resulting hydraulic conductivity relationships are shown in Figures 5.12 and 5.13 and the retention characteristics in Figure 5.14 and 5.15.

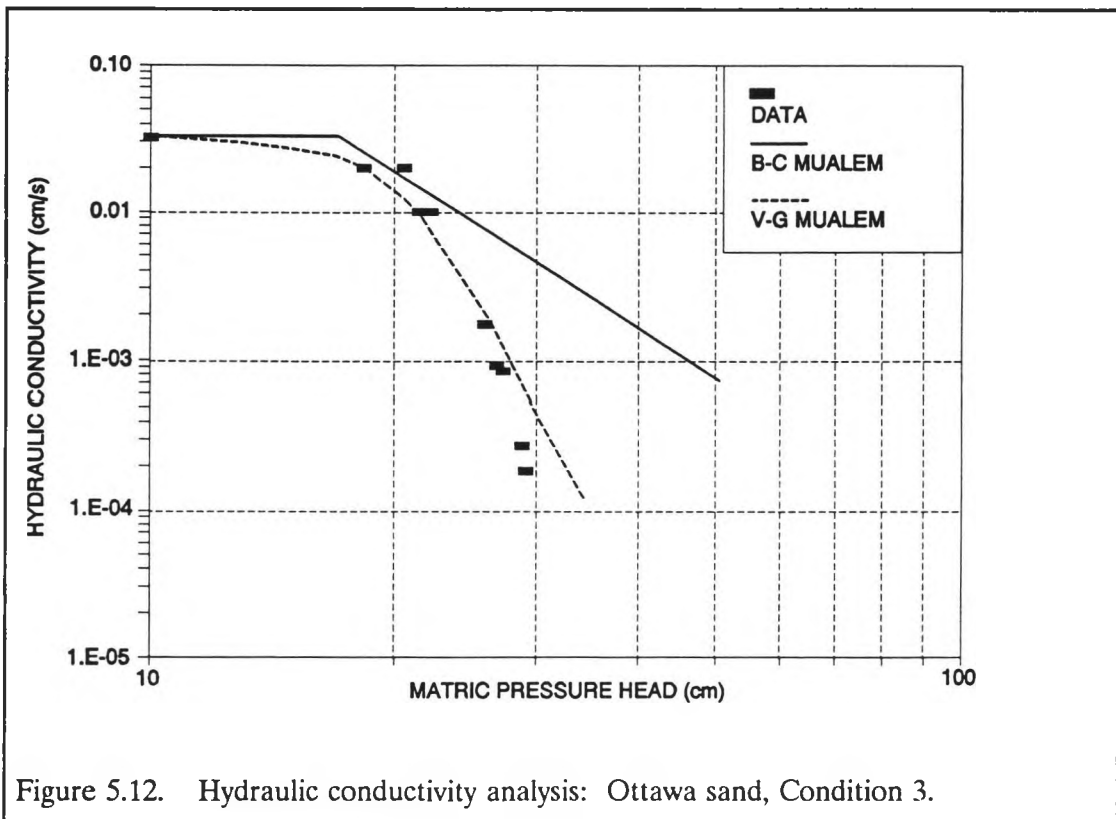
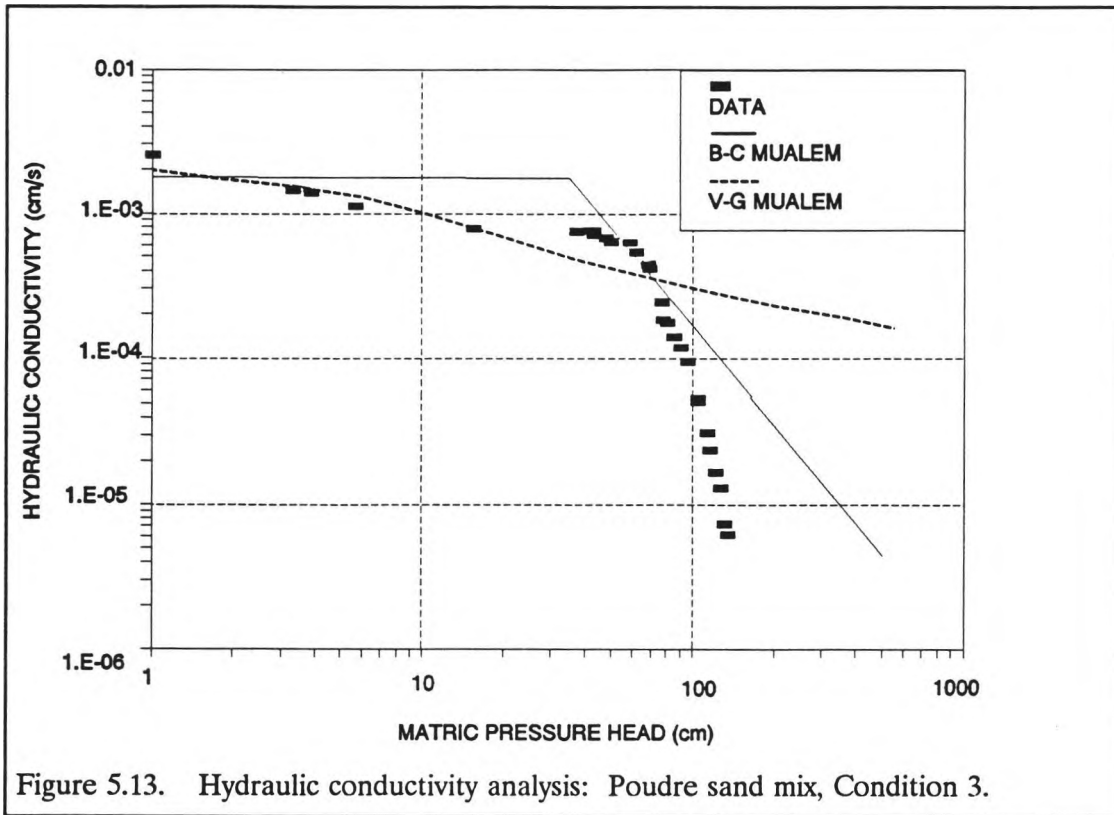


Figure 5.12. Hydraulic conductivity analysis: Ottawa sand, Condition 3.



No improvement to fitting the data concurrently has been made. Indeed, with the negative values of l obtained in Condition 3, the further examination of this exponent term by invoking retention, diffusion and hydraulic conductivity data is warranted. The following chapter attempts to do this by examining the alternative theoretical model proposed in Chapter 3.

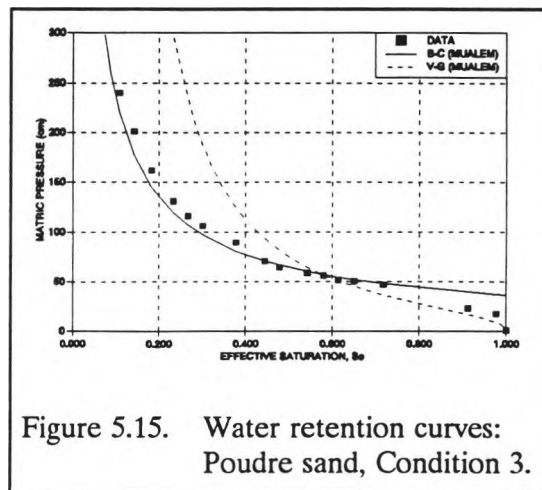
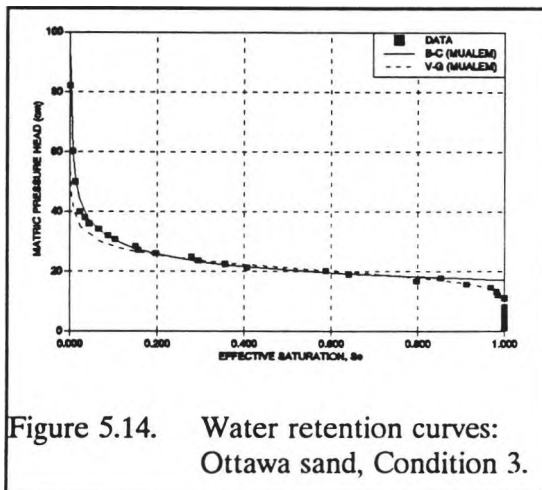


Table 5.3 Parameter optimization of the water retention (WR) and hydraulic conductivity (HC) characteristics: Ottawa sand.

Condition Variable		Brooks-Corey Retention Characteristic			Van Genuchten Retention Characteristic		
		Water retention data only	Simultaneous WR/HC (Burdine)	Simultaneous WR/HC (Mualem)	Water retention data only	Simultaneous WR/HC (Burdine)	Simultaneous WR/HC (Mualem)
1.	θ_r fixed α N l fixed Ks fixed R ²	0.0182 0.0584 3.7515 0.9897	0.0182 0.0564 4.1780 2.0000 0.03240 0.9927	0.0182 0.0568 4.0849 0.5000 0.03240 0.9933	0.0182 0.0506 7.5715 0.9944	0.0182 0.0472 10.9490 2.0000 0.03240 0.9888	0.0182 0.0467 9.7532 0.5000 0.03240 0.9903
2.	θ_r α N l fixed Ks R ²	0.0178 0.0589 3.7328 0.9897	0.0170 0.0565 4.1135 2.0000 0.03298 0.9928	0.0161 0.0569 3.9822 0.5000 0.03295 0.9934	0.0248 0.0508 7.9641 0.9948	0.0306 0.0479 11.9365 2.0000 0.03336 0.9899	0.0289 0.0474 10.5412 0.5000 0.03337 0.9914
3.	θ_r α N l Ks R ²			0.0198 0.0581 3.9911 -0.6211 0.03257 0.9935		0.0292 0.0500 9.3426 0.0735 0.03281 0.9946	0.0295 0.0490 8.8043 -0.9131 0.03277 0.9945
4.	θ_r fixed α fixed N fixed l Ks fixed R ²					0.0182 0.0494 (free) 8.8767 (free) 0.1431 0.03240 0.9039	0.0182 0.0483 (free) 8.3394 (free) -0.8366 0.03240 0.9938

Note: $\alpha = 1/h_d$ and $N = \lambda$ in Brooks and Corey Characteristic.

Table 5.4 Parameter optimization of the water retention (WR) and hydraulic conductivity (HC) characteristics: Poudre sand mix.

Condition	Variable	Brooks-Corey Retention Characteristic			Van Genuchten Retention Characteristic		
		Water Retention Data Only	Simultaneous WR/HC (Burdine)	Simultaneous WR/HC (Mualem)	Water Retention Data Only	Simultaneous WR/HC (Burdine)	Simultaneous WR/HC (Mualem)
1.	θ_r fixed α N l fixed Ks fixed R ²	0.0187 0.0301 1.0280 0.9954	0.0187 0.0259 1.0050 2.0000 0.00251 0.9923	0.0187 0.0265 1.0050 0.5000 0.00251 0.9933	0.0187 0.0261 3.1434 0.9976	0.0187 0.0245 2.5289 2.0000 0.00251 0.9505	0.0187 0.0172 1.6889 0.5000 0.00251 0.9521
2.	θ_r α N l fixed Ks R ²	0.0176 0.0301 1.0177 0.9955	0.0000 0.0235 1.0050 2.0000 0.00143 0.9883	0.0000 0.0236 1.0050 0.5000 0.00143 0.9889	0.0000 0.0274 2.9579 0.9947	0.0000 0.0139 3.9423 2.0000 0.00149 0.9727	0.0000 0.0127 3.1783 0.5000 0.00150 0.9768
3.	θ_r α N l Ks R ²		0.0258 0.0270 1.2393 -0.7961 0.00141 0.9965	0.0258 0.0272 1.2394 -1.7961 0.00141 0.9965		0.0000 0.0448 2.5651 -3.8653 0.00237 0.9878	0.0000 0.0317 1.6844 -4.5088 0.00240 0.9875
4.	θ_r fixed α fixed N fixed l Ks fixed R ²		0.0187 0.0333 0.9400 -0.5799 0.00251 0.9913			0.0187 0.0516 (free) 2.5582 (free) -3.9230 0.00251 0.9818	0.0187 0.0356 (free) 1.6829 (free) -4.5202 0.00251 0.9834

Note: $\alpha = 1/h_0$ and $N = \lambda$ in Brooks and Corey Characteristic.

CHAPTER 6
ANALYSIS AND DISCUSSION

The diffusion half-cell and hydraulic characteristic results are used to assess the dependence of the formation factor on the parameters describing the properties of the materials in this chapter. First, the half-cell results are examined for differences between the diffusion behavior in the Poudre sand mix and the Ottawa sand. This analysis yields a first estimate of the variability of the formation factors for these two materials and an indication of the dependence in other porous media. Next, guided by the results of the diffusion tests, the saturated hydraulic conductivity data, together with the hydraulic characteristic parameters of a range of porous media, are examined for the variation of the formation factor with the parameters. The algorithms derived to describe the formation factor are used to estimate the saturated hydraulic conductivity of all the materials used in the analysis. Finally, the diffusion and the unsaturated hydraulic conductivity characteristics of the Poudre sand mix and the Ottawa sand are used to estimate the dependence of the formation factor parameters on the unsaturated hydraulic characteristic parameters.

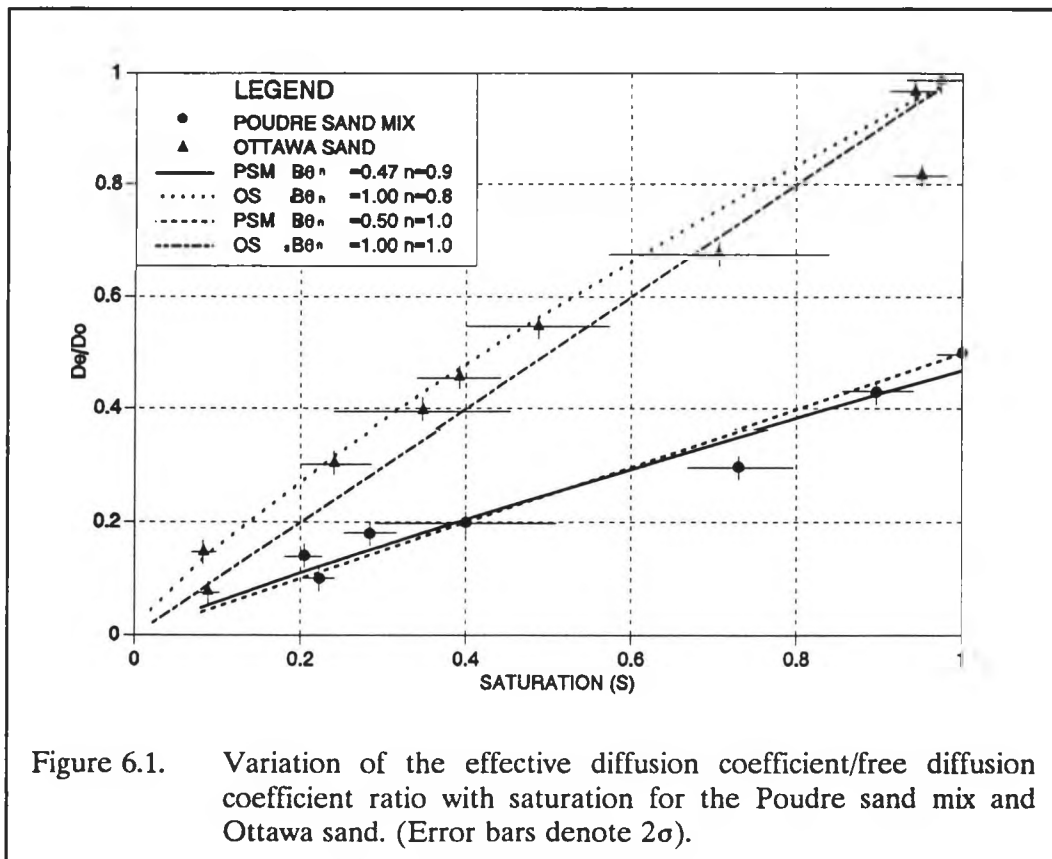
6.1 Diffusion Half-Cell Analysis

The hydraulic conductivity equation developed in Chapter 3 is written as

$$K(\theta) = \phi_e \frac{\rho g \sigma^2}{k_o \mu} B \theta_e^{n+m} \int_0^{S_e} \frac{dS_e}{P_c^2(\theta)} \quad 6.1$$

and includes the formation factor, $B\theta_e^{n+m}$, some of the parameters of which are also present in the ratio of effective to free diffusion coefficients in the form $D_e/D_o = B\theta^n$.

The variation of D_e/D_o determined in each half-cell diffusion test with the average saturation of the test is shown for the Poudre sand mix and the Ottawa sand in Figure 6.1. For each material the ratio of effective to free diffusion coefficients, D_e/D_o decreases with decreasing saturation. However, the ratios for the Poudre sand mix are significantly less than those of the Ottawa sand. Apparently the wider pore size distribution, represented by the low λ of



0.94, yields a lower formation factor (higher tortuosity and constrictivity) for the Poudre sand mix than for the Ottawa sand with the higher λ of 4. The magnitude of the diffusion formation factor at saturation $B\theta_s^n$ and the exponent, n , are examined by fitting a linear and exponential curve to each of the two data sets. The results of the fitted curves are presented

in Table 6.1. There is no significant difference between the linear and non-linear relationships representing the data, indicated by the small improvements in regression coefficient, R^2 , of the Poudre sand mix and the Ottawa sand in moving from the linear to the non-linear relationship.

Table 6.1. Results of the diffusion formation factor, D_e/D_o (or $B\theta^n$), analysis.

Poudre Sand Mix			Ottawa Sand		
$B\theta_s^n$	n	R^2	$B\theta_s^n$	n	R^2
0.50	1.00	0.9516	1.00	1.00	0.9578
0.47	0.90	0.9572	1.00	0.80	0.9765

Since the relationship D_e/D_o versus saturation for both materials have an intercept at the origin, it is evident that adsorption or ion exchange do not cause the difference in the parameter B between the two materials. The parameters derived from the data suggest that the exponent, n, increases with decreasing λ , giving further credence to the hypothesis that the formation factor D_e/D_o increases with decreasing pore size distribution. The parameters obtained in the linear relationships for the two materials and shown in Figure 6.1 are adopted in the further analysis using the hydraulic conductivity data.

6.2 Saturated Hydraulic Conductivity Analysis

The parameters determined in the previous section together with the Brooks-Corey parameters derived to describe the water retention characteristic data were used to estimate the hydraulic conductivity in which the integration in Equation 6.1 has been evaluated to yield,

$$K(S_e) = \phi_e \frac{\rho g \sigma^2}{k_o \mu P_b^2} B \theta_e^{n+m} S_e^{\frac{2+\lambda}{\lambda}} \left(\frac{\lambda}{2+\lambda} \right) \quad 6.2$$

This relationship is used to evaluate the saturated hydraulic conductivity, in which the value of $n+m = 2$ has been adopted as a first approximation. The value of B for the two materials has been derived from the diffusion half-cell results evaluated at saturation, S_e is unity and θ_e becomes the effective porosity. The results of the estimation of the saturated hydraulic conductivity are compared to the measured conductivity in Table 6.2. The measured saturated hydraulic conductivities are predicted within an accuracy of 10 percent in the case of both materials using the diffusion data together with $n+m = 2$ and the water retention parameters estimated in 5.1.

Table 6.2. Saturated hydraulic conductivity analysis.

Saturated Hydraulic Conductivity (cm/s)			
Poudre sand mix		Ottawa sand	
Measured	Predicted	Measured	Predicted
0.00251	0.00229	0.0324	0.0316

It is impossible to derive any meaningful universal relationship of the variation of the parameter, B , and the pore size distribution index based only on the two data points from the diffusion tests and the saturated hydraulic conductivity estimates of the two materials. Hence, an evaluation is performed using a larger data set, provided by the results presented in Brooks and Corey (1964) and Laliberte *et al.* (1966). The formation factors are calculated directly from the measured saturated hydraulic conductivity data and using the Burdine equation

together with the Brooks-Corey relationship for the measured retention characteristics. At saturation, the expression for the saturated hydraulic conductivity becomes,

$$K_s = \phi_c \frac{\rho g \sigma^2}{k_o \mu P_b^2} \left(\frac{1}{k_o T} \right) \left(\frac{\lambda}{2 + \lambda} \right) \quad 6.3$$

Solving for the formation factor k_o yields,

$$k_o T = \frac{K_s \mu P_b^2}{\phi_c \rho g \sigma^2} \left(\frac{\lambda + 2}{\lambda} \right) \quad 6.4$$

in which the saturated conductivity, K_s , and the fluid properties are derived from the conductivity measurements and the other parameters are derived from the measured retention characteristics. The $k_o T$ values obtained for the full set of measured properties are presented in Appendix C and are shown graphically in Figure 6.2. A summary of the data is presented in Table 6.3.

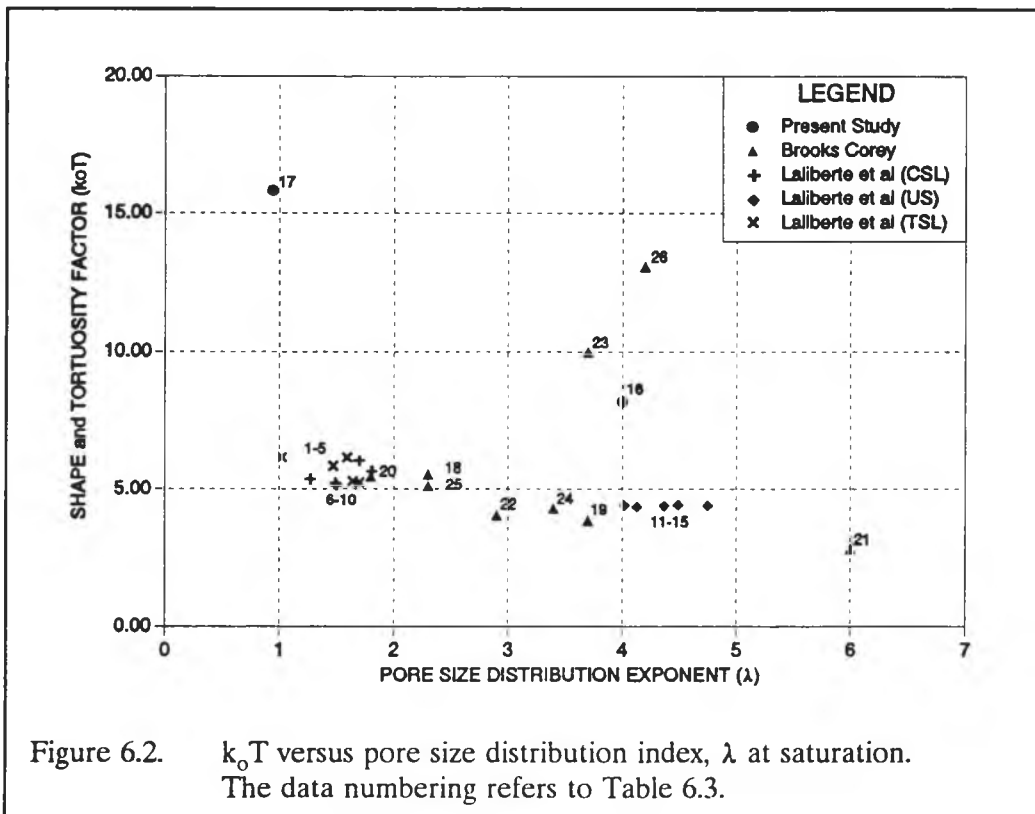


Table 6.3 Summary of porous media properties used in the k_oT analysis.

No	Porous Media	Saturated Hydraulic Conductivity (cm/s)	Bulk Density (g/cm ³)	Air Entry Pressure Head (cm)	Pore Size Distribution Index, λ	k_oT
	Laliberte <i>et al.</i>					
1	Touchet Silt Loam	1.736E-04	1.57	239.2	1.70	5.24
2		2.521E-04	1.50	202.0	1.64	5.30
3		3.218E-04	1.43	169.7	1.59	6.15
4		5.523E-04	1.36	135.5	1.47	5.85
5		6.818E-04	1.29	110.4	1.02	6.16
6	Columbia Sandy Loam	3.973E-04	1.47	156.9	1.70	6.03
7		6.180E-04	1.41	135.5	1.81	5.64
8		7.956E-04	1.37	120.8	1.50	5.13
9		1.570E-03	1.26	89.3	1.49	5.22
10		2.423E-03	1.18	70.8	1.27	5.36
11	Unconsolidated Sand	8.927E-02	1.58	15.8	4.75	4.40
12		1.016E-01	1.53	15.0	4.37	4.38
13		1.113E-01	1.51	14.4	4.49	4.42
14		1.218E-01	1.48	13.9	4.13	4.36
15		1.366E-01	1.46	13.1	4.02	4.41
	Present Study					
16	Ottawa Sand	3.240E-02	1.75	17.2	4.00	8.19
17	Poudre Sand Mix	2.510E-03	1.78	30.0	0.94	15.84
	Brooks and Corey					
18	Volcanic Sand	1.079E-02	1.68	31.8	2.30	5.54
19	Fine Sand (GE #13)	2.796E-03	1.70	81.4	3.70	3.85
20	Touchet Silt Loam	4.905E-04	1.41	149.0	1.80	5.47
21	Glass Beads	1.030E-02	1.64	57.6	6.00	2.82
22	Fragmented Mix	1.472E-02	1.48	34.2	2.90	4.04
23	Berea Sandstone	4.719E-04	2.10	85.4	3.70	9.99
24	Poudre River Sand	2.217E-02	1.69	27.8	3.40	4.29
25	Amarillo Silt Clay	2.296E-03	1.44	75.5	2.30	5.12
26	Loam	1.746E-04	1.99	107.3	4.20	13.08
	Hygiene Sandstone					

The k_oT values derived from Laliberte *et al.*, 1966 are close to a value of 5 which prompted these authors to accept this value as universal. Some of the k_oT values for the 1964 Brooks and Corey data are less than 5, being as low as 2.82 for a sample of glass beads. The k_oT values in this study are 15.84 for the Poudre sand mix and 8.19 for the Ottawa sand, both

greater than the value suggested by Laliberte *et al.*, 1966. The only other results significantly greater than 5 are those of the sandstone materials measured by Brook and Corey (1964). There is no trend in the $k_o T$ values with λ that is immediately discernable from this analysis as represented in Figure 6.2. There is also a significant difference in the $k_o T$ values for the sandstone results, being 10.0 for the Berea sandstone and 13.1 for the Hygiene sandstone which suggests that the differences in $k_o T$ observed are not entirely due to shape factor differences. These results, together with the large overall variation in $k_o T$ invite a more detailed study of the dependence of the formation factor on the properties of the porous media.

Consequently, the variation of the diffusion formation factor with pore size distribution is examined for saturated conditions. Equating 6.2 and 6.3 yields,

$$\frac{B\theta_c^{n+m}}{k_o} = \left(\frac{1}{k_o T} \right) \quad 6.5$$

Isolating the parameter B is difficult since the values of n and m are not known for the materials examined by Laliberte *et al.* (1966) and Brooks and Corey (1964). However, the square of the saturation has been found to be relatively successful in representing the variation of the formation factor with saturation in these studies. It must be noted, however, that Brooks and Corey (1966) reported the exponent of the effective saturation term predicted from retention characteristic measurements differed from that estimated from hydraulic conductivity measurements by as much as 3.9. While this could be due, to some extent, to experimental error, it could also signify a flaw in the common assumption of $n+m = 2$. However, proceeding with $n+m = 2$ and assuming that the shape factor for all materials can be represented by $k_o = 2.5$, the diffusion formation factor can be derived for saturated conditions from Equation 6.5 as,

$$B\theta_s = \left(\frac{1}{k_o T} \right) \left(\frac{2.5}{\theta_c^2} \right) \theta_s \quad 6.6$$

For this expression to represent the true diffusion formation factor, the porous media must have a value of n of unity, which is the value attributed to the Poudre sand mix and the Ottawa sand in this present study, but may not be the case for other materials. The variation of $B\theta_s$ with the pore size distribution index, λ , is shown in Figure 6.3.

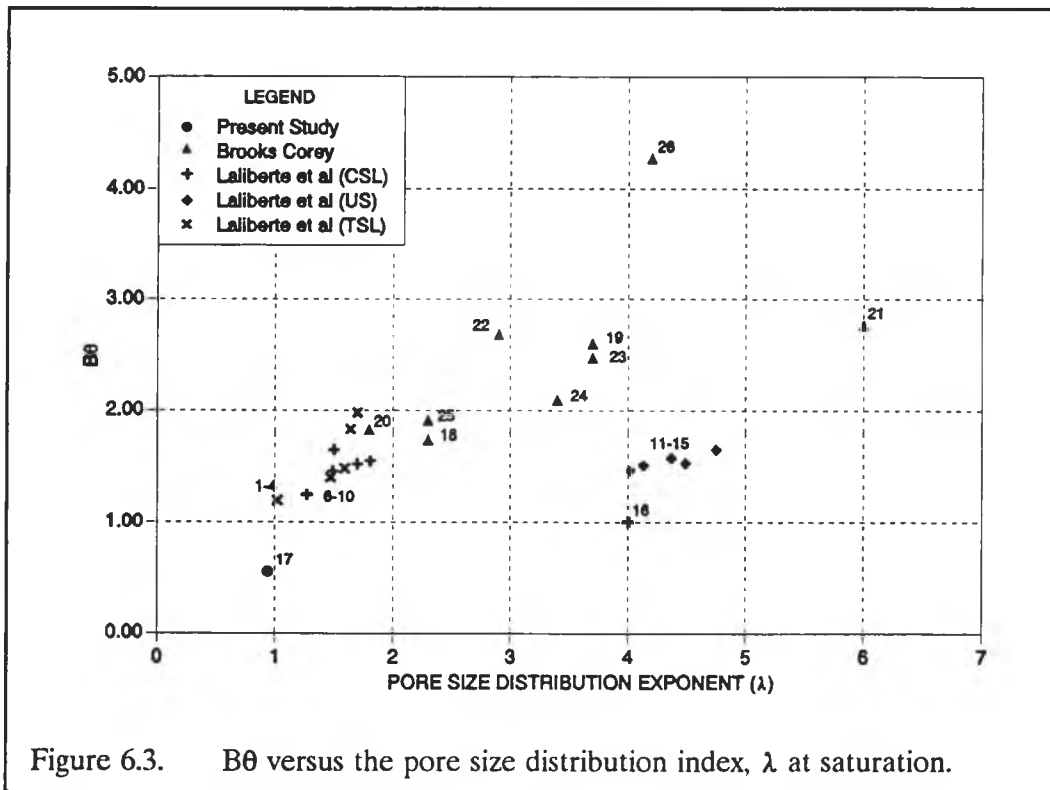


Figure 6.3. $B\theta$ versus the pore size distribution index, λ at saturation.

This analysis shows that, in general, the formation factor increases with increasing λ . However, the data are apparently grouped in different sets of curves which suggest an additional influence on the relationship between $B\theta$ and λ . The data for the Ottawa sand and the data for an unconsolidated sand, packed at different densities, used by Laliberte *et al.* (1966) for instance, do not coincide with the general trend suggested by the other data. Both the Ottawa sand and the unconsolidated sand, however, have hydraulic conductivities with an order of magnitude greater than the rest of the data. The air entry pressure is also

lower than the other materials. This suggests that a further influence on the formation factor exists other than the pore size distribution index. It is suggested that the air entry pressure, h_b , and the effective water content, θ_e , may contribute to the relationship between the formation factor and the hydraulic properties of the porous media. This is evident in models for the hydraulic conductivity and formation factor derived using percolation and effective medium theory such as in Katz and Thompson (1987) and Doyen (1988). In one study the saturated hydraulic conductivity and formation factor are represented by Katz and Thompson (1987), respectively, as

$$K_s = D r_h^2 \frac{EC}{EC_w} \quad 6.7$$

and

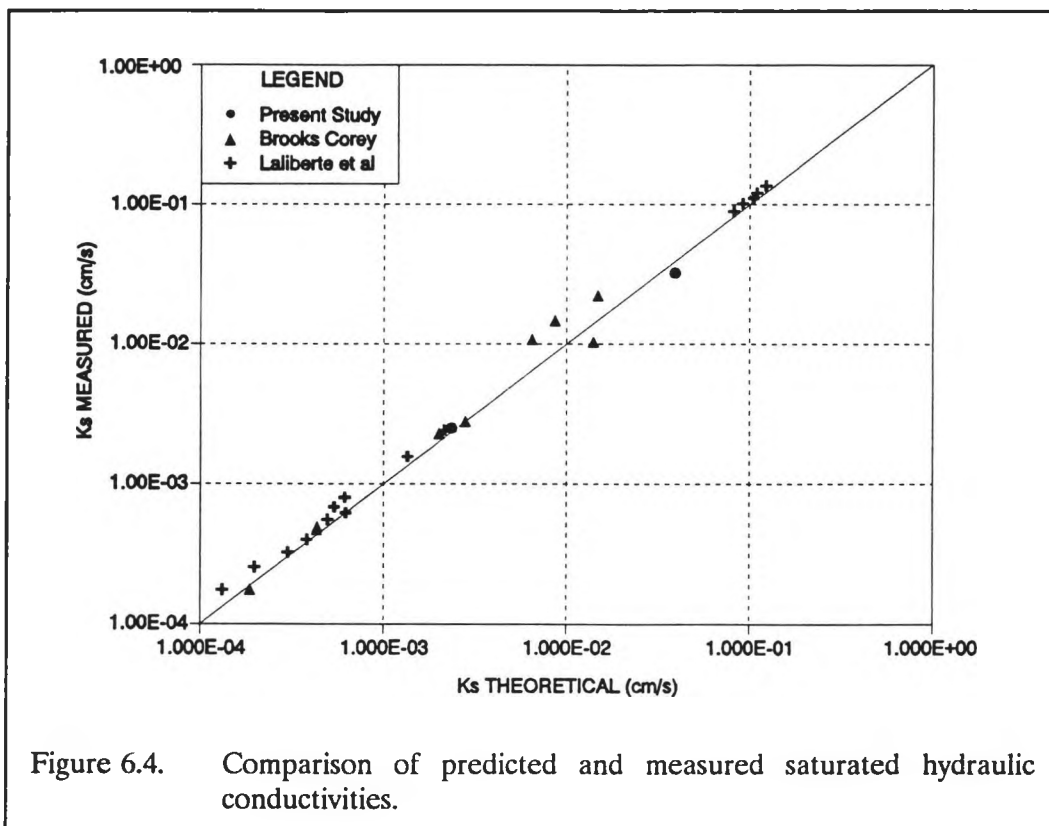
$$\frac{EC_b}{EC_w} = E \phi \frac{r_e}{r_h} S(r_{max}) \quad 6.8$$

where r_h , r_e and r_{max} are determined from the pore size distribution and D and E are constants. Swansen (1981) also presents an analysis using a pressure and porosity ratio to determine saturated hydraulic conductivities. Consequently, an analysis is performed to examine the dependence of B on h_b , θ_e and λ . A curve fitting exercise aimed at minimizing the regression coefficient between measured and predicted saturated hydraulic conductivities, resulted in the relationship,

$$B = \left(1 + 0.173 \left(\frac{h_b}{\theta_e} \right)^{\frac{\lambda}{2+\lambda}} \lambda^{0.185} \right) \quad 6.9$$

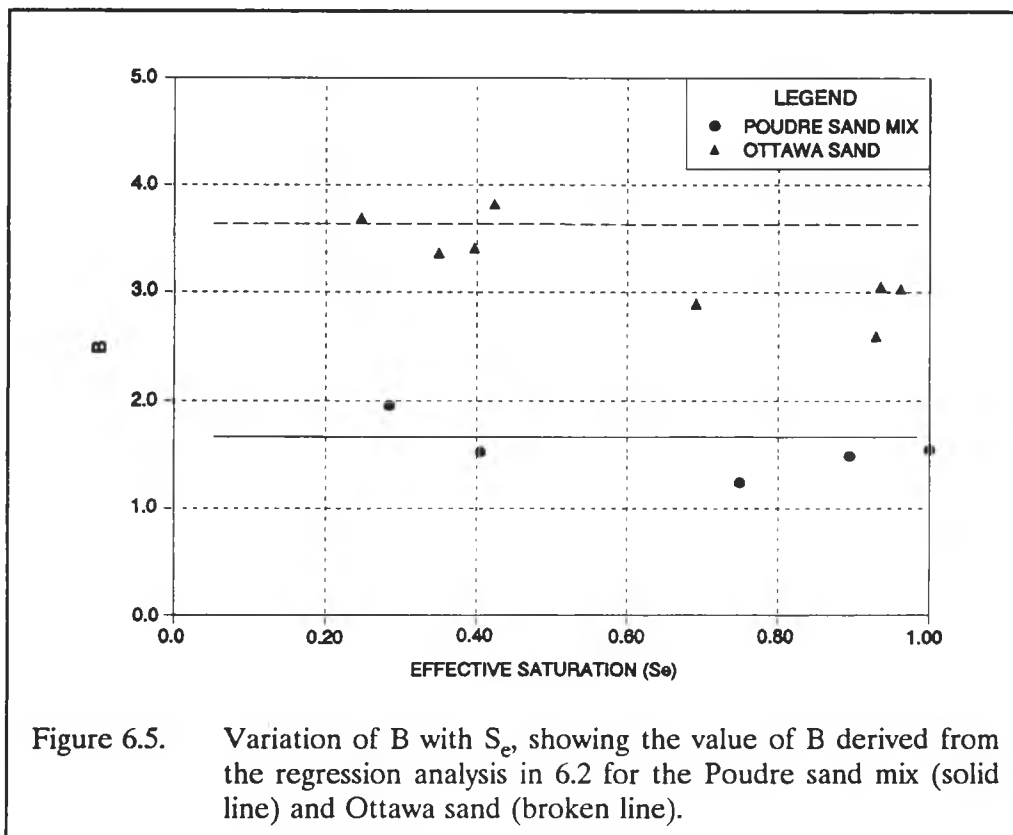
The values of B obtained from this expression varied from typical high values of 18.278, 10.932 and 9.827 for the Hygiene sandstone, Berea sandstone and glass beads, respectively, to a low value of 1.599 for the Poudre sand mix. Using Equation 6.9 to evaluate $B\theta_e$ for the Poudre sand mix and the Ottawa sand used in this study, resulted in values of 0.551 and 1.006

respectively. These results compare favorably to those estimated from the diffusion tests of these materials. The saturated hydraulic conductivities predicted using the expression for B presented in Equation 6.9 in the theoretical hydraulic conductivity expression represented by Equation 6.2 are compared to the measured saturated hydraulic conductivities in Figure 6.4. The regression coefficient between predicted and measured conductivities is 0.9952, indicating a successful estimation of B for the 26 porous media over four orders of magnitude. Analysis is continued on the variation of B and $n+m$ with unsaturated hydraulic properties.



6.3 Unsaturated Hydraulic Conductivity Analysis

The diffusion half-cell results of the Poudre sand mix and the Ottawa sand are now used together with the unsaturated hydraulic properties of these materials to determine the dependence of B and $n+m$ on the pore size distribution and the saturation. The value of B is calculated from the diffusion data represented in Figure 6.1, using $n=1$, and displayed in Figure 6.5. Also shown in Figure 6.5 is the value of B estimated by the regression analysis resulting in Equation 6.9. The estimated value of B for the Ottawa sand is 3.6, while the average value of B from the diffusion data close to this value, is 3.2. Similar agreement is obtained for the Poudre sand mix, with an estimated value for B of 1.8 and an average of the diffusion estimates of 1.6. While the maximum range of B is approximately 30 percent, the estimated value is considered sufficiently accurate to be adopted as a constant for all saturations.



Variations in $n+m$, however, could cause order of magnitude differences in the calculated conductivities at any saturation. The variation of $n+m$ can be examined by solving Equation 6.2 for $n+m$, which yields,

$$n+m = \frac{\log\left(\frac{2.5K_s\mu P_b^2}{\phi_e\rho g\sigma^2 B} \left(\frac{\lambda+2}{\lambda S_e^{\frac{2+\lambda}{\lambda}}}\right)\right)}{\log(\theta_e)} \quad 6.10$$

The values of $n+m$ derived using measured values for the unsaturated hydraulic conductivity and the pore size distribution parameters from the water retention characteristics are displayed in Figure 6.6. The values of $n+m$ vary from a minimum of 1.07 to a maximum of 2.37 for the Poudre sand mix and from 1.08 to 2.13 for the Ottawa sand. Simple relationships

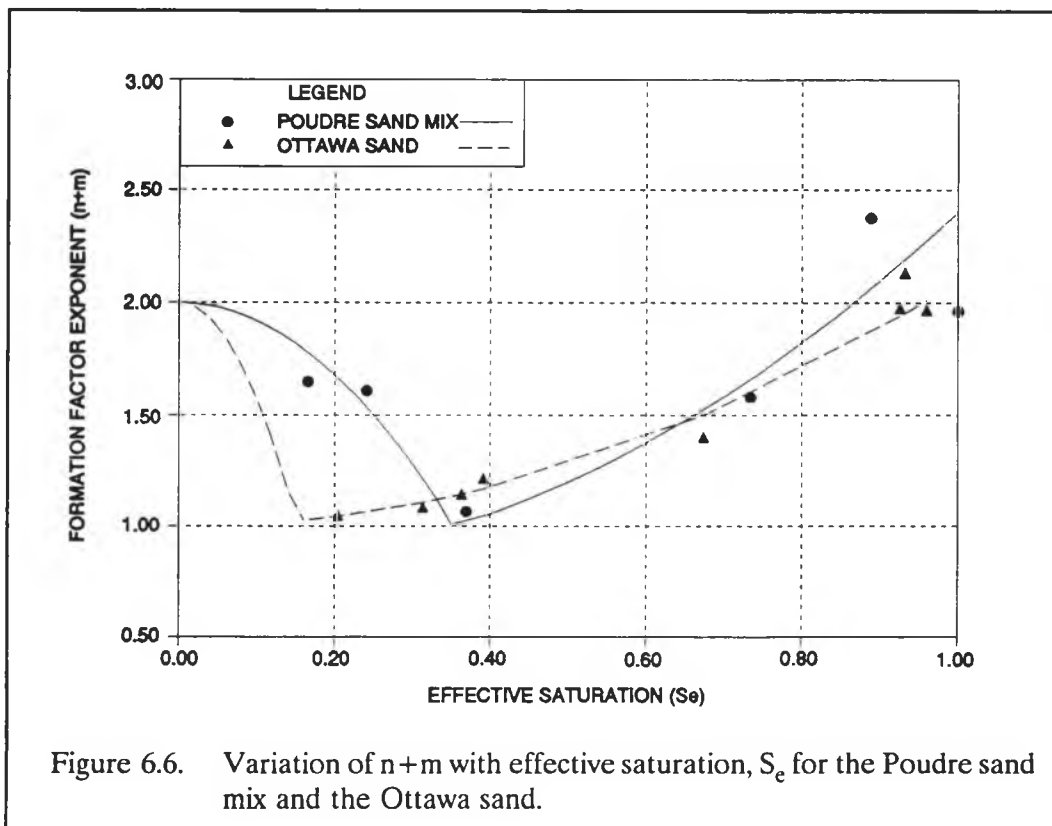


Figure 6.6. Variation of $n+m$ with effective saturation, S_e for the Poudre sand mix and the Ottawa sand.

have been fitted to the $n+m$ data as shown by the lines in Figure 6.6. These can be expressed as a function of the pore size distribution index as

$$n+m = a_1 + b_1 S_e^2 \quad \theta_c < \theta < \theta_s \quad 6.11a$$

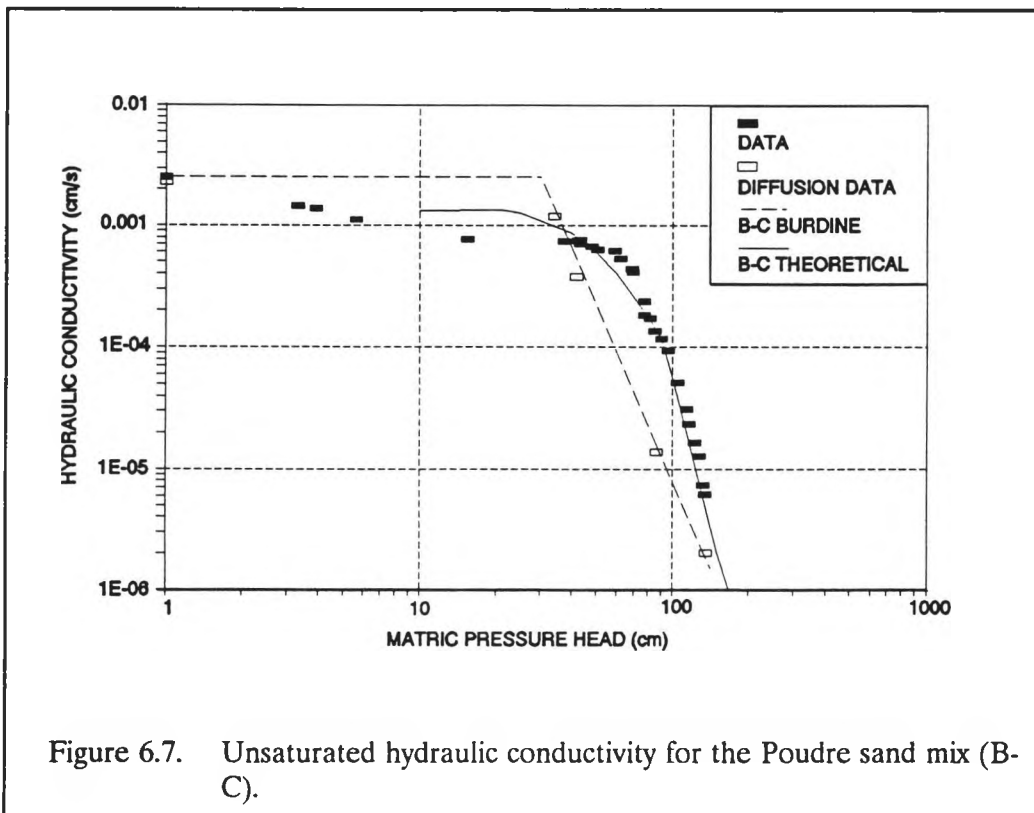
and

$$n+m = a_2 + b_2 S_e^2 \quad \theta_i < \theta < \theta_c \quad 6.11b$$

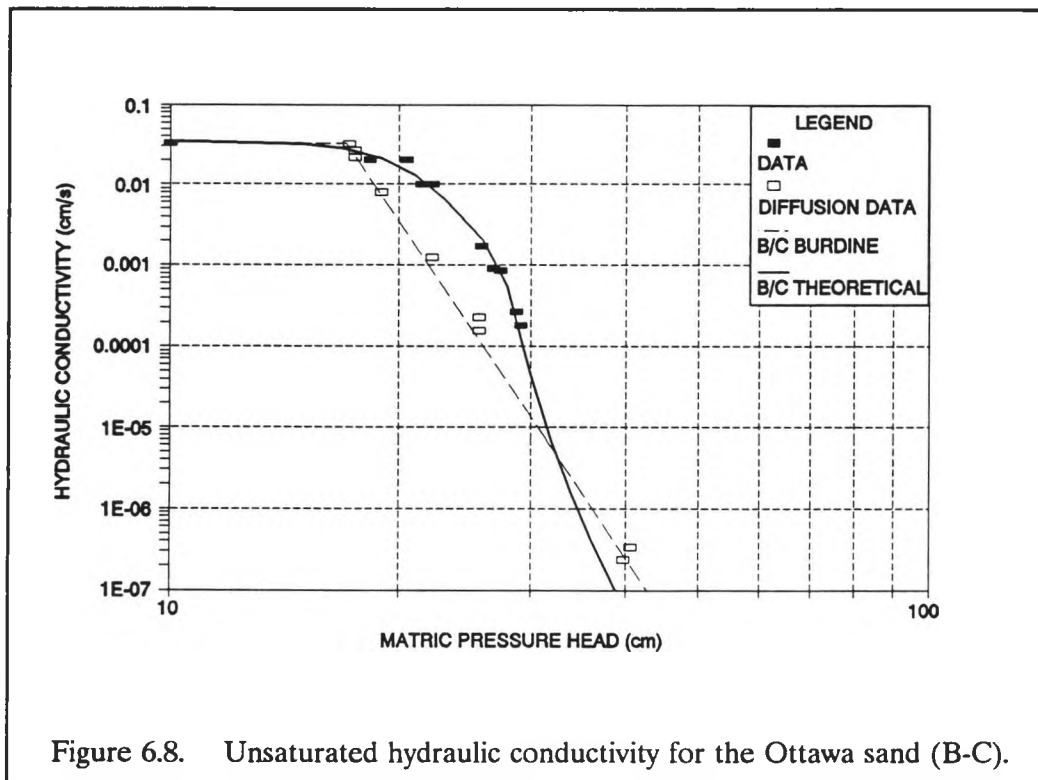
where,

$$\begin{aligned} a_1 &= 0.739 + 0.065\lambda \\ b_1 &= 1.884 + 0.196\lambda \\ a_2 &= 2.000 \\ b_2 &= -2.752 + 11.438\lambda \quad \text{and} \\ \theta_c &= 0.411 - 0.0654\theta \end{aligned}$$

Applying these theoretical expressions to the unsaturated hydraulic conductivity function given in Equation 6.2 yields a reasonable fit to the hydraulic conductivity measurements for



the Poudre sand mix and the Ottawa sand as shown in Figures 6.7 and 6.8. Also shown in these figures are the hydraulic conductivity relationship using the Brooks-Corey (B-C) retention characteristics in the Burdine equation as well as the hydraulic conductivities predicted using the diffusion data, B value in Equation 6.2 and using $n+m=2$. The theoretical relationship clearly produces the best fit to the observed data. This is to be expected since the measured hydraulic conductivities were used to derive the relationships for $n+m$.



A similar exercise is performed using the Van Genuchten (V-G) relationships for the retention characteristics. Solving the Burdine relationship for hydraulic conductivity using the Van Genuchten expression for the effective saturation and solving for $n+m$ yields:

$$n+m = \frac{\log \left(\frac{2.5 \mu K(S_e)}{\phi_e \rho g \sigma^2 \alpha^2 B \left(1 - \left(1 - S_e \frac{1}{M} \right)^M \right)} \right)}{\log(\theta_e)} \quad 6.12$$

This expression yields a similar relationship between $n+m$ and the effective saturation, as shown in Figure 6.9. A set of expressions for the curves fitted to the data are identical to

Equation 6.11, except that,

$$\begin{aligned} a_1 &= 0.658 + 0.0452N, \\ b_1 &= 2.126 - 0.1355N, \\ b_2 &= -16.85 + 7.9041N \text{ and} \\ \theta_c &= 0.492 - 0.0452N, \end{aligned}$$

where $M=1-2/N$.

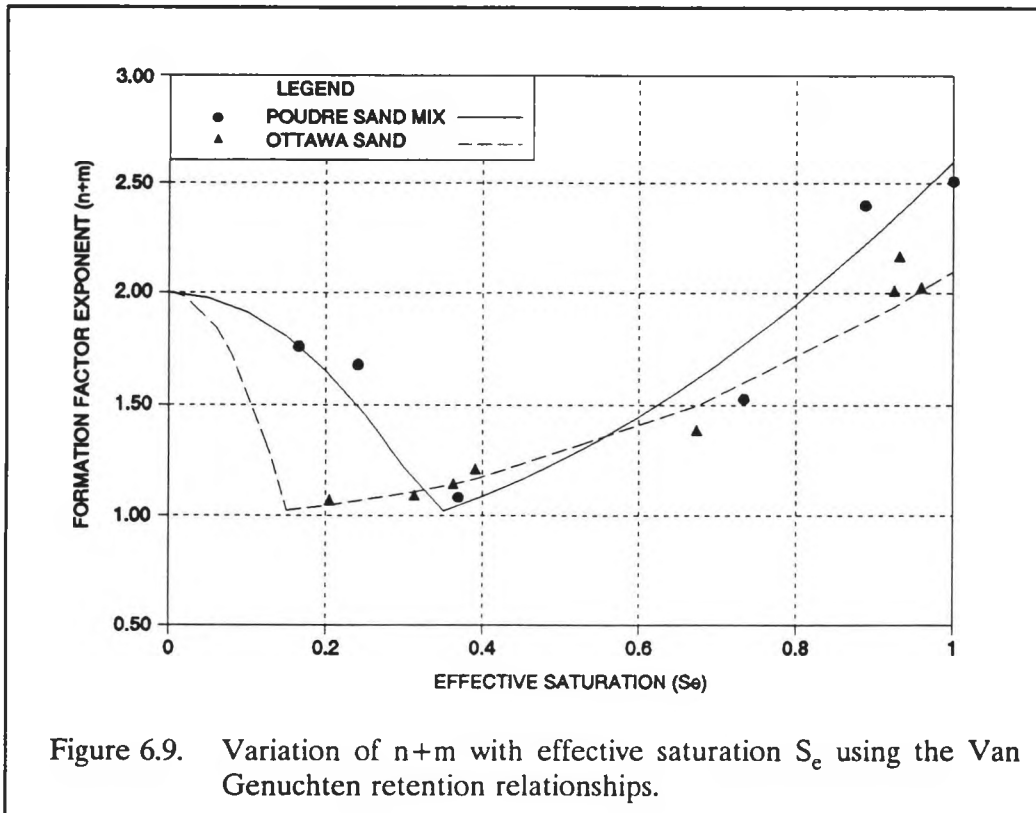


Figure 6.9. Variation of $n+m$ with effective saturation S_e using the Van Genuchten retention relationships.

These expressions yield the hydraulic conductivity curves shown in Figures 6.10 and 6.11. Also shown in these figures is the hydraulic conductivity relationship derived using the Van Genuchten retention relationship in the Burdine equation. Again, the theoretical relationships provide the best fit to the measured conductivity data.

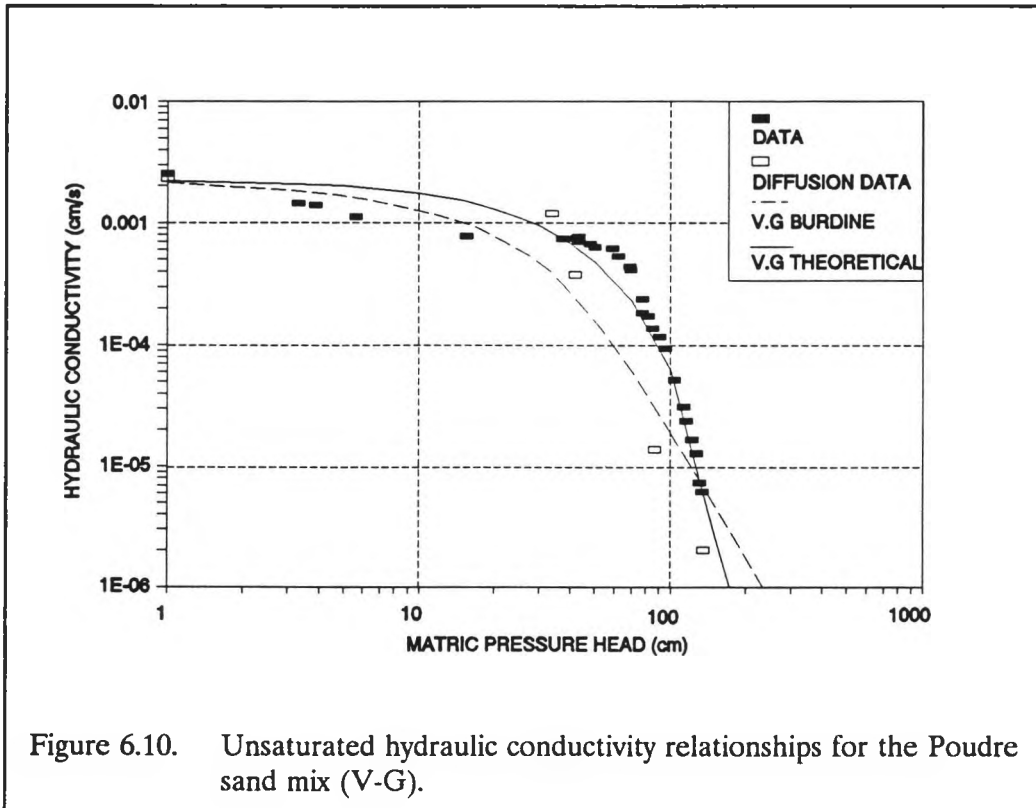
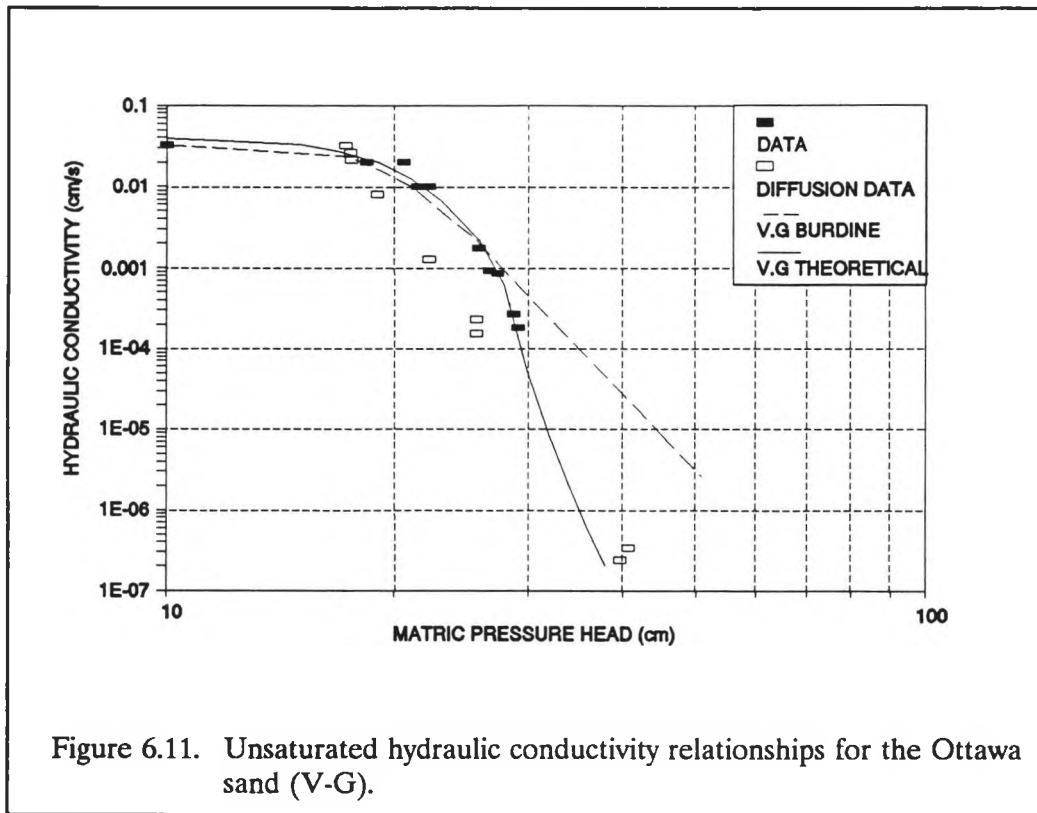


Figure 6.10. Unsaturated hydraulic conductivity relationships for the Poudre sand mix (V-G).

The observations of the dependence of $n+m$ on effective saturation and pore size distribution index made here are based on the limited data afforded by the Poudre sand mix and Ottawa sand analyses. In addition, the variation of $n+m$ with effective saturation is determined primarily by the curvature of the measured hydraulic conductivity/ matric pressure head data. While this curvature is not typical of the straight line relationship predicted by the Brooks-Corey retention function, the data for both materials display the curvature well beyond the Brooks-Corey air entry pressure, justifying the application of the observed conductivity relationships to the analysis.



A few significant observations can be made on the results of the retention, solute diffusion and hydraulic conductivity analyses for the two materials in this study. There is an apparent difference between the influence of n on the diffusion behavior and the influence of m on the hydraulic conductivity behavior of the porous media tested. While the value of n derived from the diffusion analysis varied by a maximum of 0.2, the variation of $m+n$, derived from the conductivity analysis, was greater than 1.0. Hence, it is evident that the hydraulic conductivity is more strongly influenced by tortuosity and constrictivity fluctuations than the diffusion process. This observation is supported in a "bond shrinkage" model developed in Wong *et al.* (1984). It is also evident that the variation of $n+m$ can be related to the pore size distribution index, as speculated upon in Wyllie and Spangler (1952), although the relationships derived are limited by the small number of porous media tested in this study.

The variation of $n+m$ with effective saturation results in a severely non-linear expression for unsaturated hydraulic conductivity and would constrain analytical solutions to problems of flow in porous media. Some plausible explanation for this variation may result from further detailed testing. However, present speculation of the behavior of $n+m$ is restricted to that represented in Figures 6.6 and 6.9. The exponent, $n+m$, significantly reduces the a maximum at saturation where liquid discharges through the full spectrum of pore size variations, thereby contributing to a strong influence of the tortuosity and constrictivity on the hydraulic conductivity. As saturation decreases, the variation of sizes and constrictions through which the fluid flows may decrease to a minimum at some specific saturation, after which, with further reduction in saturation, the variation in flow depths between fluid filled pores and film flow over particles may again be significant. Hence, despite the observations being limited to only two porous media, some fruitful avenues for future research can be identified.

CHAPTER 7

CONCLUSIONS AND RECOMMENDATIONS

7.1 Problem Summary

Common mathematical models of the relative unsaturated hydraulic conductivity of porous media represent the tortuosity and constrictivity of flow pathways within the media as a function of the effective saturation. The form of the variation of tortuosity and constrictivity of flow pathways, or formation factor with effective saturation, has been based on observations of the variation of either the electrical conductance or the relative hydraulic conductivity with effective saturation. These observations have led to simple expressions for the formation factor as the effective saturation raised to an exponent. The square of the effective saturation is used in the Burdine model, and the root of the effective saturation is used in the Mualem model. Recent attempts at using these models to describe observed unsaturated hydraulic conductivities have allowed optimization of the effective saturation exponent in fitting the model to the observed conductivities. A wide variation in the value of this exponent has resulted, casting some uncertainty on three aspects of these relationships. First, the structure and formulation of the models may be unrealistic; secondly, the manner in which the tortuosity and constrictivity are represented may be too simplistic; and thirdly, the manner in which the measurements are made or the data represented may not be commensurate with the model formulation. This study investigated the second aspect and, in particular, determining how the porous media characteristics affect the tortuosity and constrictivity. Previous studies have relied on one of two methods to account for tortuosity and constrictivity. In the first method, observations of diffusion or electrical conductivity

made on various porous media are used to develop a universal relationship for the dependence of the formation factor on effective saturation (Wyllie and Spangler, 1952; Brooks and Corey, 1966). This relationship is then applied to relative hydraulic conductivity models. The second method relied on a regression analysis of relative unsaturated hydraulic conductivity data for many different porous media to derive the optimum form of the formation factor (Mualem, 1976). Concurrent observations of the diffusion or electrical conductivity characteristics in addition to the hydraulic conductivity and retention characteristics were never made on the same porous media. This study was, therefore, conducted to make such concurrent observations as well as to determine the properties of the porous media that could account for the wide variation in the fitted exponent used to represent the formation factor.

7.2 Summary of This Study

This study begins with a review of the different approaches in representing the formation factor both in electrical conductivity and hydraulic conductivity models. Some fundamental differences between the approaches are highlighted. A theoretical development is presented that develops simple relationships for the diffusion and hydraulic conductivity in porous media, treating the contributions to the formation factors of each of these two processes separately. The theoretical development resulted in simple expressions for the ratio of effective diffusion to free diffusion coefficient as,

$$\frac{D_e}{D_o} = B \theta^n \quad 7.1$$

and for the unsaturated hydraulic conductivity as,

$$K(S_e) = \phi_e \frac{\rho g \sigma^2}{k_o \mu P_b^2} B \theta_e^{n+m} S_e^{\frac{2+\lambda}{\lambda}} \left(\frac{\lambda}{2+\lambda} \right) \quad 7.2$$

where the variables are defined in the list of symbols.

In order to examine the dependence of the variables B, n, and m on the characteristics of porous media, two porous media with distinctly different pore size distributions were tested to establish their diffusion, retention and hydraulic conductivity characteristics. The first material, a mixture of Poudre sand size fractions, had a pore size distribution index of 0.94, and the second material, an Ottawa sand, had a pore size distribution index of 4. The results of the diffusion measurements revealed a significant difference between the variable, B, for the materials. Further examination of the variable, B, was conducted by expanding the data base, using a set of results of measurements on other porous media that were extracted from the literature. A relationship between the variable, B, and the pore size distribution index, the effective porosity, and the air entry pressure was established. This allowed a universal relationship for the saturated hydraulic conductivity to be established from the retention characteristics of the materials. Further examination of the results of the diffusion, retention and hydraulic conductivity analyses of the two materials prepared in this study concluded in the definition of relationships between n, m, and the pore size distribution index. Specific conclusions and recommendations can be made from the results of these analyses.

7.3 Conclusions

The conclusions that can be drawn from the results of this study are as follows.

- The ratio of effective diffusion coefficient to free diffusion coefficient at saturation, expressed as $B\theta_s^n$ was 0.5 for the Poudre sand mix and approximately unity for the Ottawa sand.
- By examination of the saturated conductivity data of the Poudre sand mix, the Ottawa sand and a range of other porous media, the variable, B, was found to be dependent, not only on the pore size distribution index, but on the effective porosity and the air entry pressure of the materials as well, as defined by the Brooks and Corey retention relationship. A relationship for the saturated hydraulic conductivity was defined using these variables to successfully predict measured saturated hydraulic conductivities, ranging between 1.113E-01 cm/s and 1.736E-04 cm/s and including 26 porous media.
- The exponent variable, n, defining the variation of the formation factor with saturation in the diffusion process did not appear to differ markedly between the Poudre sand mix and the Ottawa sand (materials with significantly different pore size distributions).
- The exponent variable, m, influenced by the hydraulic conductivity process, was found to vary to a greater extent than n for the two materials tested.
- Using the unsaturated hydraulic conductivity data for the Poudre sand mix and the Ottawa sand, the exponent variable, m, was found to vary as a function of effective saturation.

7.4 Recommendations

The following recommendations are made based on the outcome of this study.

- The dependence of the formation factor on porous media hydraulic characteristics defined in this study should be verified through additional testing on a wide range of porous media in which the diffusion, retention and hydraulic conductivity characteristics are observed with each porous media in the same morphological state for each of the three characteristic tests.
- The model of the formation factor defined in this study should be further developed to establish the influence of an "effective pore size" parameter as well as the pore size distribution and effective porosity on the formation factor.
- Measurements of the diffusion, retention and hydraulic conductivity characteristics should be conducted on the drying and wetting cycles to establish the dependence of the formation factor on parameters defined from the drying and wetting characteristics.

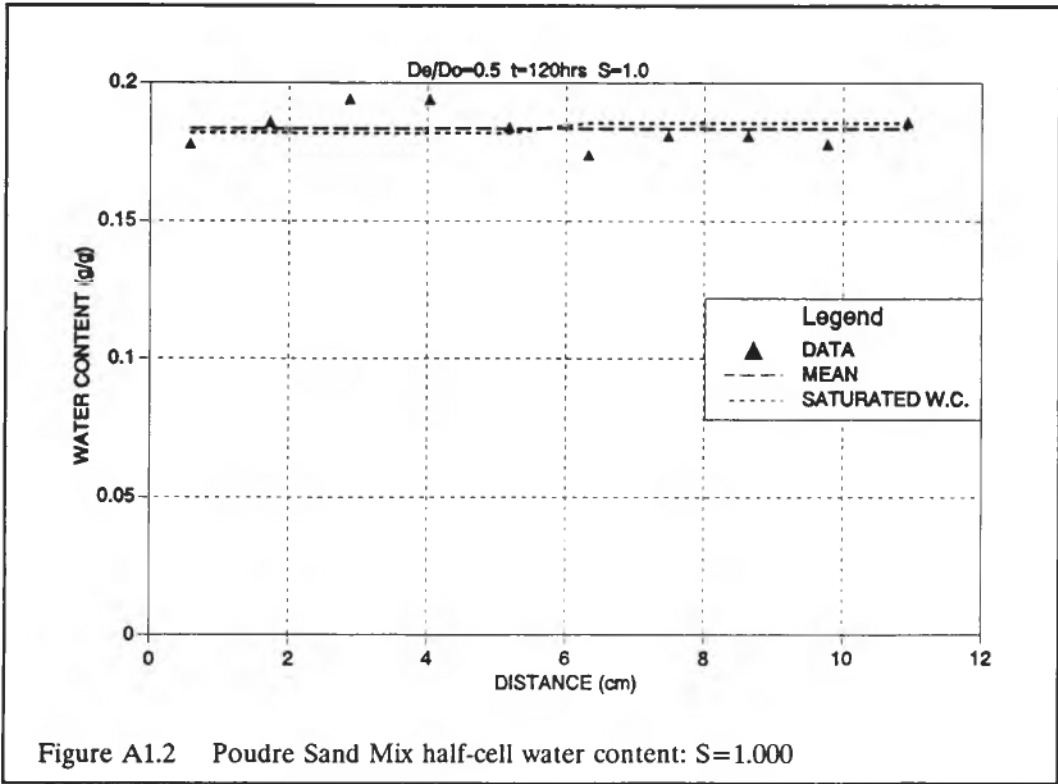
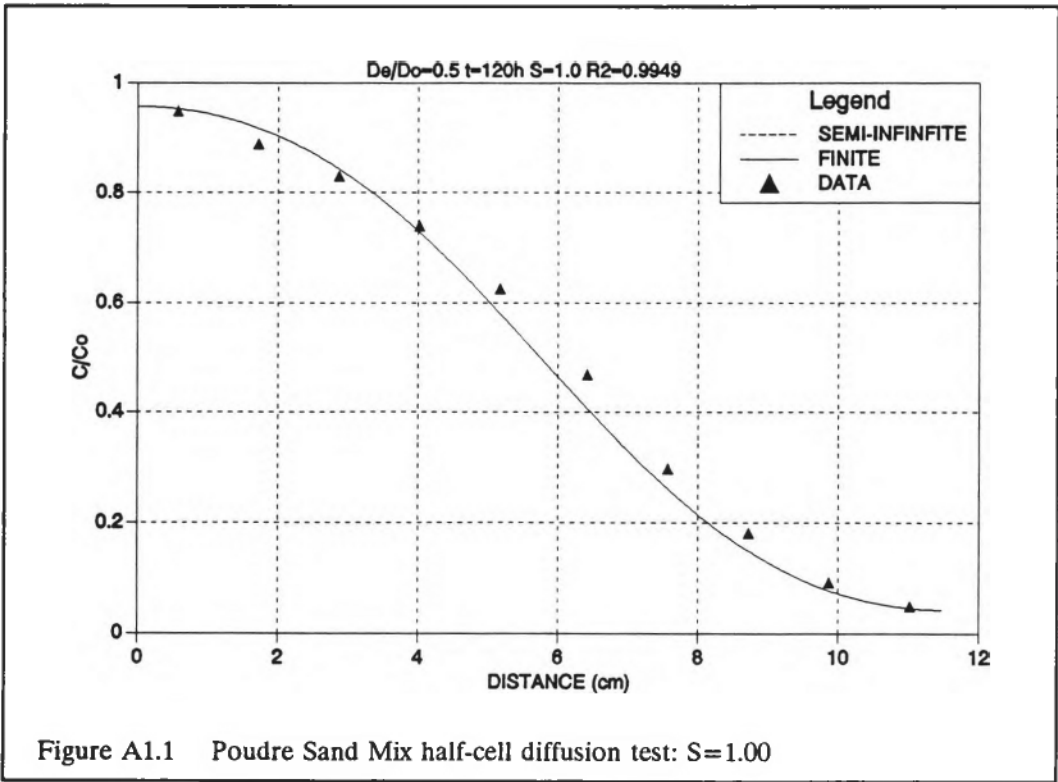
REFERENCES

- Alexander, L. and R.W. Skaggs. 1986. Predicting the unsaturated hydraulic conductivity from the soil water characteristic. *Trans. A.S.A.E.* 29(1):176-184.
- Arah, J.R.M. and B.C. Ball. 1994. A functional model of soil porosity used to interpret measurements of gas diffusion. *European Journal of Soil Science.* 44:135-144.
- Bear, J. 1972. *Dynamics of Fluids in Porous Media.* American Elsevier Publishing Co. Inc. New York, NY.
- Brooks, R.H. and A.T. Corey. 1964. Hydraulic properties of porous media. Colorado State University: Hydrology Paper No. 3. Fort Collins, CO. 24 p.
- Brooks, R.H. and A.T. Corey. 1966. Hydraulic properties of porous media. *Proc. Amer. Soc. Civil Eng. Irrig. and Drainage Div.* 92(IR2):61-88.
- Burdine, N.T. 1953. Relative permeability calculations from pore size distribution data. *Trans. A.I.M.E.* 193:71-78.
- Carman, P.C. 1937. Fluid flow through granular beds. *Trans. Inst. Chem. Eng.* 15:150-166.
- Childs, E.C. and N. Collis-George. 1950. The permeability of porous media. *Proc. Royal Soc. A(201):*392-405.
- Collin, M. and A. Rasmuson. 1988. A Comparison of gas diffusivity models for unsaturated porous media. *Soil Sci. Soc. Am. J.* 52:1559-1565.
- Corey A.T. 1986. *Mechanics of Immiscible Fluids in Porous Media.* Water Resources Publications. Littleton, CO.
- Cornell, D. and D. L. Katz. 1953. Flow of gases through consolidated porous media. *Ind. Eng. Chem.* 45(10):2145-2152.
- Dullien, F.A.L. 1992. *Porous Media. Fluid Transport and Pore Structure,* 2nd Ed. Academic Press, San Diego, CA.
- Doyen, P.M. 1988. Permeability, conductivity, and pore geometry of sandstone. *J. Geophys. Res.* 93(B7):7729-7740.
- Faris, S.R., L.S. Gournay, L.B. Lipson, and T.S. Webb. 1954. Verification of tortuosity equations. *Bull. Amer. Assoc. Petrol. Geol.* 38(3):2226-2232.
- Katz, A.J. and A.H. Thompson. 1987. Prediction of rock electrical conductivity from mercury injection measurements. *J. Geophys. Res.* 92(B1):599-607.
- Klute, A. and J. Letey. 1958. The Dependence of Ionic Diffusion on the Moisture Content of Nonadsorbing Porous Media. *Soil Sci. Soc. Am. Proc.* 22:213-215.

- Laliberte, G.E., A.T. Corey and R.H. Brooks. 1966. Properties of unsaturated porous media. Colorado State University. Hydrology Paper 17, Fort Collins CO.
- Lenhard, R.J., J.C. Parker and J.J. Kaluarachchi. 1991. Comparing simulated and experimental hysteretic two-Phase transient fluid flow phenomena. *Water Resour. Res.* 27(8):2113-2124.
- Millington, R.J. and R.C. Quirk. 1960. Diffusion in aggregated porous media. *Soil Science.* 111(6):372-378.
- Mishra, S. and J.C. Parker. 1990. On the relation between saturated conductivity and capillary retention characteristics. *Ground Water.* 28(5):775-777.
- Mualem, Y. 1976. A new model for predicting hydraulic conductivity of unsaturated porous media. *Water Resour. Res.* 12(3):513-522.
- Mualem, Y. and G. Dagan. 1978. Hydraulic conductivity of soils: Unified approach to the statistical models. *Soil Sci. Soc. Am. J.* 42:392-395.
- Mualem, Y. 1986. Hydraulic conductivity of unsaturated soils: Prediction and formulas. *In Klute A., Ed. Methods of Soil Analysis, Part 1. Physical and Mineral Methods. Agronomy Monograph No 9., Madison, WI.*
- Mualem, Y. and S.P. Friedman. 1991. Theoretical prediction of electrical conductivity in saturated and unsaturated soil. *Water Resour. Res.* 27(10):2771-2777.
- Perkins, F.M., J.S. Osaba and K.H. Ribe. 1956. Resistivity of sandstones as related to the geometry of their interstitial water. *Geophysics.* 21(4):1071-1086.
- Purcell, W.R. 1949. Capillary pressures--Their measurement using mercury and the calculation of permeability therefrom. *Trans. A.I.M.E.* 186:39-48.
- Rawls, W.J., D.L. Brakensiek and S.D. Logsdon. 1993. Predicting saturated hydraulic conductivity utilizing fractal principles. *Soil Sci. Soc. Am. J.* 57:1193-1197.
- Rhoades, J.D., P.A.C. Raats and R.J. Prather. 1976. Effects of liquid-phase EC, θ and surface conductivity on bulk soil EC. *Soil Sci. Soc. Am. J.* 40:651-655.
- Rieu, M. and G. Sposito. 1991. Fractal fragmentation, soil porosity and soil water properties: I theory. *Soil Sci. Soc. Am. J.* 55:1231-1238.
- Schuh, W.M. and R.L. Cline. 1990. Effect of soil properties on unsaturated hydraulic conductivity pore-interaction factors. *Soil Sci. Soc. Am. J.* 54:1509-1519.
- Shepard, J.S. 1993. Using a fractal model to compute the hydraulic conductivity function. *Soil Sci. Soc. Am. J.* 57:300-306.
- Stephens, D.B. and K.R. Rehfeldt. 1985. Evaluation of closed-form analytical models to calculate conductivity in a fine sand. *Soil Sci. Soc. Am. J.* 49:12-19.
- Swanson, B. F. 1981. A simple correlation between permeabilities and mercury capillary pressures. *J. Pet. Tech.* 1981(Dec):2498-2504.

- Van Brakel, J. and P.M. Heertjes. 1974. Analysis of diffusion in macroporous media in terms of a porosity, a tortuosity and a constrictivity factor. *Int. J. Heat and Mass Transfer.* 17:1093-1103.
- Van Genuchten, M.Th. 1980. A closed-form equation for predicting the hydraulic properties of unsaturated soils. *Soil Sci. Soc. Am. J.* 44:892-898.
- Van Genuchten, M.Th. and D.R. Nielsen. 1985. On describing and predicting the hydraulic properties of unsaturated soils. *Ann. Geophys.* 3:615-628.
- Van Genuchten, M.Th., F.J. Leij and S.R. Yates. 1991. The RETC code for quantifying the hydraulic functions of unsaturated soils. EPA/600/2-91/065, Ada, Oklahoma.
- Vereecken, H. 1995. Estimating the unsaturated hydraulic conductivity from theoretical models using simple soil properties. *Geoderma.* 65:81-92.
- Wong, P., J. Koplik and J.P. Tomanic. 1984. Conductivity and permeability of rocks. *Phys. Rev. B.* 30(11):6606-6614.
- Wyllie, M.R.J. and M.B. Spangler. 1952. Application of electrical resistivity measurements to problem of fluid flow in porous media. *Bulletin Amer. Assoc. Petr. Geol.* 36:359-403.
- Wyllie, M.R.J. and A.R. Gregory. 1955. Fluid flow through unconsolidated porous media. *Ind. Eng. Chem.* 47:1379-1388.
- Wyllie, M.R.J. and G.H.F. Gardner. 1958. The generalized Kozeny-Carman equation; Its application to problems of multiphase flow in porous media: Part 2 A novel approach to problems of fluid flow. *World Oil. Production Section.* April 1958:210-228.
- Yates, S.R., M.Th. Van Genuchten, A.W. Warrick and F.J. Leij. 1992. Analysis of measured, predicted, and estimated hydraulic conductivity using RETC computer program. *Soil Sci. Soc. Am. J.* 56:347-354.

APPENDIX A
DIFFUSION HALF-CELL RESULTS



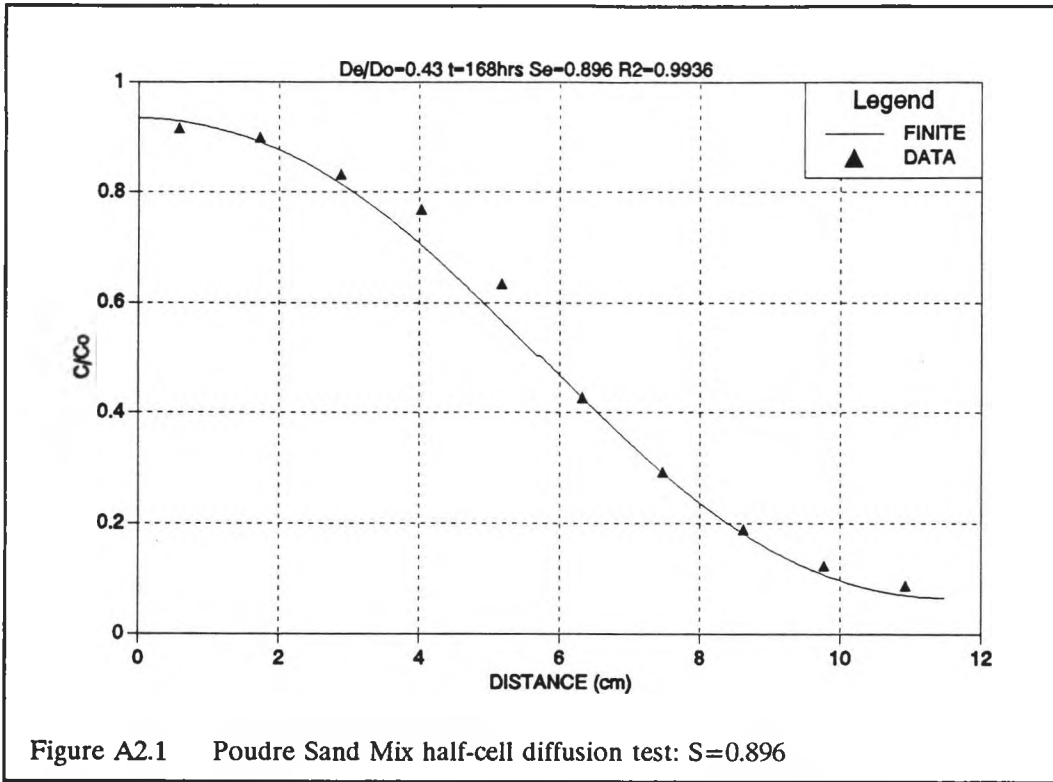


Figure A2.1 Poudre Sand Mix half-cell diffusion test: $S=0.896$

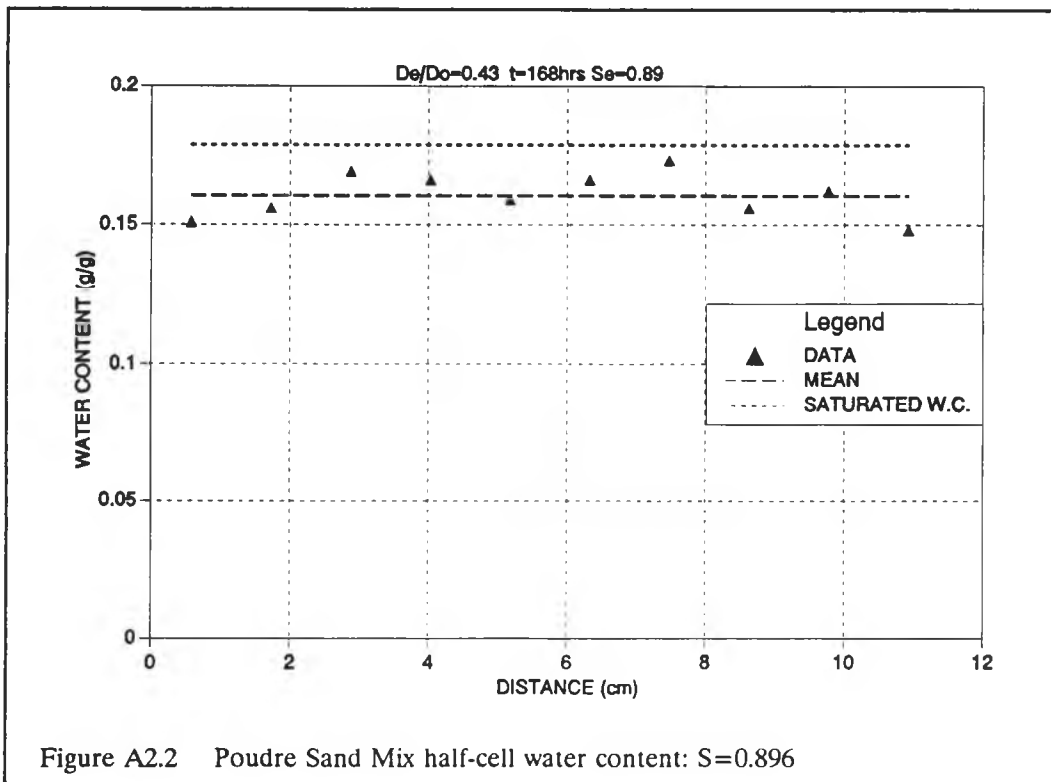
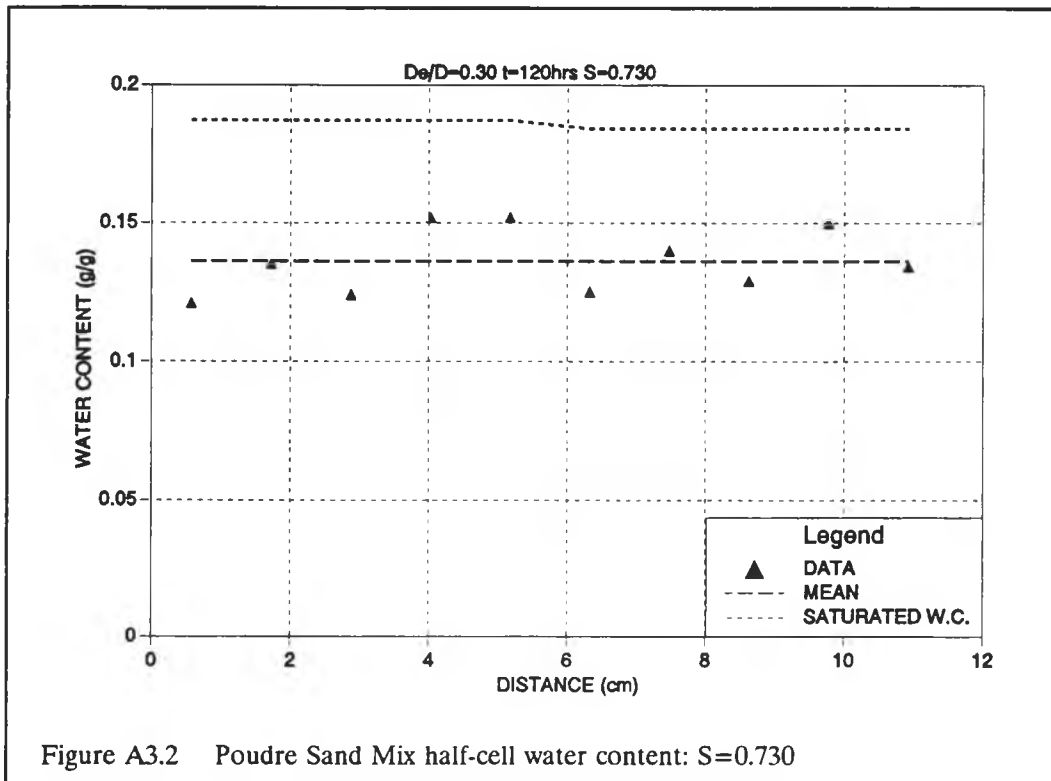
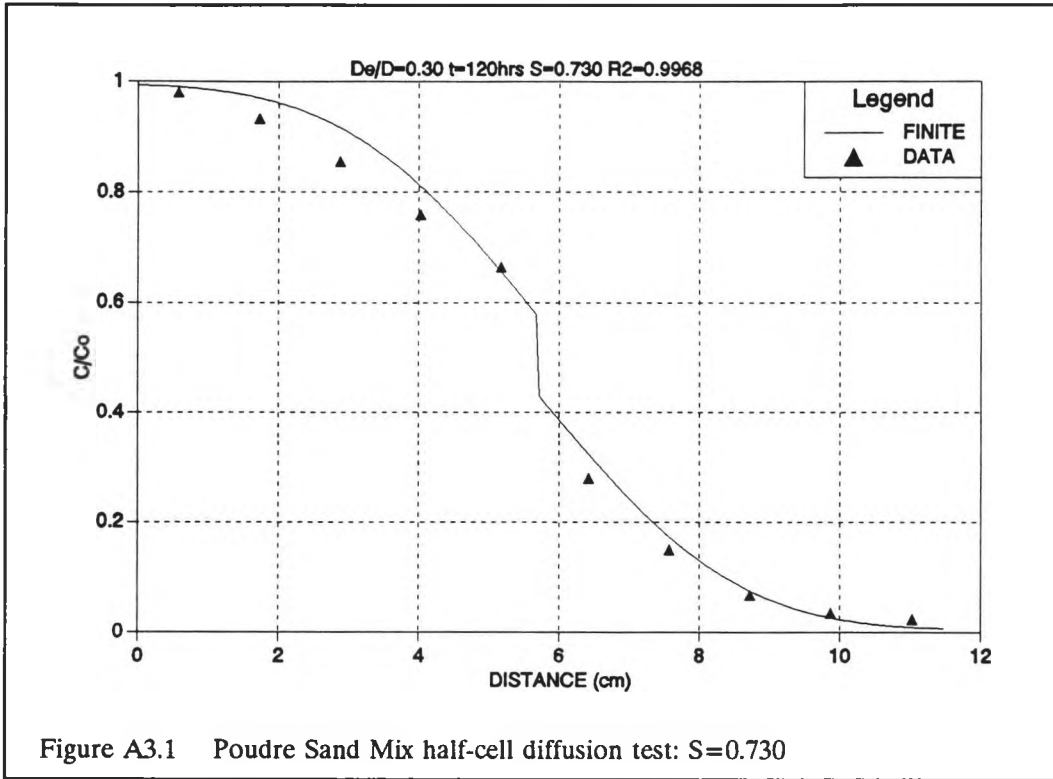


Figure A2.2 Poudre Sand Mix half-cell water content: $S=0.896$



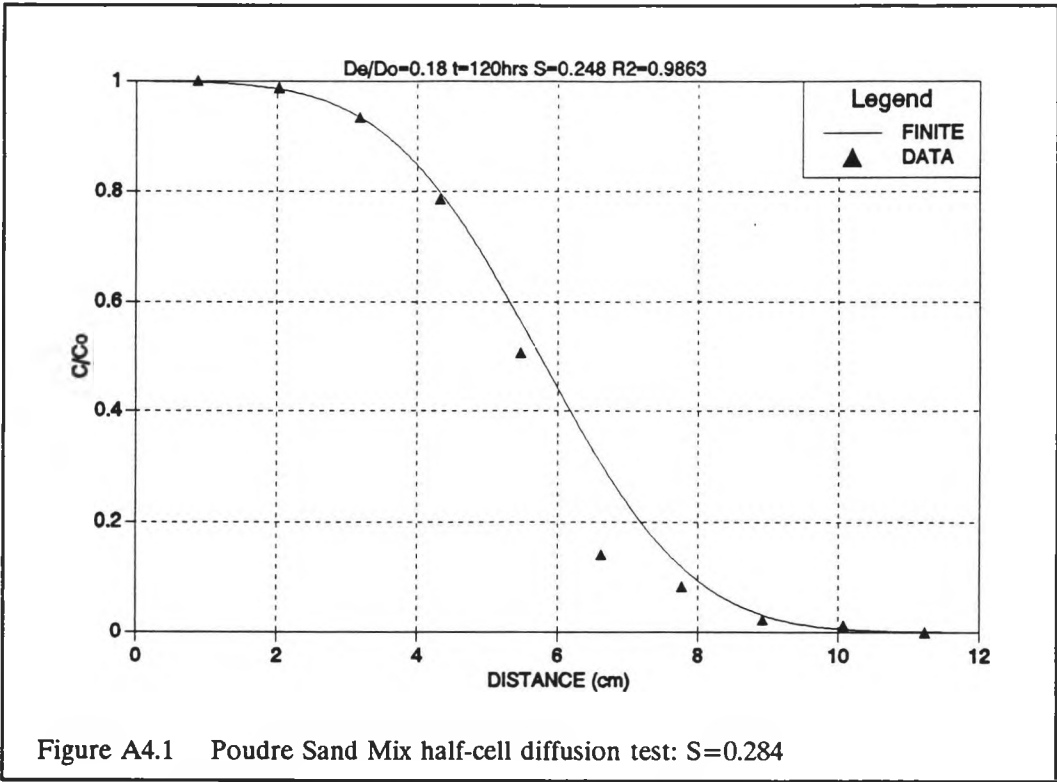


Figure A4.1 Poudre Sand Mix half-cell diffusion test: $S=0.284$

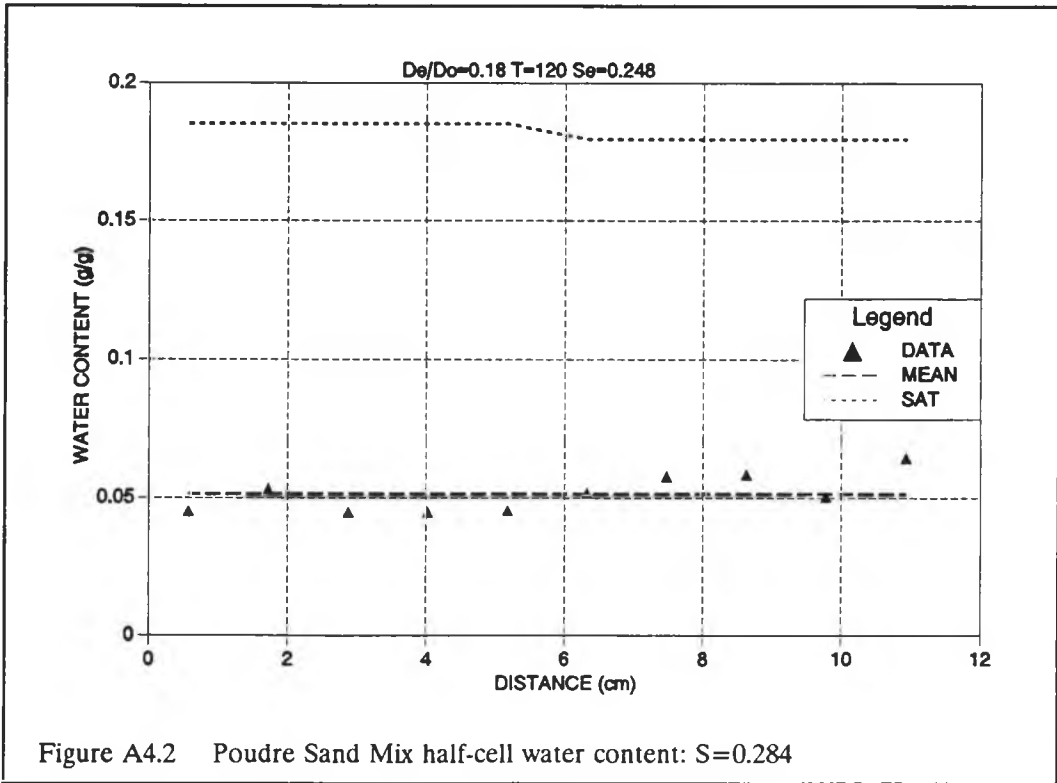
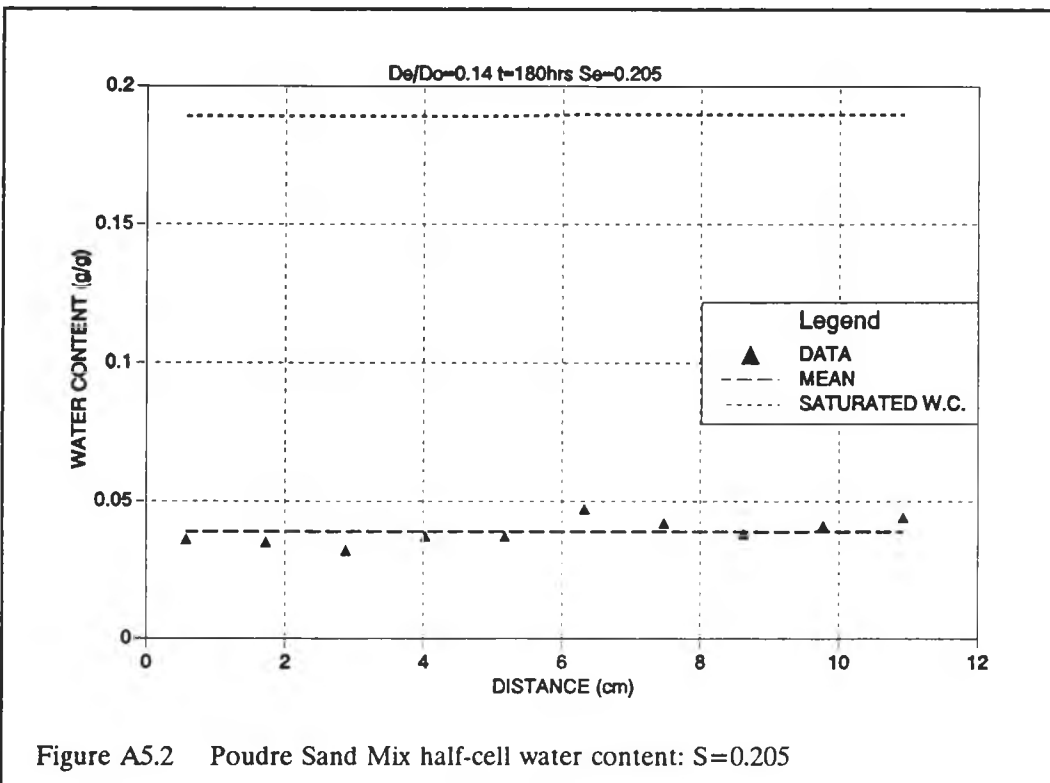
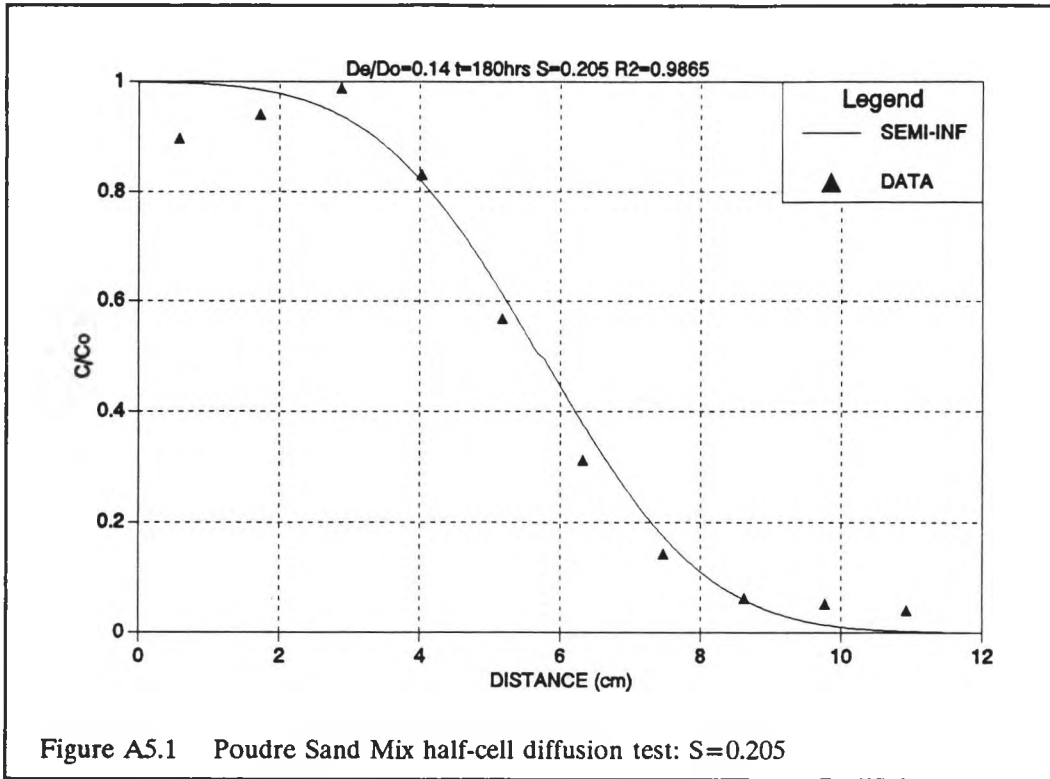


Figure A4.2 Poudre Sand Mix half-cell water content: $S=0.284$



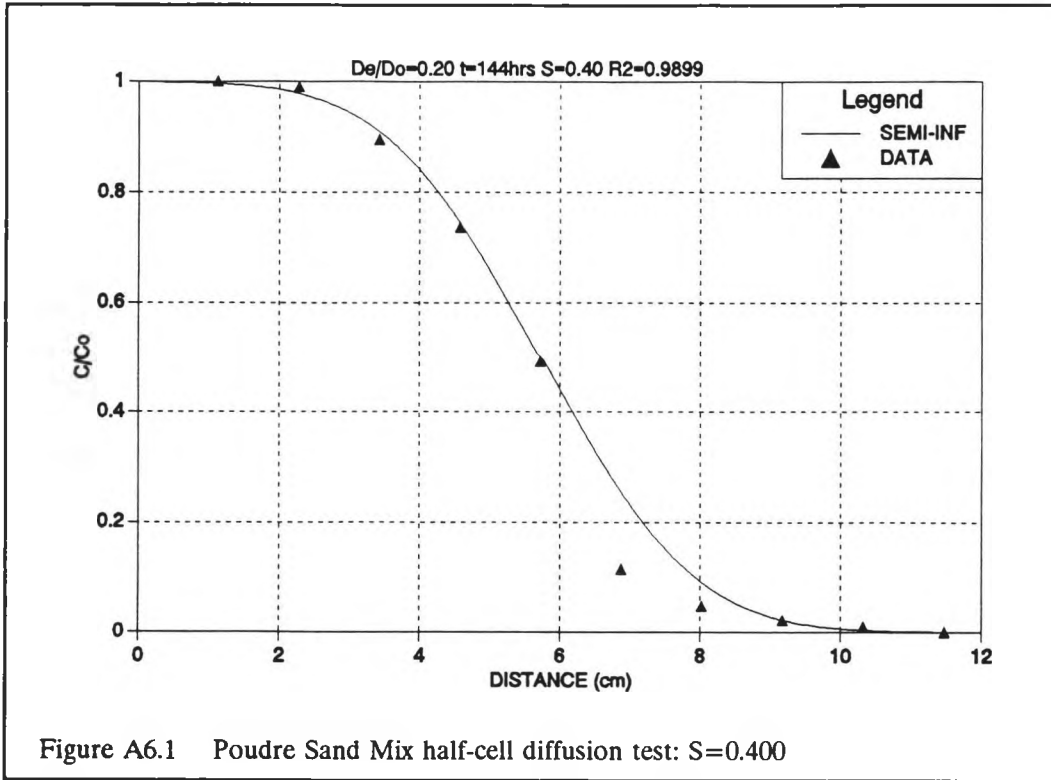


Figure A6.1 Poudre Sand Mix half-cell diffusion test: $S=0.400$

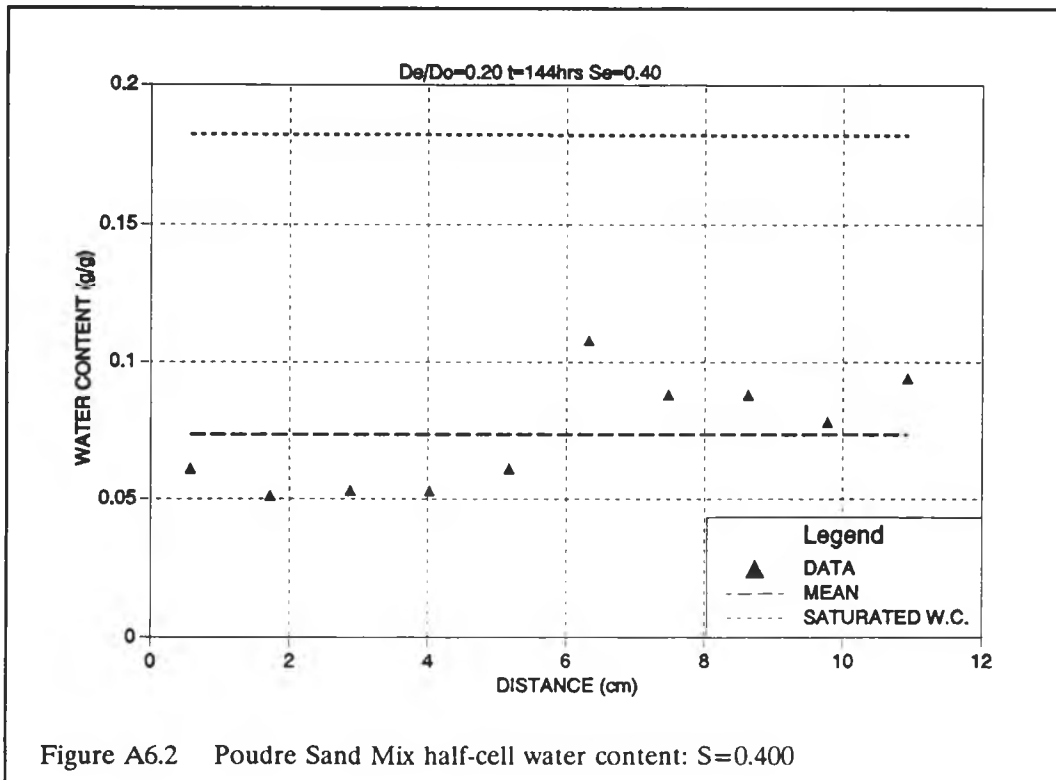


Figure A6.2 Poudre Sand Mix half-cell water content: $S=0.400$

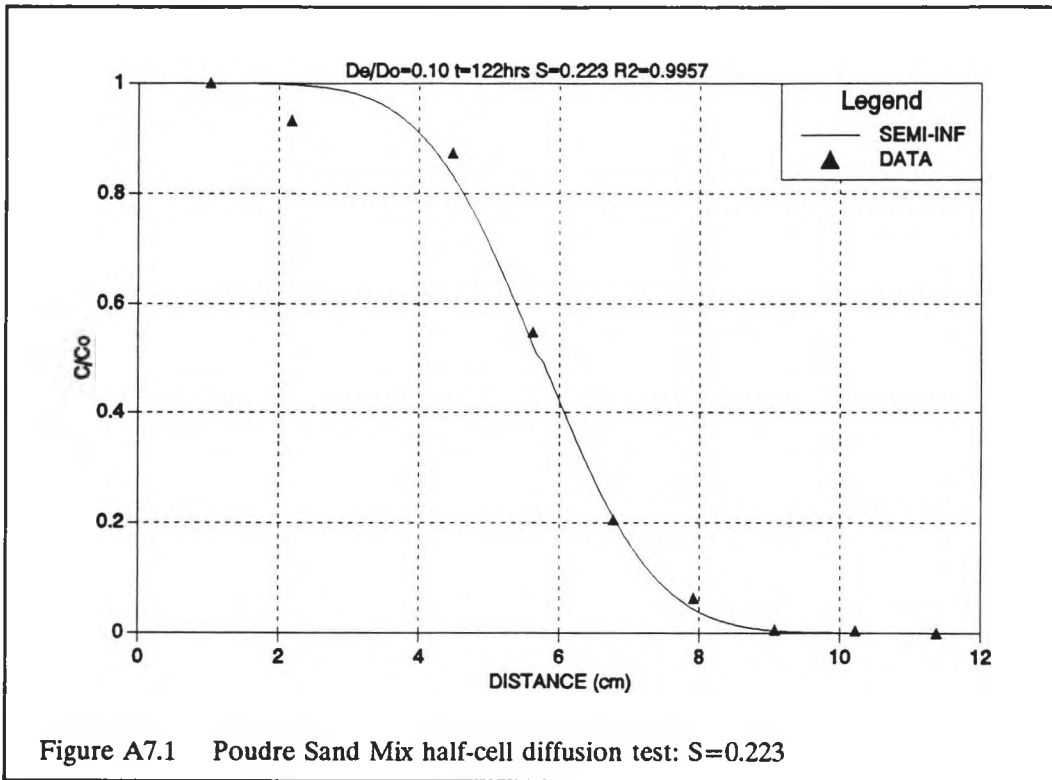


Figure A7.1 Poudre Sand Mix half-cell diffusion test: $S=0.223$

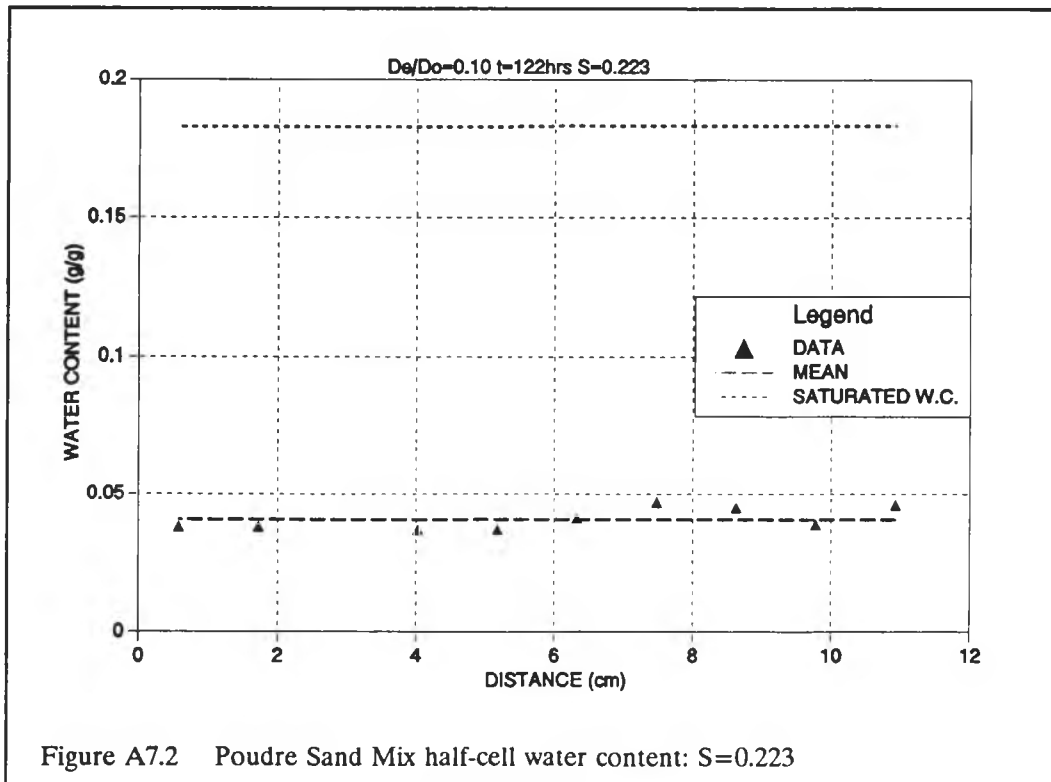


Figure A7.2 Poudre Sand Mix half-cell water content: $S=0.223$

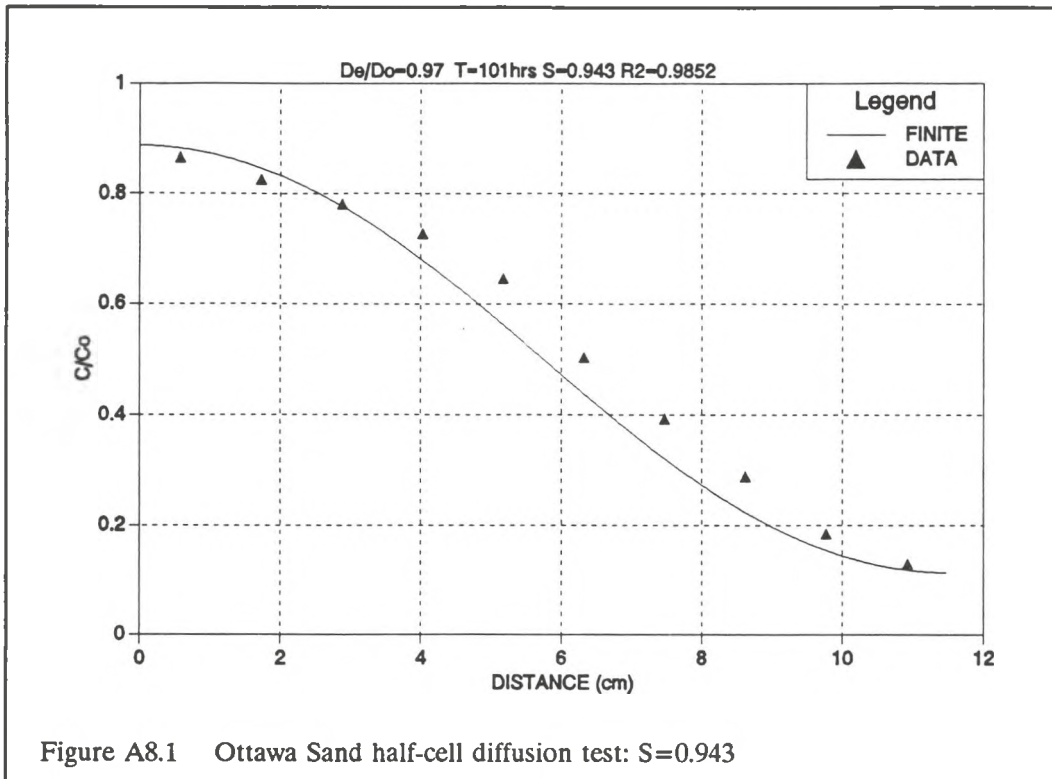


Figure A8.1 Ottawa Sand half-cell diffusion test: $S=0.943$

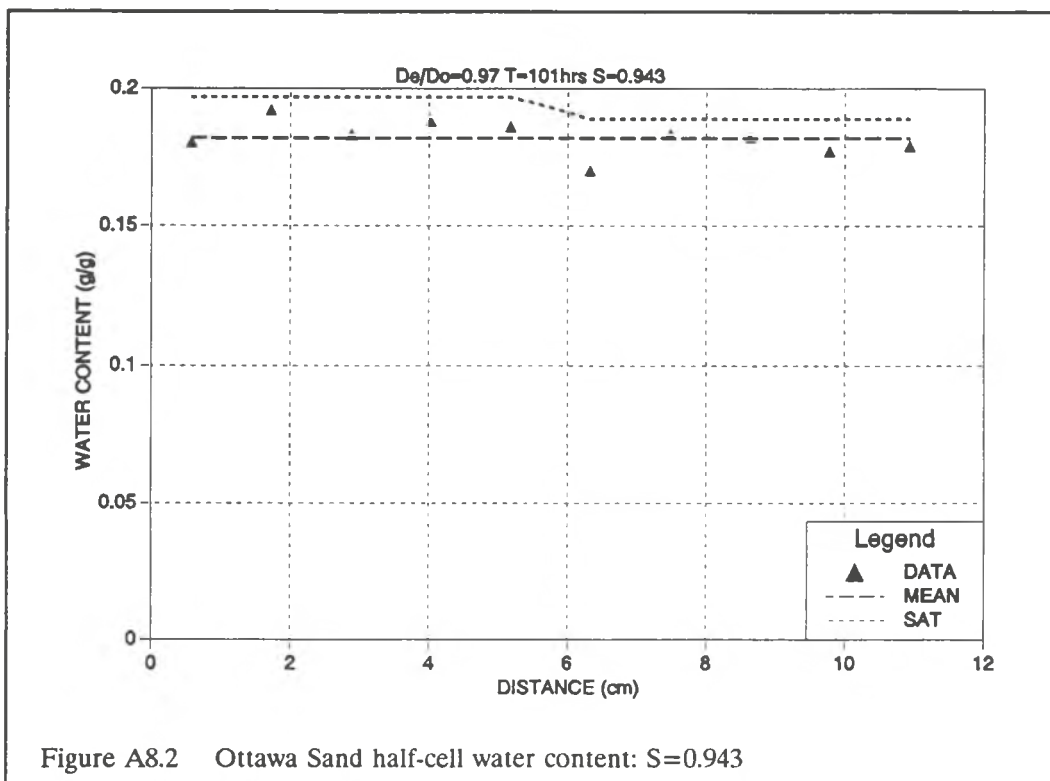


Figure A8.2 Ottawa Sand half-cell water content: $S=0.943$

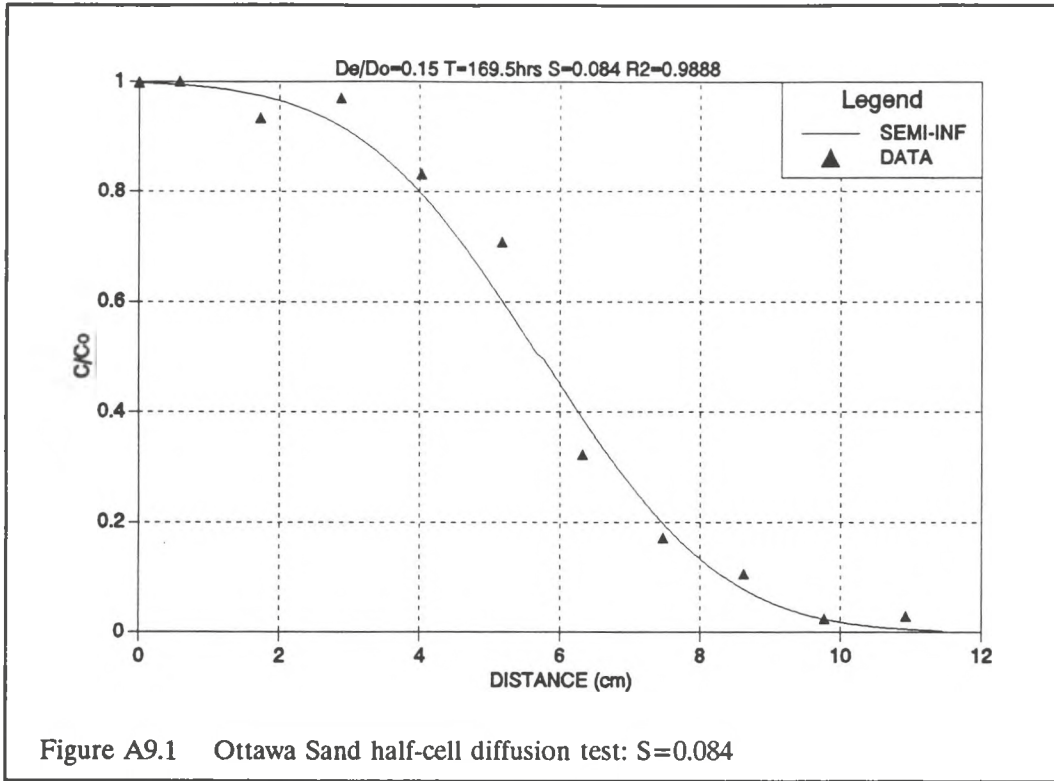


Figure A9.1 Ottawa Sand half-cell diffusion test: $S=0.084$

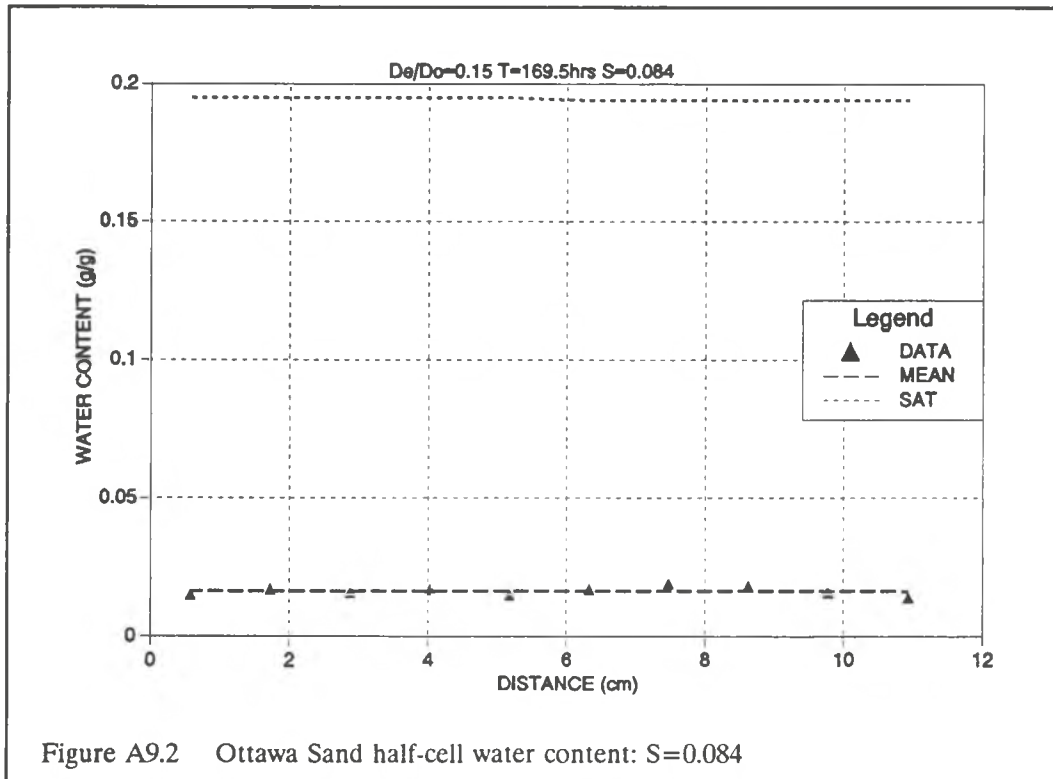
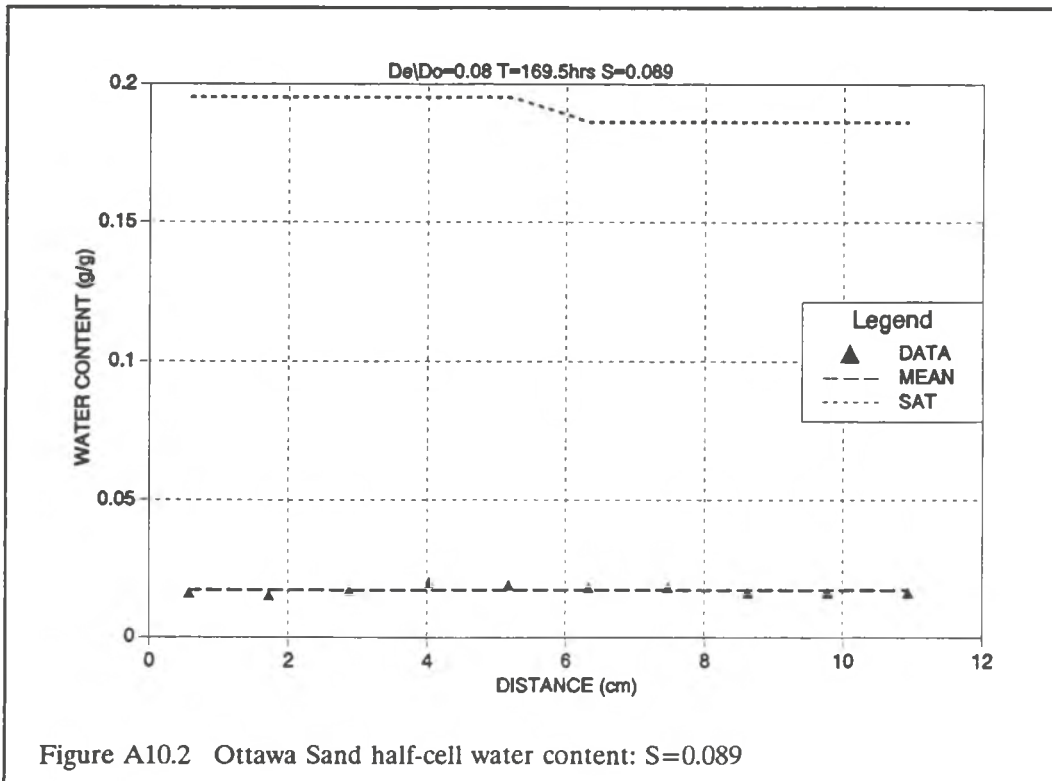
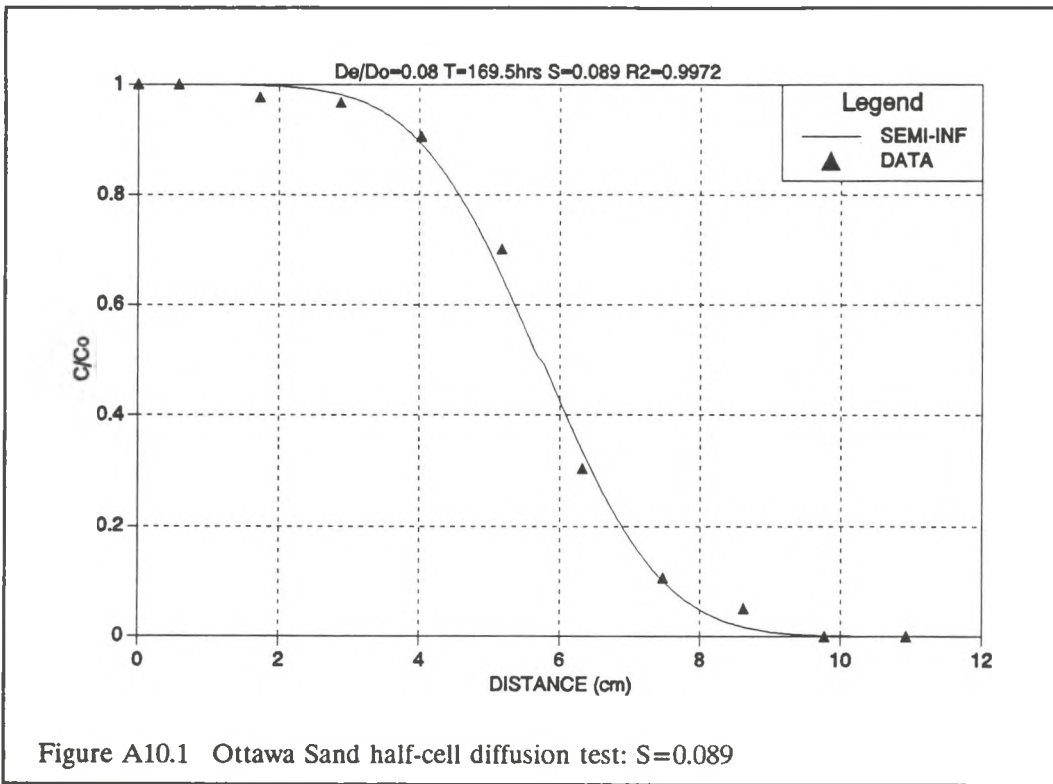


Figure A9.2 Ottawa Sand half-cell water content: $S=0.084$



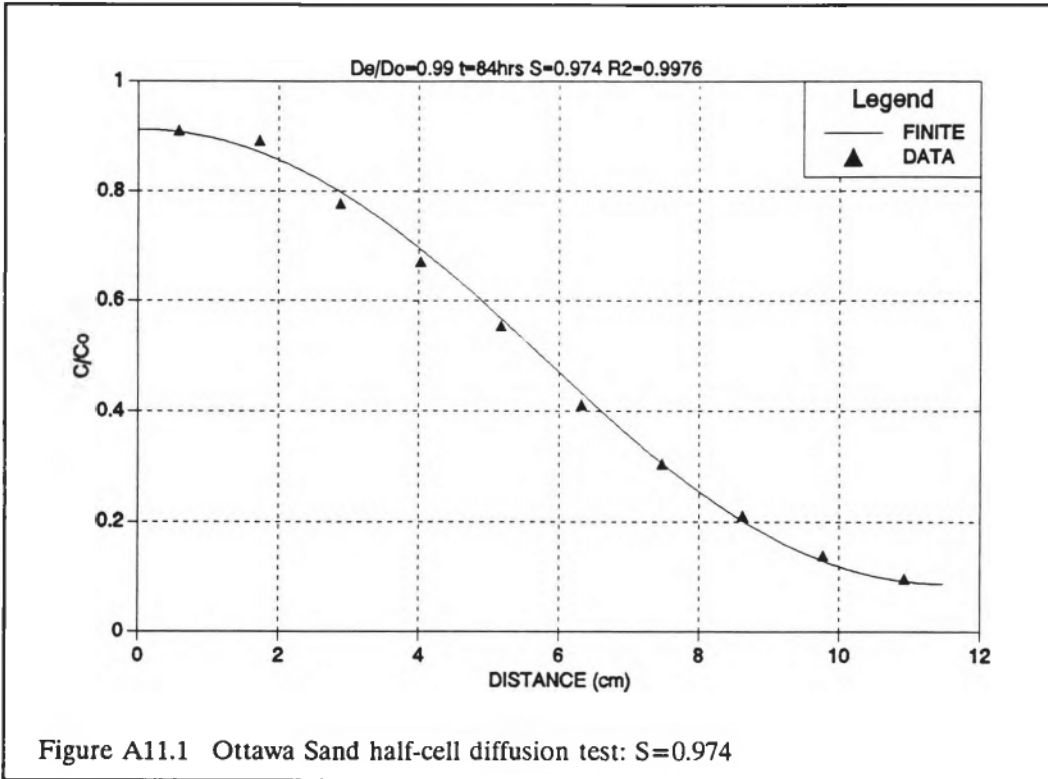


Figure A11.1 Ottawa Sand half-cell diffusion test: $S=0.974$

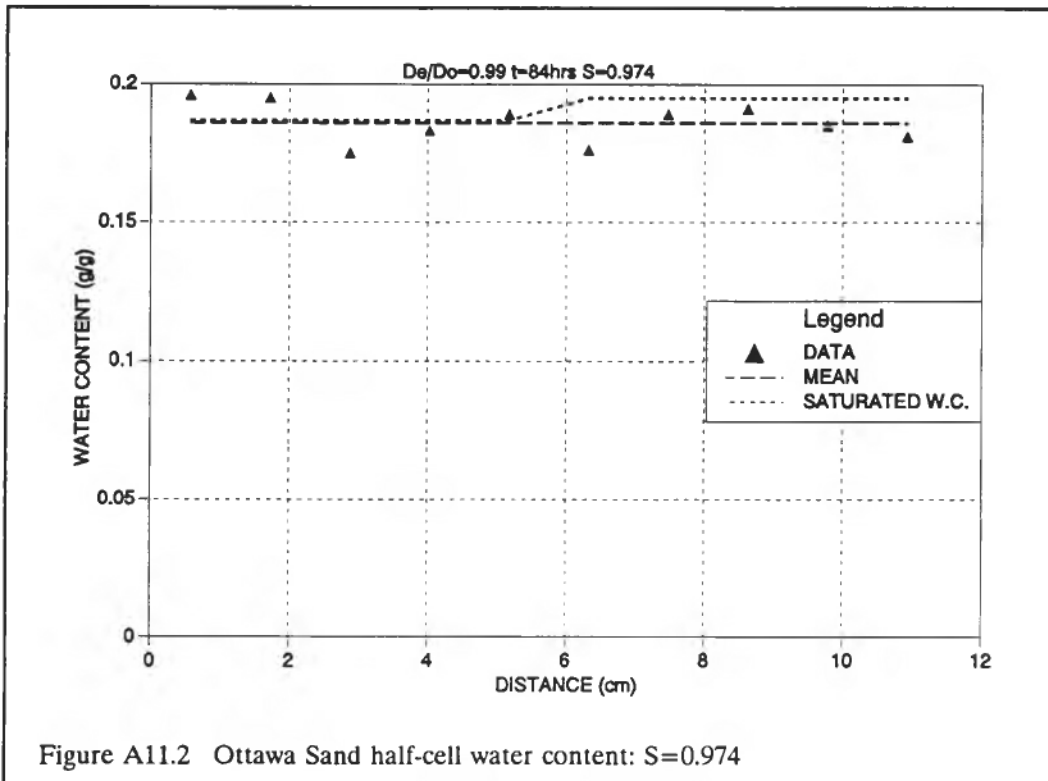
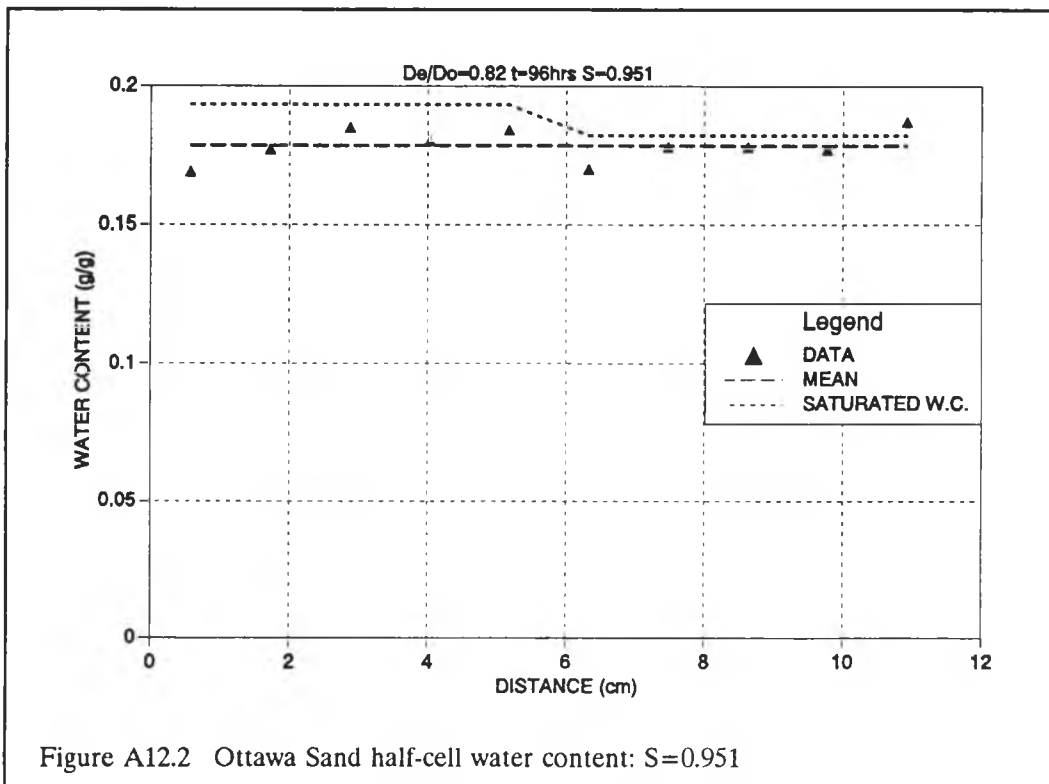
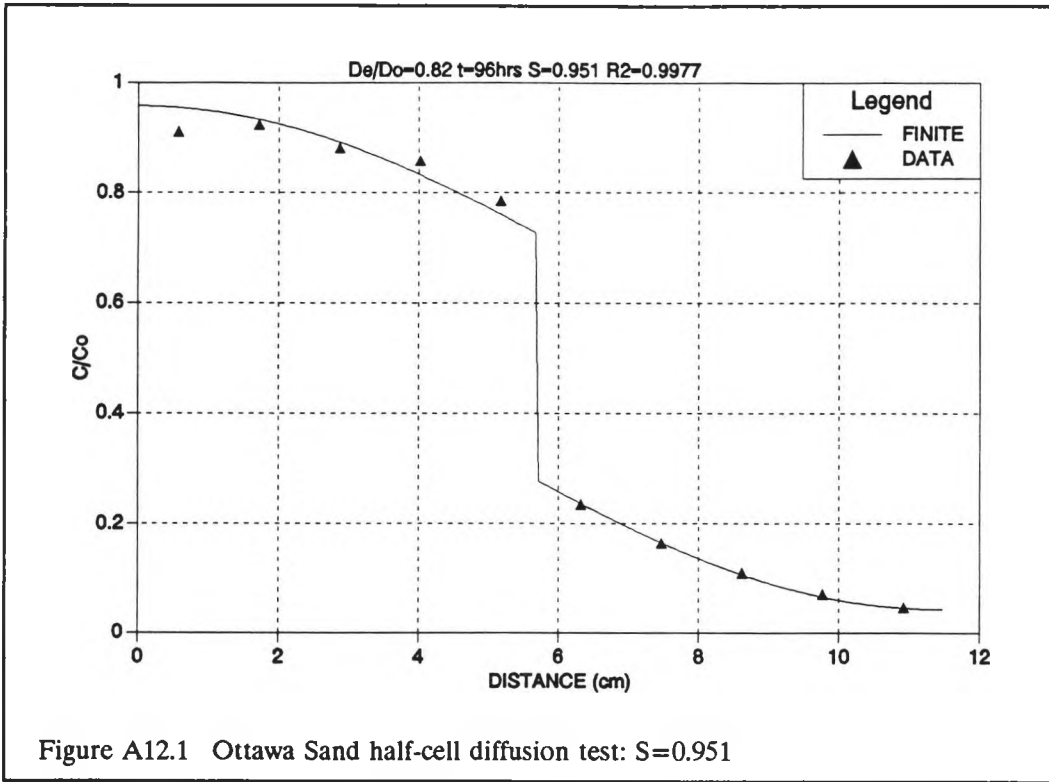
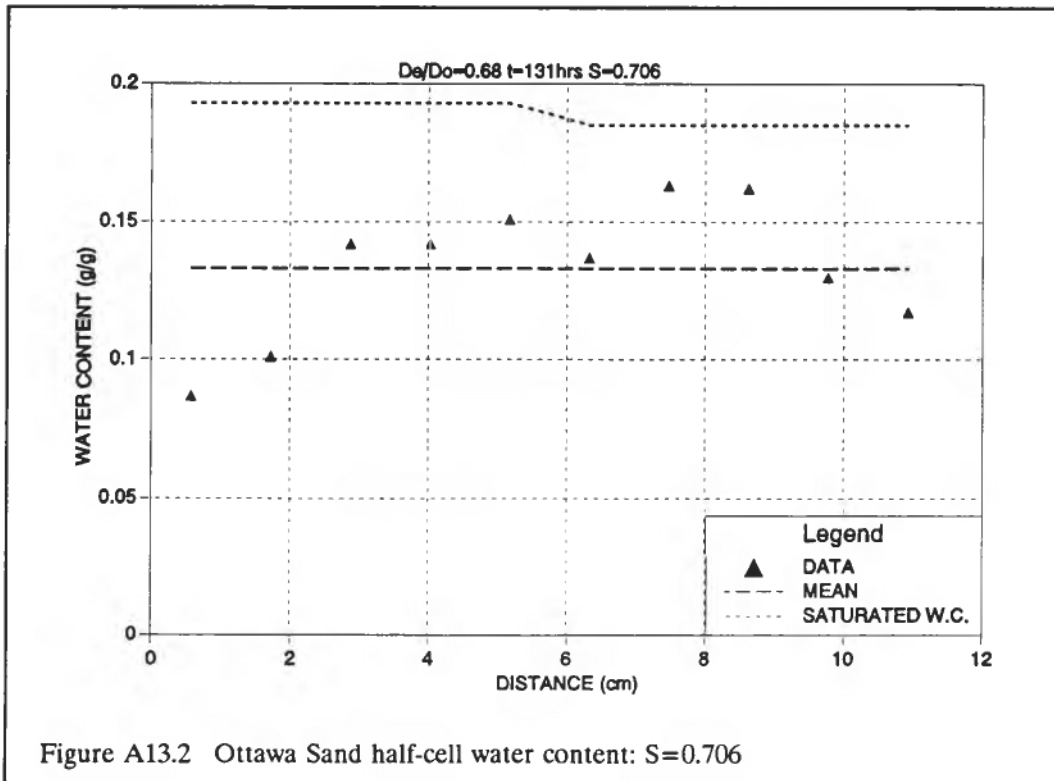
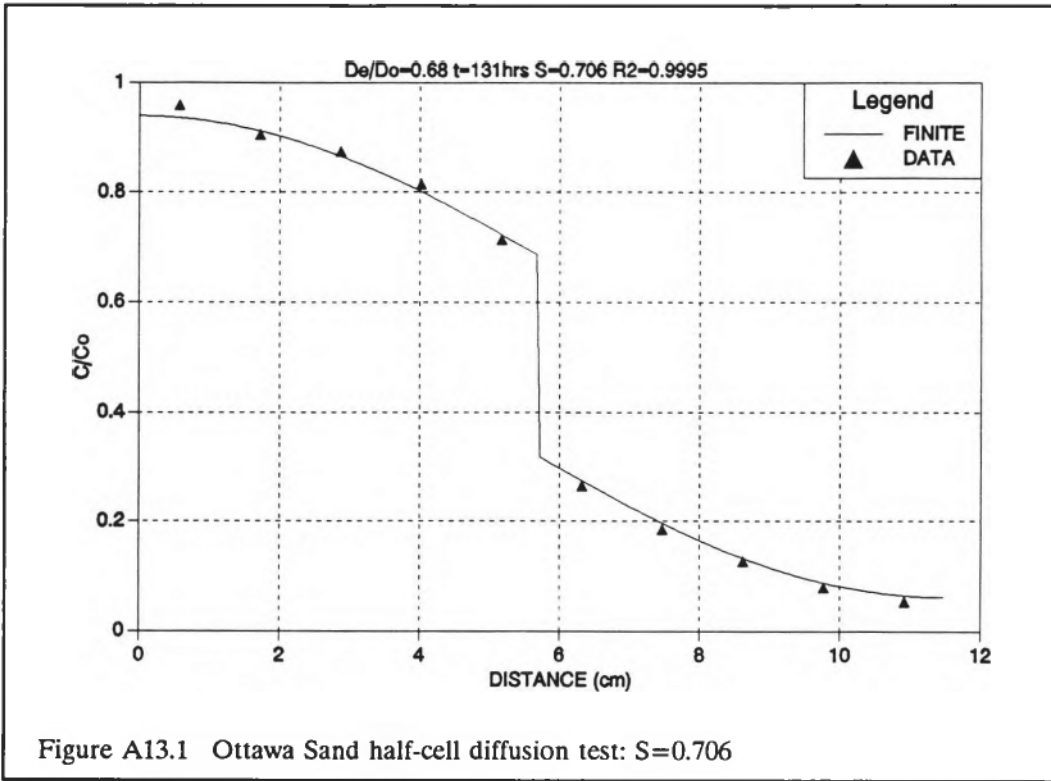


Figure A11.2 Ottawa Sand half-cell water content: $S=0.974$





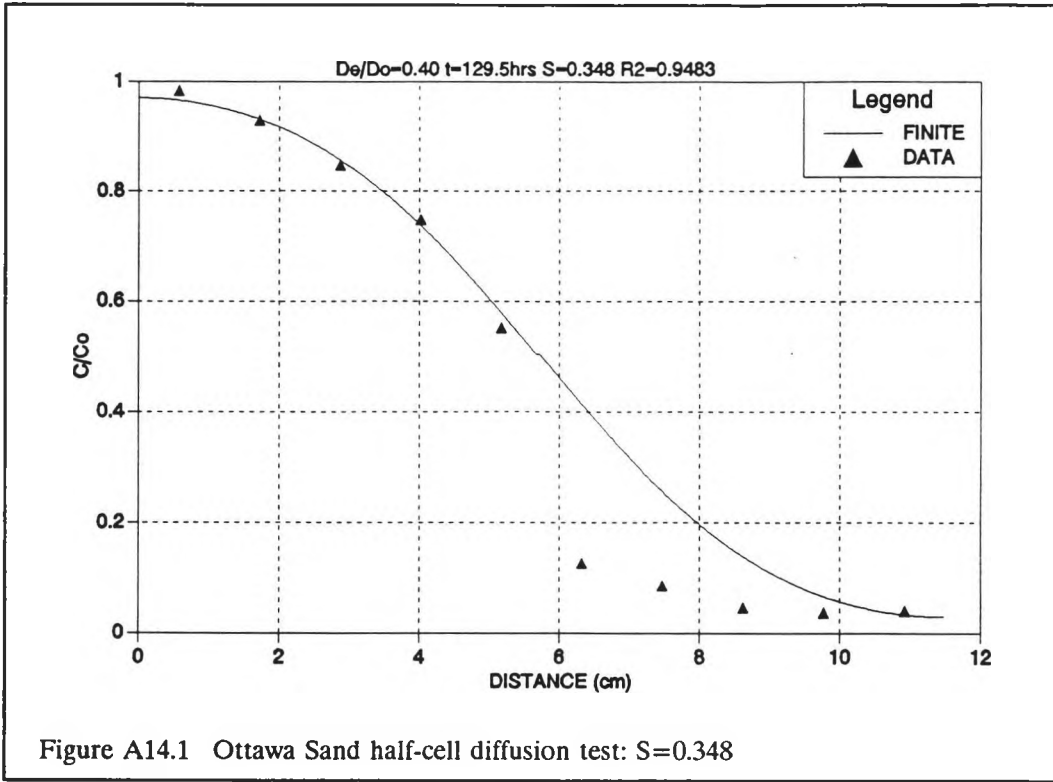


Figure A14.1 Ottawa Sand half-cell diffusion test: $S=0.348$

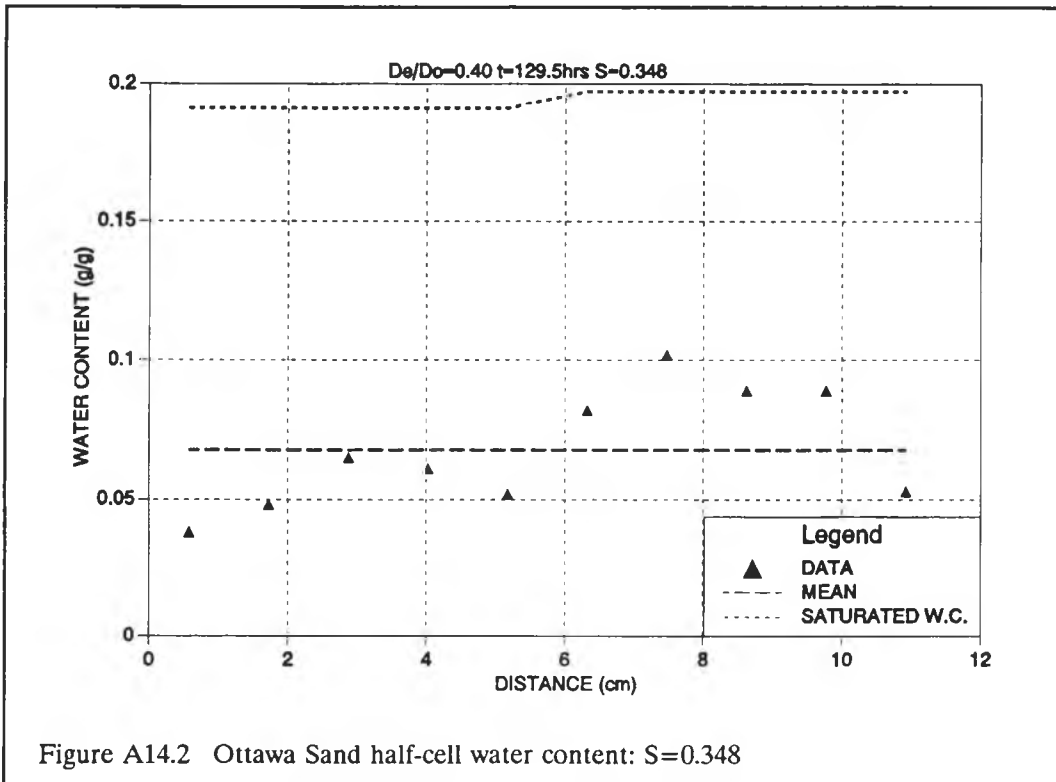
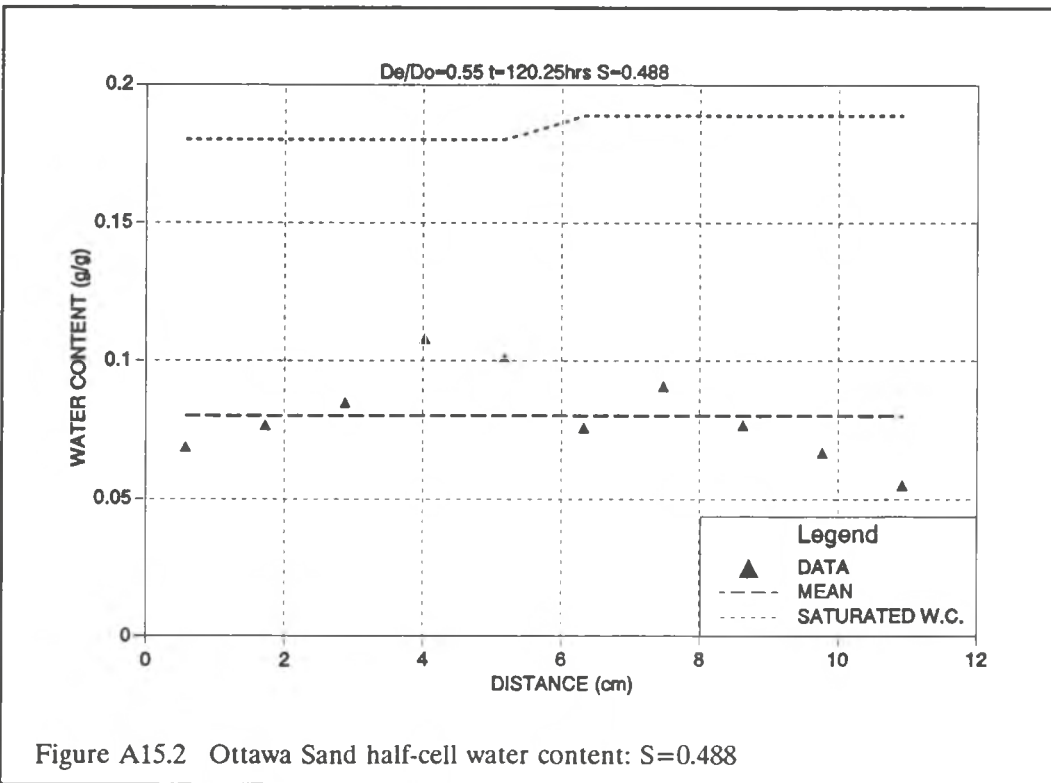
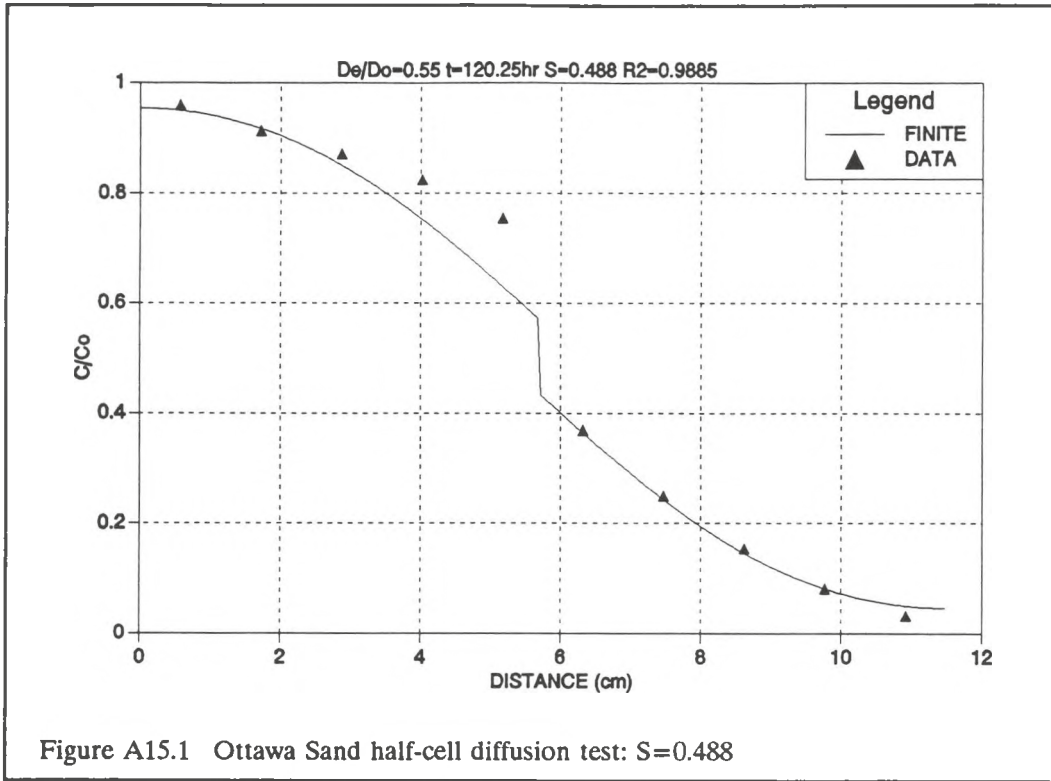
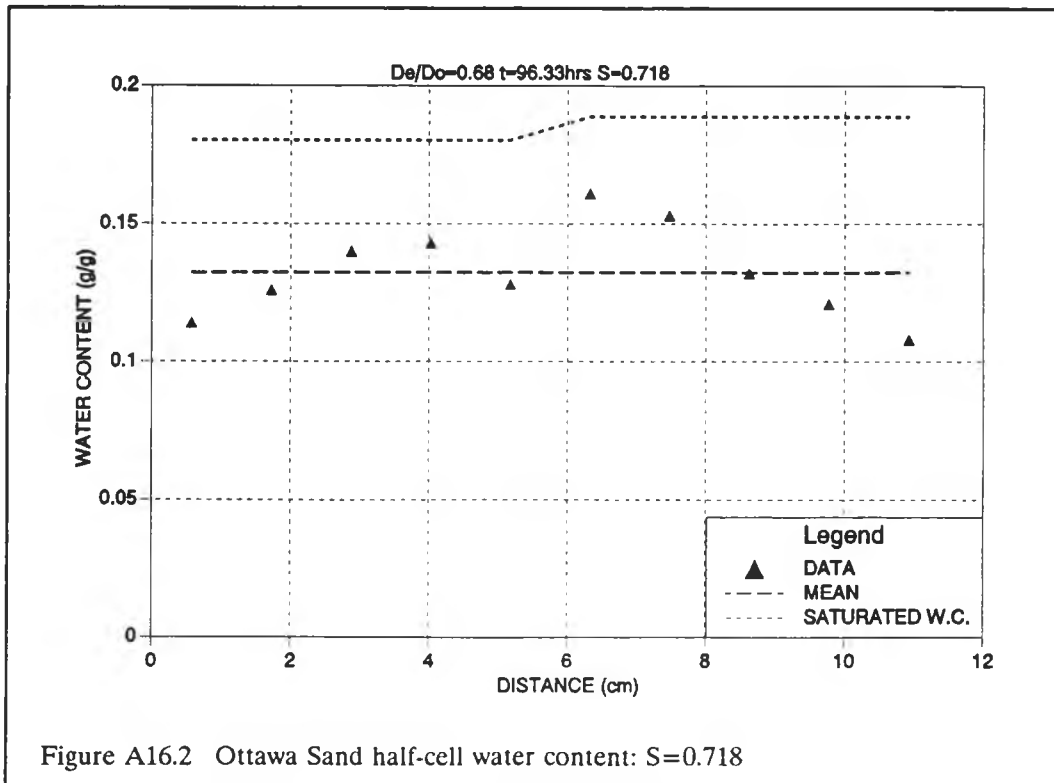
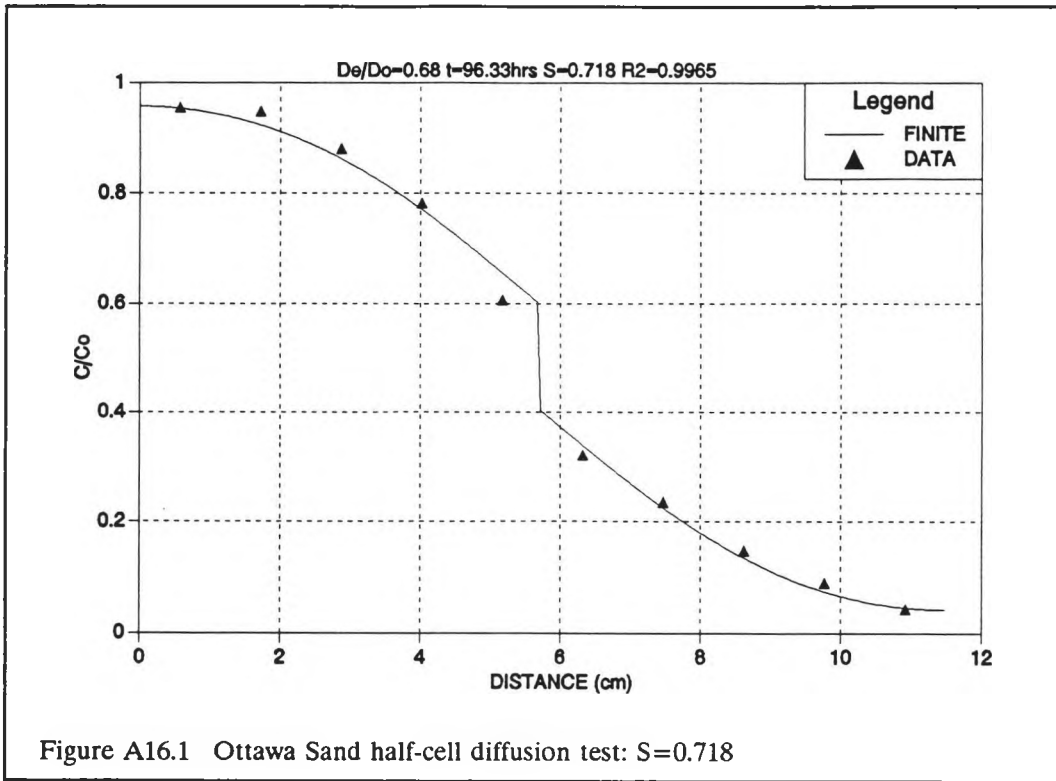


Figure A14.2 Ottawa Sand half-cell water content: $S=0.348$





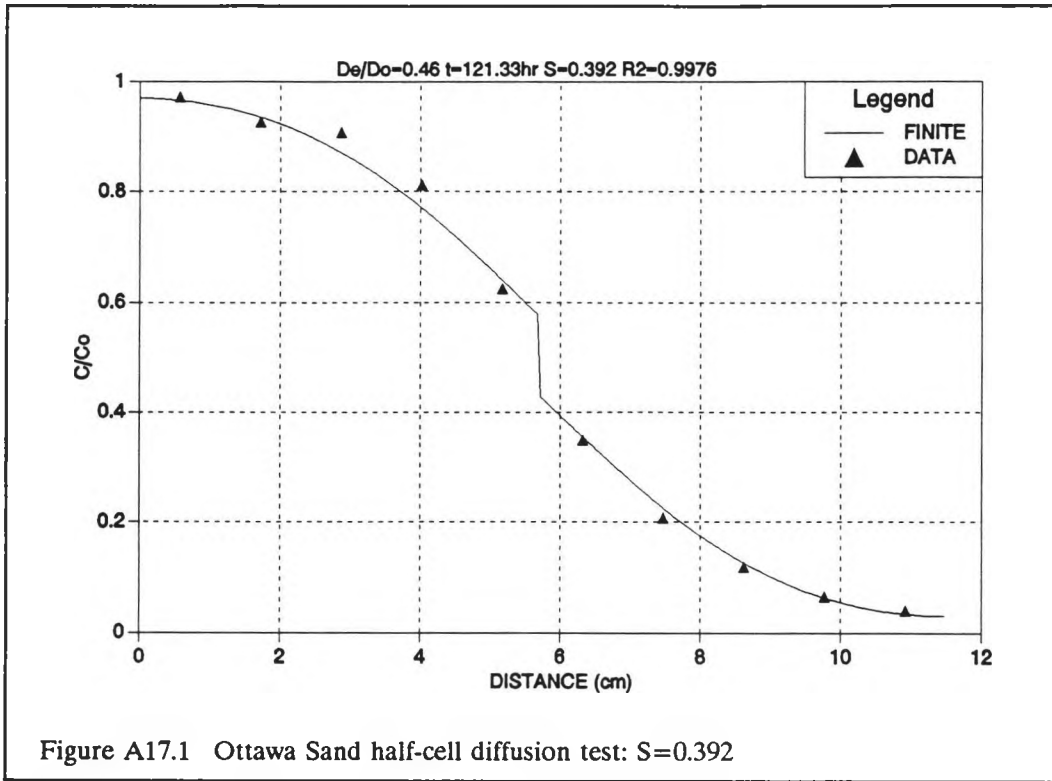


Figure A17.1 Ottawa Sand half-cell diffusion test: S=0.392

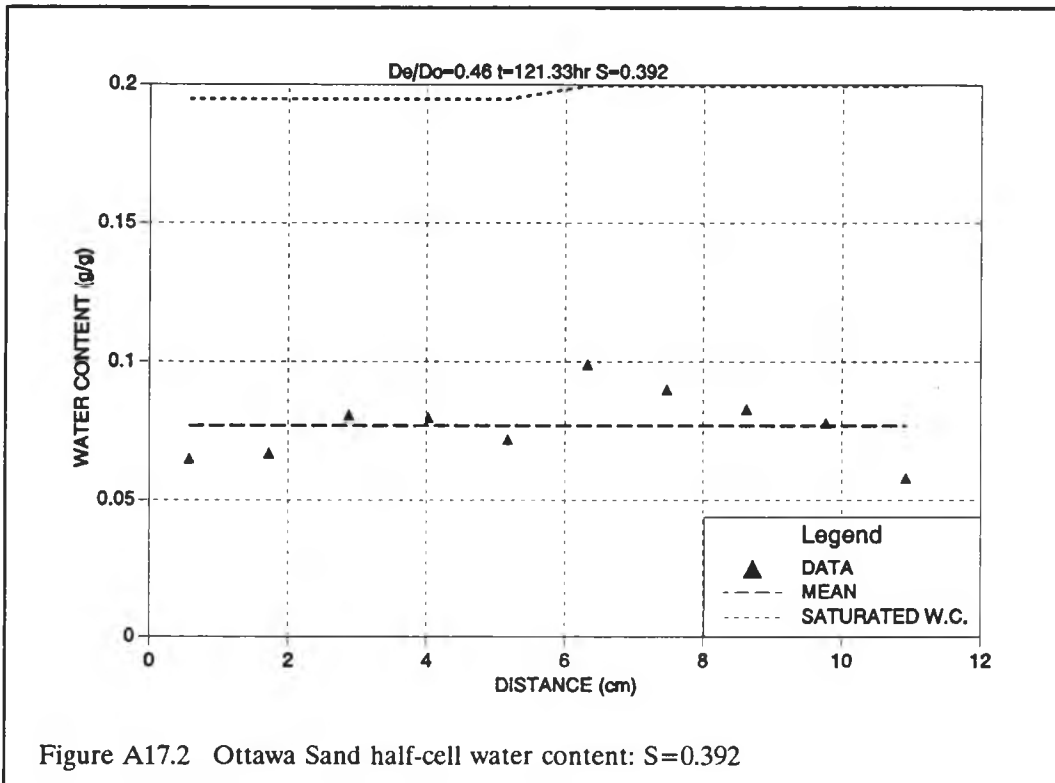


Figure A17.2 Ottawa Sand half-cell water content: S=0.392

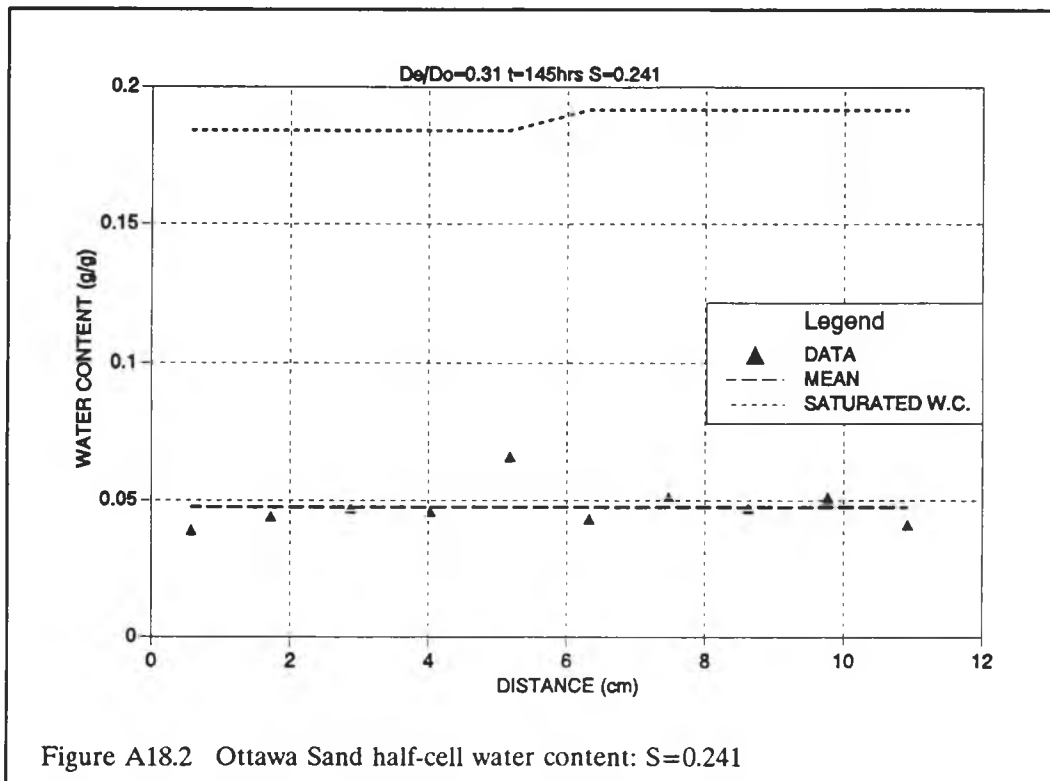
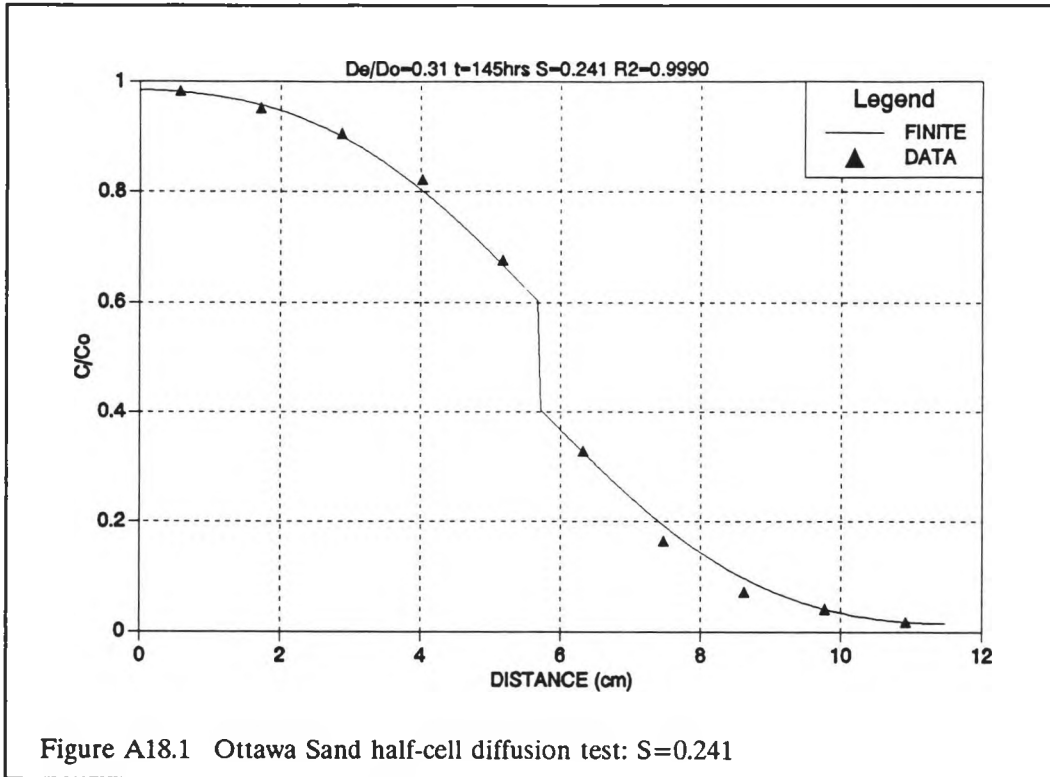


Table A1. Results of half-cell diffusion tests.					
Test #	Section #	Water Content w (g/g)	Cl ⁻ Concentration C (mg/l)	Average Bulk Density of Each Half-Cell ρ_b (g/cm ³)	Average Porosity of Each Half-Cell ϕ (cm ³ /cm ³)
PS 1	1	0.178	3130		
	2	0.186	2932		
	3	0.194	2740	1.788	0.320
	4	0.194	2441		
	5	0.184	2062		
	6	0.174	1547		
	7	0.181	981		
	8	0.181	598	1.776	0.325
	9	0.178	304		
	10	0.186	163		
PS 2	1	0.151	2842		
	2	0.156	2787		
	3	0.169	2580	1.798	0.316
	4	0.166	2382		
	5	0.159	1965		
	6	0.166	1324		
	7	0.173	905		
	8	0.156	586	1.798	0.316
	9	0.162	381		
	10	0.148	269		
PS 3	1	0.121	3329		
	2	0.135	3167		
	3	0.124	2905	1.771	0.327
	4	0.152	2579		
	5	0.152	2254		
	6	0.125	945		
	7	0.140	508		
	8	0.129	227	1.780	0.323
	9	0.150	116		
	10	0.134	80		

Table A2. Results of half-cell diffusion tests.

Test #	Section #	Water Content w (g/g)	Cl ⁻ Concentration C (mg/l)	Average Bulk Density of Each Half-Cell ρ_b (g/cm ³)	Average Porosity of Each Half-Cell ϕ (cm ³ /cm ³)
PS 4	1	0.045	3000		
	2	0.053	2962		
	3	0.045	2802	1.768	0.328
	4	0.045	2357		
	5	0.045	1516		
	6	0.052	419		
	7	0.058	246		
	8	0.058	68	1.785	0.321
	9	0.050	38		
	10	0.064	0		
PS 5	1	0.036	1793		
	2	0.035	1880		
	3	0.032	1976	1.765	0.329
	4	0.037	1662		
	5	0.037	1136		
	6	0.047	622		
	7	0.042	286		
	8	0.038	125	1.763	0.330
	9	0.041	105		
	10	0.044	80		
PS 6	1	0.061	3353		
	2	0.051	3318		
	3	0.053	3000	1.787	0.321
	4	0.053	2469		
	5	0.061	1649		
	6	0.108	384		
	7	0.088	159		
	8	0.088	71	1.788	0.320
	9	0.078	34		
	10	0.094	0		

Table A3. Results of half-cell diffusion tests.

Test #	Section #	Water Content w (g/g)	Cl ⁻ Concentration C (mg/l)	Average Bulk Density of Each Half-Cell ρ_b (g/cm ³)	Average Porosity of Each Half-Cell ϕ (cm ³ /cm ³)
PS 7	1	0.038	3216		
	2	0.038	2796		
	3	-	-	1.785	0.321
	4	0.037	2621		
	5	0.037	1644		
	6	0.041	615		
	7	0.047	189		
	8	0.045	18	1.783	0.322
	9	0.039	12		
	10	0.046	0		
OS 1	1	0.180	2814		
	2	0.192	2684		
	3	0.183	2538	1.741	0.343
	4	0.188	2363		
	5	0.186	2098		
	6	0.170	1636		
	7	0.183	1277		
	8	0.182	937	1.766	0.334
	9	0.177	599		
	10	0.179	419		
OS 2	1	0.015	3438		
	2	0.017	3212		
	3	0.016	3336	1.747	0.341
	4	0.017	2864		
	5	0.015	2436		
	6	0.017	1109		
	7	0.019	589		
	8	0.018	363	1.750	0.340
	9	0.016	84		
	10	0.014	98		

Table A4. Results of half-cell diffusion tests.

Test #	Section #	Water Content w (g/g)	Cl ⁻ Concentration C (mg/l)	Average Bulk Density of Each Half-Cell ρ_b (g/cm ³)	Average Porosity of Each Half-Cell ϕ (cm ³ /cm ³)
OS 3	1	0.016	3080		
	2	0.016	3010		
	3	0.016	2982	1.746	0.341
	4	0.018	2789		
	5	0.018	2158		
	6	0.019	936		
	7	0.020	327		
	8	0.017	155	1.774	0.331
	9	0.015	0		
	10	0.016	0		
OS 4	1	0.196	2822		
	2	0.195	2767		
	3	0.175	2410	1.772	0.331
	4	0.183	2081		
	5	0.189	1715		
	6	0.176	1277		
	7	0.189	944		
	8	0.191	652	1.747	0.341
	9	0.185	430		
	10	0.181	300		
OS 5	1	0.169	2960		
	2	0.177	3001		
	3	0.185	2865	1.752	0.339
	4	0.180	2789		
	5	0.184	2551		
	6	0.170	764		
	7	0.178	531		
	8	0.178	355	1.787	0.326
	9	0.177	228		
	10	0.187	150		

Table A5. Results of half-cell diffusion tests.

Test #	Section #	Water Content w (g/g)	Cl ⁻ Concentration C (mg/ℓ)	Average Bulk Density of Each Half-Cell ρ_b (g/cm ³)	Average Porosity of Each Half-Cell ϕ (cm ³ /cm ³)
OS 6	1	0.087	3019		
	2	0.101	2850		
	3	0.142	2753	1.753	0.338
	4	0.142	2564		
	5	0.151	2247		
	6	0.137	834		
	7	0.163	583		
	8	0.162	397	1.778	0.329
	9	0.130	246		
	10	0.117	168		
OS 7	1	0.038	3000		
	2	0.048	2835		
	3	0.065	2587	1.758	0.337
	4	0.061	2279		
	5	0.052	1681		
	6	0.082	384		
	7	0.102	261		
	8	0.089	139	1.740	0.343
	9	0.089	113		
	10	0.053	121		
OS 8	1	0.069	2974		
	2	0.077	2828		
	3	0.085	2701	1.793	0.323
	4	0.108	2554		
	5	0.101	2340		
	6	0.076	1146		
	7	0.091	773		
	8	0.077	477	1.766	0.334
	9	0.067	252		
	10	0.055	98		

Table A6. Results of half-cell diffusion tests.

Test #	Section #	Water Content w (g/g)	Cl ⁻ Concentration C (mg/l)	Average Bulk Density of Each Half-Cell ρ_b (g/cm ³)	Average Porosity of Each Half-Cell ϕ (cm ³ /cm ³)
OS 9	1	0.114	3009		
	2	0.126	2987		
	3	0.140	2773	1.748	0.340
	4	0.143	2464		
	5	0.128	1909		
	6	0.161	1013		
	7	0.153	742		
	8	0.132	464	1.733	0.346
	9	0.121	283		
	10	0.108	138		
OS 10	1	0.065	3110		
	2	0.067	2962		
	3	0.081	2903	1.751	0.339
	4	0.080	2598		
	5	0.072	1994		
	6	0.099	1114		
	7	0.090	664		
	8	0.083	377	1.740	0.343
	9	0.078	208		
	10	0.058	129		
OS 11	1	0.041	3372		
	2	0.051	3262		
	3	0.047	3105	1.781	0.328
	4	0.051	2818		
	5	0.043	2318		
	6	0.066	1125		
	7	0.046	564		
	8	0.047	249	1.757	0.337
	9	0.044	143		
	10	0.039	62		

APPENDIX B
HYDRAULIC PROPERTIES OF POROUS MEDIA

Table B1. Water retention analysis Ottawa sand		
Ottawa Sand $\rho_b = 1.75 \text{ g/cm}^3$ $\phi = 0.340$		
$\lambda = 4.0$ $hd = 17.2 \text{ cm}$ $\theta_r = 0.0187$		
Matric Pressure Head h_c (cm)	Water Content θ (cm^3/cm^3)	Saturation S
11.0	0.340	1.0
12.1	0.335	0.985
13.2	0.334	0.982
14.5	0.330	0.971
15.6	0.312	0.918
16.7	0.275	0.809
17.8	0.293	0.862
19.0	0.225	0.662
21.2	0.150	0.441
22.4	0.134	0.394
24.8	0.109	0.321
26.0	0.083	0.244
28.3	0.068	0.200
32.0	0.048	0.141
34.1	0.041	0.121
36.0	0.034	0.100
38.0	0.031	0.091
40.0	0.027	0.079
50.0	0.024	0.071
60.2	0.022	0.065
82.1	0.020	0.059
99.8	0.019	0.056

Table B2. Water retention analysis Poudre sand		
Poudre Sand $\rho_b = 1.78 \text{ g/cm}^3$ $\phi = 0.323$		$\lambda = 0.94$ $hd = 30 \text{ cm}$ $\theta_r = 0.0185$
Matric Pressure Head h_c (cm)	Water Content θ (cm^3/cm^3)	Saturation S
0	0.323	1.00
17.5	0.316	0.978
22.9	0.297	0.920
46.5	0.239	0.740
50.0	0.219	0.678
51.5	0.208	0.644
56.0	0.198	0.613
58.5	0.187	0.579
64.2	0.168	0.520
70.5	0.158	0.489
89.2	0.138	0.427
106.2	0.115	0.356
116.0	0.105	0.325
131.0	0.095	0.294
161.5	0.075	0.232
201.0	0.064	0.198
240.0	0.054	0.167
3000.0	0.022	0.068
1500.0	0.019	0.059

Table B3. Unsaturated hydraulic conductivity Ottawa sand		
Ottawa Sand $K_s = 3.24 \times 10^{-2} \text{ cm/s}$ $\rho_b = 1.751 \text{ g/cm}^3$		
Matric Pressure h_c (cm)	Relative Conductivity K_r	Unsaturated Hydraulic Conductivity $K(h_c)$ (cm/s)
0	1.0	0.03240
18.4	0.617	0.02000
21.5	0.309	0.01000
25.8	0.054	0.00174
26.7	0.028	0.00091
27.3	0.026	0.00085
28.7	0.008	0.00027
29.1	0.006	0.00018

Table B4. Unsaturated hydraulic conductivity Poudre sand		
Poudre Sand $K_s = 2.51 \times 10^{-3}$ cm/s $P_b = 1.78$ g/cm ³		
Matric Pressure Head h_c (cm)	Relative Conductivity K_r	Unsaturated Hydraulic Conductivity $K(h_c)$ (cm/s)
3.00	1	1.40×10^{-3}
3.90	0.96	1.34×10^{-3}
5.62	0.77	1.08×10^{-3}
10.05	0.72	1.01×10^{-3}
20.40	0.72	1.01×10^{-3}
48.00	0.62	8.68×10^{-4}
55.00	0.52	7.28×10^{-4}
47.00	0.463	6.48×10^{-4}
52.00	0.43	6.02×10^{-4}
59.00	0.422	5.91×10^{-4}
64.00	0.37	5.18×10^{-4}
69.00	0.31	4.34×10^{-4}
70.00	0.285	3.99×10^{-4}
77.00	0.165	2.31×10^{-4}
79.00	0.125	1.75×10^{-4}
82.00	0.117	1.64×10^{-4}
86.00	0.093	1.30×10^{-4}
91.00	0.081	1.13×10^{-4}
95.00	0.065	9.10×10^{-5}
105.00	0.036	5.04×10^{-5}
115.00	0.021	2.94×10^{-5}
118.00	0.0165	2.31×10^{-5}
121.00	0.0112	1.57×10^{-5}
128.00	0.0088	1.23×10^{-5}
130.00	0.0053	7.42×10^{-6}
135.00	0.0043	6.02×10^{-6}

APPENDIX C
HYDRAULIC PROPERTIES OF POROUS MEDIA
EXTRACTED FROM THE LITERATURE

TABLE C1. Hydraulic properties of porous media.

	Saturated Hydraulic Conductivity (cm/s)	Bulk Density (g/cm ³)	Particle Density (g/cm ³)	Porosity (cm ³ /cm ³)	Residual Sat.	Effective Water Content (cm ³ /cm ³)	Air Entry Pressure (cm)	Lambda	k _o	k _o T	D ₀
Laliberte et al.											
Touchet SiLm	1.736E-04	1.57	2.60	0.396	0.220	0.309	239.2	1.70	2.5	5.24	1.9801
	2.521E-04	1.50	2.60	0.423	0.220	0.330	202.0	1.64	2.5	5.30	1.8339
	3.218E-04	1.43	2.60	0.450	0.220	0.351	169.7	1.59	2.5	6.15	1.4847
	5.523E-04	1.36	2.60	0.477	0.200	0.381	135.5	1.47	2.5	5.85	1.4013
	6.818E-04	1.29	2.60	0.504	0.180	0.413	110.4	1.02	2.5	6.16	1.1978
Columbia SaLm											
	3.973E-04	1.47	2.66	0.448	0.220	0.350	156.9	1.70	2.5	6.03	1.5208
	6.180E-04	1.41	2.66	0.471	0.220	0.367	135.5	1.81	2.5	5.64	1.5474
	7.956E-04	1.37	2.66	0.486	0.220	0.379	120.8	1.50	2.5	5.13	1.6482
	1.570E-03	1.26	2.66	0.527	0.210	0.416	89.3	1.49	2.5	5.22	1.4572
	2.423E-03	1.18	2.66	0.557	0.180	0.457	70.8	1.27	2.5	5.36	1.2459
Unconsolidated Sa											
	8.927E-02	1.58	2.71	0.416	0.091	0.378	15.8	4.75	2.5	4.40	1.6522
	1.016E-01	1.53	2.71	0.435	0.088	0.396	15.0	4.37	2.5	4.38	1.5778
	1.113E-01	1.51	2.71	0.442	0.086	0.404	14.4	4.49	2.5	4.42	1.5309
	1.218E-01	1.48	2.71	0.453	0.085	0.415	13.9	4.13	2.5	4.36	1.5131
	1.366E-01	1.46	2.71	0.460	0.084	0.422	13.1	4.02	2.5	4.41	1.4660
This Study											
Ottawa Sa	3.240E-02	1.75	2.65	0.340	0.055	0.321	17.2	4.00	2.5	8.19	1.0063
Poudre Sa Mix	2.510E-03	1.78	2.63	0.323	0.056	0.305	30.0	0.94	2.5	15.84	0.5511
Brooks-Corey											
Volcanic Sa	1.079E-02	1.68	2.65	0.365	0.157	0.308	31.8	2.30	2.5	5.54	1.7397
Fine Sa (GE #13)	2.796E-03	1.70	2.65	0.360	0.167	0.300	81.4	3.70	2.5	3.85	2.5985
Touchet SiLm	4.905E-04	1.41	2.65	0.469	0.270	0.342	149.0	1.80	2.5	5.47	1.8301
Glass Beads	1.030E-02	1.64	2.65	0.383	0.085	0.350	57.6	6.00	2.5	2.82	2.7634
Fragmented Mix	1.472E-02	1.48	2.65	0.441	0.276	0.319	34.2	2.90	2.5	4.04	2.6794
Berea Sandstone	4.719E-04	2.10	2.65	0.206	0.299	0.144	85.4	3.70	2.5	9.99	2.4720
Poudre River Sa	2.217E-02	1.69	2.65	0.364	0.125	0.319	27.8	3.40	2.5	4.29	2.0904
Amarillo SiCILm	2.296E-03	1.44	2.65	0.455	0.250	0.341	75.5	2.30	2.5	5.12	1.9076
Hygiene Sandstone	1.746E-04	1.99	2.65	0.250	0.577	0.106	107.3	4.20	2.5	13.08	4.2720

Note : Bulk density of Brooks-Corey porous media are calculated from reported wetting phase porosity and assumed particle density, 2.65 g/cm³.
 Sa = Sand; Si = Silt; Cl = Clay; Lm = Loam